SYNTHESIS OF HYBRID NANOMATERIALS THROUGH AMPHIPHILIC SELF-ASSEMBLY

Qingjie Luo

A DISSERTATION

in

Chemistry

Presented to the Faculties of the University of Pennsylvania

in

Partial Fulfillment of the Requirements for the

Degree of Doctor of Philosophy

2016

Supervisor of Dissertation

_____

So-Jung Park, Adjunct Associate Professor of Chemistry

Graduate Group Chairperson

_____

Gary A. Molander, Hirschmann-Makineni Professor of Chemistry

Dissertation Committee

Zahra Fakhraai, Assistant Professor of Chemistry
Larry G. Sneddon, Professor of Chemistry
Robert Riggleman, Assistant Professor of Chemical and Biomolecular Engineering

SYNTHESIS OF HYBRID NANOMATERIALS THROUGH AMPHIPHILIC SELF-ASSEMBLY

ABSTRACT
SYNTHESIS OF HYBRID NANOMATERIALS THROUGH AMPHIPHILIC SELF-ASSEMBLY

Qingjie Luo

So-Jung Park

There have been tremendous efforts toward combining nanoparticles, polymers, biomolecules in material synthesis and device fabrication in order to take advantage of the unique properties of each component. The ability to construct multicomponent hybrid nanomaterials with controllable structure and properties is critical to truly exploit the potential of these functional materials in many applications. This thesis presents the construction of self-assemblies of various components including nanoparticles, synthetic block copolymers, DNA block copolymers, and lipid molecules.

The location of nanoparticles in colloidal block copolymer assemblies is controlled by using nanoparticles modified with mixed surface ligands. Different morphologies including micelles, Janus-like micelles, and interfacial assemblies, are obtained by varying gold nanoparticles ligand composition. This work also reveals the surface energy calculations to explain the experimental findings, which offers guidelines for the generation of colloidal self-assemblies with predesigned structures and properties. We also demonstrated the compartmentalization of two different types of nanoparticles in colloidal polymer assemblies by using mixed ligand gold nanoparticles.

The self-assembly of DNA block copolymers and synthetic block copolymer is also presented. The binary self-assembly results in giant polymersomes which can be

connected through specific DNA interactions and form DNA rafts at junction area. These results demonstrate that DNA hybridization induces effective phase segregation in polymer assemblies to form multiple DNA linkages. We further showed that phase segregation has important implications in DNA melting properties, as mixed block copolymer assemblies with low DNA content can still exhibit useful DNA melting properties that are characteristic of DNA nanostructures with high DNA density.

Finally we developed a strategy to self-assemble DNA-functionalized gold nanoparticles into macroscopic sheets assisted by DNA-tethered lipid bilayers. By varying the amount of gold nanoparticles input, the surface coverage can be tuned. Our approach provides a new method for the preparation of versatile scaffolds for nanofabrication and paves the way for organizing functional nanoparticles in a micrometer space.

TABLE OF CONTENTS

LIST OF TABLES

LIST OF FIGURES

LIST OF SCHEMES

CHAPTER 1. Introduction

1.1 Solution phase self-assembly of amphiphilic block copolymers

1.1.1 Amphiphilic block copolymers solution phase self-assemblies and their applications. Amphiphilic block copolymers consist of two chemically distinct blocks which are covalently bound together. The two immiscible blocks can microphase separate and later self-organize into enormous morphologies in solution phase, such as spherical micelles, cylinders, lamellae, vesicles, and other hierarchical assemblies, *etc.*, as shown in Figure 1.1.[1-3] Self-assembly is a common phenomenon in daily life, for instant, cell membranes constructed by the self-assembly of phospholipids, or soap bubbles originated from the self-assembly of small molecule surfactants. Amphiphilic block copolymers self-assemblies are superior to those formed by small molecule surfactants in terms of stability and durability due to their better mechanical and physical properties. Therefore, self-assembly of amphiphilic block copolymers is a very active area in material science, and has been extensively exploited for applications in many domains, including biomateirals, biomedicine, microelectronics, catalysts, *etc*.[4]

There are couples of popular methods to prepare amphiphilic block copolymers assemblies reported on previously published literatures. Among them, slow water addition (or co-solvent method) is the most frequently used method to generate small assemblies in chemistry lab. In this method, block copolymers are dissolved in a good solvent, followed by the slow addition of water which is a nonsolvent to intrigue

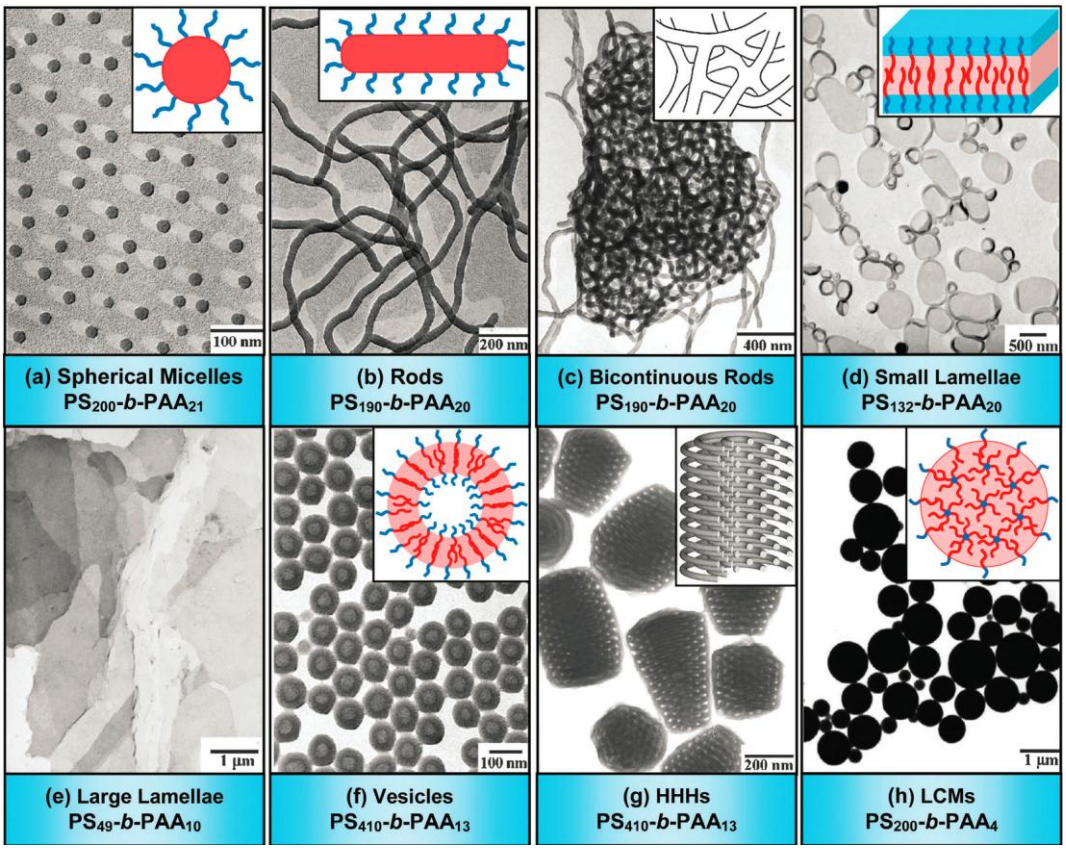

Figure 1.1. Transmission electron microscopy (TEM) images and corresponding pictorial images of various morphologies formed by different degrees of polymerization for each block. In the pictorial drawings, red represents hydrophobic polystyrene part, while blue strands denote hydrophilic polyacrylic acid. In TEM images, only hydrophobic PS parts are visible. HHHs: hexagonally packed hollow hoops; LCMs: large compound micelles. Figure reprint with permission from ref. [2] and [3].

the self-assembly process. Typically, this method produces nanometer to several micrometer sizes assemblies. For the generation of giant vesicles in micrometer sizes range, film hydration is particularly useful.[5-7] There are other approaches utilized for the preparation of vesicles including electroformation and layer-by-layer assembly.[8,9] The developments of microfluidics techniques in recent years have opened promising ways to form monodisperse vesicles with controllable size.[10]

As mentioned above, one can observe a spectrum of morphologies of assemblies obtained by amphiphilic block copolymers, ranging from spherical micelles through rods, bicontinous rods, bilayers, to large compound micelles, as shown in Figure 1.1. Spherical micelles and vesicles, two of the most important morphologies, will be discussed in the following paragraphs.

Simple spherical micelles are composed of hydrophobic core surrounded by hydrophilic corona. The hydrophilic corona chains maintain the solubility in aqueous solution to avoid assemblies precipitating, while the hydrophobic cores offer a perfect compartment for the incorporation of hydrophobic functional materials, for example, drugs, fluorescent probes, nanoparticles, and a wide range of biomolecules including genes and proteins.[11-13] Hence, spherical micelles have been extensively used for applications in bioimaging and drug/gene delivery. Moreover, during the preparations of self-assemblies, spherical micelles are usually first generated. Therefore, they are considered as the simplest beginning aggregate to build up more complicated morphologies.

Vesicles consist of hydrophilic hollow cavity with a hydrophobic bilayer wall

sandwiched by hydrophilic external and internal coronas. They are known as super amphiphiles, for the reason that their molecular weights are several orders of magnitude higher than those of phospholipids. The higher molecular weight results in increased wall thickness and coil interpenetration and entanglement, which makes amphiphilic block copolymers vesicles more robust, stable and improved mechanical properties, compared to liposomes.[14,15] Vesicles have drawn significant attention because of their unique morphologies as well as their potential applications, and over thousands of papers have been published on this topic.[16-19] Various technologies have been applied in order to acquire desired functionalities, for example, vesicle surface modification and encapsulation. Specific ligands, such as biotin can be conjugated onto hydrophilic block and incorporated into vesicle coronas which subsequently can be decorated by avidinylated/streptavidinylated ligands or nanoparticles *via* strong affinity between avidin/streptavidin and biotin.[20] Surface modification of vesicle walls allows for the attachment of hydrophobic molecules,[21] nanoparticles,[22,23] and proteins, *etc*.[19,24,25] The hydrophobic wall also enables the encapsulation of molecules mentioned above to create dual system.[26,27] Nucleic acids and proteins need carriers for cellular delivery as they are too polar to enter cells.[28] Vesicles provide the capabilities of encapsulation and delivery of these bioactive agents, and thus show promising aspect in gene or protein therapies.[28,29]

1.1.2 Incorporation of nanoparticles into block copolymer assemblies. It is well known that amphiphilic block copolymers self-assemble into assemblies with a wide range of morphologies in selective solvents, allowing them to provide as

templates to direct the organization of incorporated nanoparticles. Through the self-assembly of amphiphilic block copolymer and nanoparticles in selective solvents, one can spatially organize nanoparticles in the resultant polymer matrices. Nanoparticles, as one of the most powerful popular building blocks encapsulated into amphiphilic block copolymers, have found a number of applications in electron devices, catalysis, nanoelectronics, and biodiagnostics.[30] The forming nanocomposites often have advantages over individual constituent, show enhanced stability and unique functions for certain applications,[31-34] and depend on the distribution and ordering of incorporated nanoparticles.

It should be noted that nanoparticles are not just passively encapsulated into polymer metrics, and indeed play an active role during the self-assembly process. The co-assembly of nanoparticles and amphiphilic block copolymers is a very complex process, and the introduction of nanoparticles even increases its complexity. The self-assembly of amphiphilic block copolymers in co-solvent system involves six major χ-parameters (Flory-Huggins interaction parameter) including χ_{AB}, χ_{AS}, χ_{AN}, χ_{BS}, χ_{BN}, χ_{SN}, where A and B represent the two polymer blocks, S denotes the good solvent for both blocks, N denotes nonsolvent for both blocks.[3] When nanoparticles incorporate into amphiphilic block copolymers, there are at least five more parameters needed to be considered, namely χ_{PA}, χ_{PB} (where P represents nanoparticles), nanoparticle size, shape and volume fraction. If nanoparticle-nanoparticle interaction is strong, it is not negligible. Among them, the polymer-nanoparticle interaction is an enthalpic parameter which is determined by the polymer and

nanoparticle's coordinating ligand and makes major contribution to the location of nanoparticles. For example, Taton and coworkers have reported the encapsulation of citrate-immobilized gold nanoparticles into poly(methacrylate)-*block*-poly(acrylic acid) (PMMA-*b*-PAA) micelles through the addition of dodecanethiol. Small amount of dodecanethiol was intentionally added to nanoparticle surface to increase hydrophobicity and favorable interaction between PMMA block and dodecanethiol, subsequently solubilize nanoparticles into polymer micelles.[35] In another case, Eisenberg and coworkers have successfully fabricated PS-*block*-poly(ethylene oxide) (PS-*b*-PEO) vesicles with polystyrene-*block*-PAA (PS-*b*-PAA) decorated gold nanoparticles inside vesicle walls mediated by hydrophobic interaction.[23] The incorporation of gold nanoparticles presented in Chapter 2 relies on the surface chemistry, which is mainly the interaction between ligand and polymers, to dictate the location within polymer micelles.

Other parameters also play important roles in the co-assembly process. For example, nanoparticles size, from the entropic side, the less favorable the polymer-nanoparticle interaction, if the inclusion is larger.[36-38] Many efforts have been made in the nanoparticle synthesis techniques for various types of nanoparticles to control over these parameters, including gold,[39,40] magnetic,[40] and semiconducting nanoparticles.[41]

1.2 DNA block copolymers

1.2.1 Preparation of DNA block copolymers. Previously, researchers are only interested in block copolymers that consist of exclusively synthetic polymers;

however, more and more investigations have explored nucleic acid and polymer hybrids (known as DNA block copolymers) which combine organic materials and biomacromolecules. The properties of block copolymers are determined by monomer chemical nature, the length of each block, and the block length ratio. This also holds true for DNA block copolymer which is a novel class of block copolymer architectures. DNA block copolymers provide several advantages over conventional block copolymers. Firstly, the nucleotide precision of DNA segments can be perfectly controlled over by automated synthesis facilitating the fabrication of hybrid materials with precise length and digital information of DNA blocks. Another key feature of DNA block copolymer is their DNA recognition property from single-stranded DNA on surface which can hybridize with complementary sequence by Watson-Crick base-pairing. Furthermore, the conjugation of hydrophilic DNA onto polymers leads to supramolecular assemblies in aqueous solution because of the amphiphilicity of DNA block copolymers. With careful selection of DNA sequences and polymers, it allows for adjusting of material properties for designated applications in gene or oligonucleotide delivery, biomaterials, and DNA detection.[42,43]

The first paper which reported DNA polymer hybrid materials synthesis came out around the late 1980s. DNA-*block*-poly(L-lysine) (DNA-*b*-PLL) was synthesized by grafting nucleotide onto PLL backbone and proved to be an effective antiviral agent inhibiting the production of vesicular stomatitis virus.[44,45] Since then, the field of DNA polymer hybrid materials has been gaining tremendous momentum. There are handful of strategies for the coupling of linear DNA block copolymers

which allow for the prefabrication of DNA sequences and polymers, including the variation of length and base information of biological building blocks and molecular weight of polymer building blocks. Generally speaking, two synthetic schemes have been employed for the coupling, coupling in solution and on solid support. In solution coupling, different reactions have been achieved (Scheme 1.1). In the first reaction, carboxylic acid terminated polymers were conjugated onto amine modified DNA sequences.[46,47] In Chapter 3 and 4, DNA block copolymers were formed *via* this chemistry reaction. The second reaction is the formation of disulfide bond between thiolated polymers and DNA sequences.[48] The third reaction relies on Michael addition, with acrylate- or maleimide-functionalized polymers and thiolated DNA sequences as Michael acceptor and donors, respectively.[49,50] The copper (I)-catalyzed Huisgen cyclo-addition as the premier example of click reaction was also utilized for the attachment of DNA block copolymers. However, it has drawback resulting from the cleavage of DNA strand induced by copper ions. Recently, improvements were made by adding copper chelating agents and it becomes feasible for DNA coupling.[51] Despite the fact that DNA block copolymers are easily synthesized through all of the solution-phase methods discussed above, their coupling efficiencies are drastically low and they are limited to hydrophilic polymers. As the solution coupling requires both reactants to have sufficient solubility in water.

Meanwhile, huge progress was made on solid-phase synthesis of DNA block copolymers. Mirkin and coworkers first reported the successful coupling of DNA block copolymer using solid-phase strategy, and this work was a landmark in the

Scheme 1.1. DNA block copolymer synthesis in solution phase.

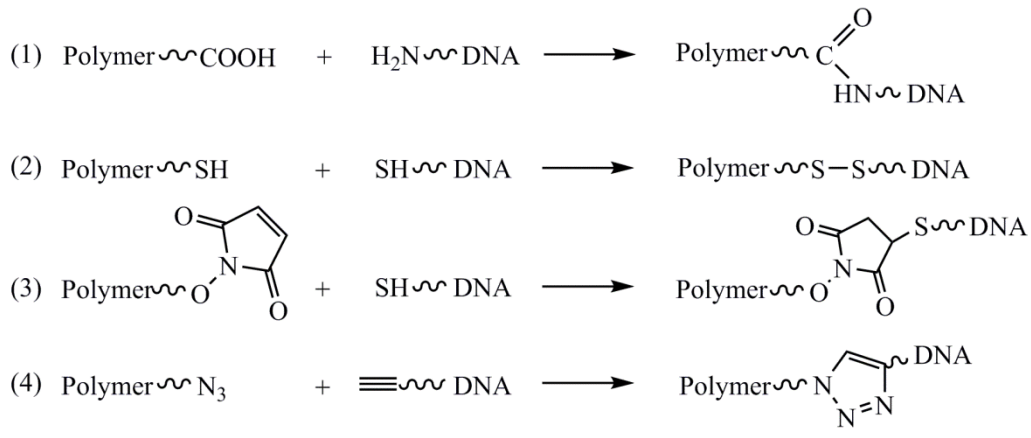

preparation of DNA block copolymer.[52] The DNA block copolymers were prepared on controlled pore glass beads (CPG) (Scheme 1.2). In this method, alcohol terminated polymer was treated with chlorophosphoramadite to obtained activated polymer phosphoramadite which was a crucial reagent.[53] The polymer phosphoramadite was later coupled to oligonucleotide either using "syringe synthesis technique" or in a conventional DNA synthesizer. The former method developed by Mirkin group has some drawbacks as it lacks of reproducibility and exposure of polymer phosphoramadite to solid support. The second method was established by Herrmann group and carried out "in line" coupling of a polymer phosphoramadite to the detritylated 5'-hydroxyl end oligonucleotide bound on resin in a DNA synthesizer.[54] This method was modified later on. It was discovered phosphoramadite polymer which is a sensitive intermediate can be replaced in the coupling. Some chemistry reactions listed on Scheme 1.1 were utilized for the conjugation by mixing DNA sequences bound on CPG with polymers in organic solvents. The two blocks were both modified with specific functional end groups.[55] And the reactions were performed outside DNA synthesizer. The DNA block copolymers were cleaved from resin and purified through polyacrylamide gel electronphoresis (PAGE) or anion exchange chromatography. In Chapter 3 and 4, modified solid-phase method was adopted for the synthesis of DNA block copolymer *via* the formation of amide bond between carboxylic acid terminated polymers and amine terminated DNA.

Scheme 1.2. Phosphoramadite chemistry.

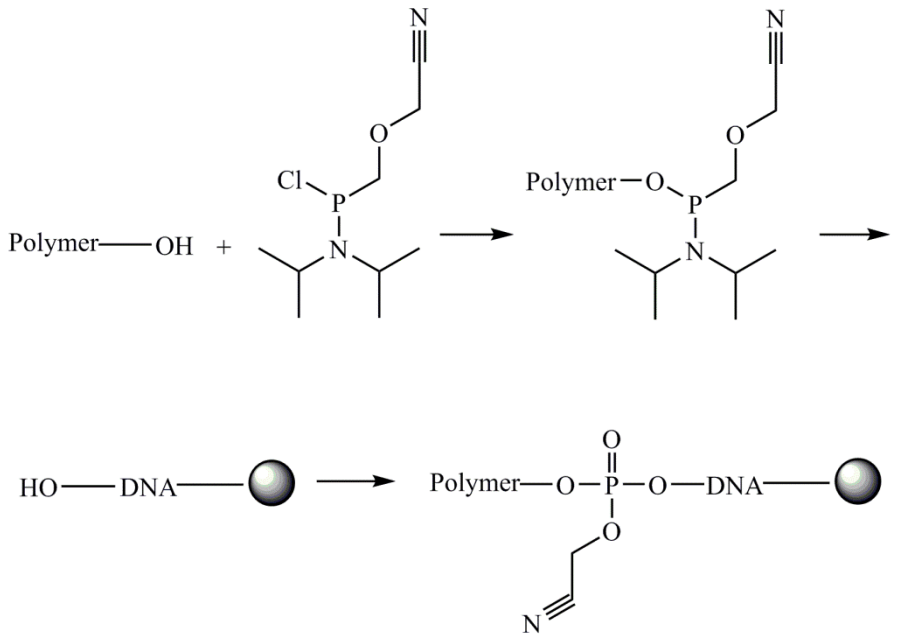

1.2.2 DNA block copolymer assemblies and their applications. The combination of organic polymers with DNA molecules offers new opportunities to fabricate functional DNA hybrid material, the key benefit of which is from the programmability of DNA sequences manipulating structures with subnanometer precision. In prior work, DNA-modified inorganic nanoparticles were bridged by linker DNA to form 3D assemblies and showed sharp melting transitions, which has been exploited for applications in DNA detection.[56] This concept was extended to the field of DNA-polymer amphiphilies to generate organic micelles network by Mirkin group. DNA-*block*-polystyrene (DNA-*b*-PS) was prepared by solid-phase method. Due to their amphiphilicty, DNA-*b*-PS form stable micelle suspensions in water solution. The DNA binding properties of micelles were studied, and sharp melting transitions were also observed for DNA block copolymer micelles originating from high DNA density on assembly surface.[52] It is expected that DNA block copolymer micelles can also be used as building blocks to fabricate higher-ordered structures *via* hybridization with biomaterials that have complementary DNA.

Inorganic nanoparticles, as the core materials of DNA-modified nanoparticles, serve one purpose which is essential in the context of material, device, and probe design. That is, they offer extraordinary chemical and physical properties, for example, colorimetric, plasmonic, quenching, catalytic, and scattering.[57-59] On the other hand, polymers which are another type of DNA-modified nanoparticles core materials could be biocompatible and possess excellent loading or releasing capacity. Drug delivery applications were successfully achieved with pristine DNA block

copolymer micelles or mixed micelles. Hydrophobic anticancer drug molecules were incorporated into DNA block copolymer micelle hydrophobic cores, while folic acid which is the corresponding ligand of folate receptors on cancerous human colon adenocardnoma cell membranes could be coupled to complementary DNA sequences and then hybridize with DNA sequences and equipped onto micelle surfaces (Figure 1.2).[60] This fast and convenient approach turns DNA block copolymer assemblies into multifunctional nanoscale vehicles. The extremely easy and straightforward preparation of DNA block copolymer assemblies gives access to combinational platform of drug delivery vehicles.

Besides pure DNA block copolymer assemblies, it is useful to introduce other functional polymers to prepare mixed assemblies. For example, micellar structures formed by Pluronic triblock copolymers polyethylene oxide-*block*-polypropylene oxide-*block*-polyethylene oxide (PEO-*b*-PPO-*b*-PEO) can be loaded drug molecules into hydrophobic cores, and possess biocompatibility from PEO moieties on micelle corona. However, the shortcoming of Pluronic-based drug delivery system is the missing of targeting units. On the other hand, although DNA block copolymer micelles can easily get to desired targeting units by DNA hybridization, their *in vivo* applications are limited to the immune response caused by high local salt and DNA concentrations. By simply mixing both block copolymers to prepare mixed assemblies, problems can be resolved. PEO polymer blocks provide stealth function, while DNA sequences of DNA block copolymers implement specific addressability.[61] In Chapter 3 and 4, DNA block copolymers were mixed with block copolymers to

form mixed assembly structures which show fast phase separation speed and sharp melting transitions. The successful mixing of block copolymers enables further *in vivo* studies in the context of drug targeted delivery and release, circulation lifetimes, and immunogenicity.

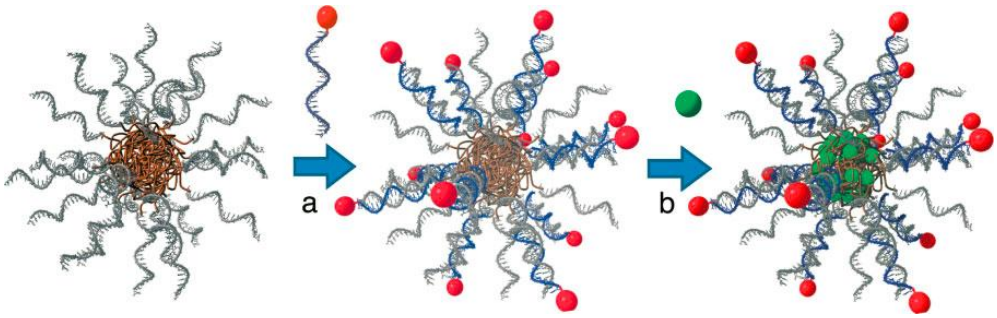

Figure 1.2. Schematic representation of DNA block copolymer drug delivery system. (a) Folic acid molecules (red dots) attached to complementary sequences are equipped to nanoparticle surface by hybridization. (b) Hydrophobic drug molecules are incorporated into hydrophobic micelle core. Figure reprint with permission from ref. [60].

The DNA units of DNA block copolymers allow for the functionalization of the nanosized objects by hybridization with complementary sequences attached to other materials. Moreover, it has been reported that the hybridization event can induce morphology changes of DNA block copolymer assemblies to create dynamic structures. In general, volume fraction and electrostatic govern the overall morphologies of assembled amphiphiles.[62] Therefore, Gianneschi *et al* reported morphology changes of DNA block copolymer amphiphile by manipulating the magnitude of volume fraction and electrostatic repulsions in the micelle shells which is controlled by DNA sequence-selective interactions. Three types of sequence-selective interactions involve the DNA-programmed micelle phase transition, namely, enzymatic cleavage, hybridization of complementary single-stranded DNA, and thermal melting and annealing of DNA duplexes. Two morphologies are obtained upon the addition of stimuli, sphere or cylinder (Figure 1.3).[63] This work demonstrated the use of DNA sequence as an informational intrigue tool for morphology shift in nanoscale polymeric materials. In a broader context, one can expect DNA block copolymers and their self-assemblies undergo designated morphology changes in response to stimuli and give the versatility in a wide range of applications, for instance, drug delivery, soft polymer templates, and self-healing and switching materials.

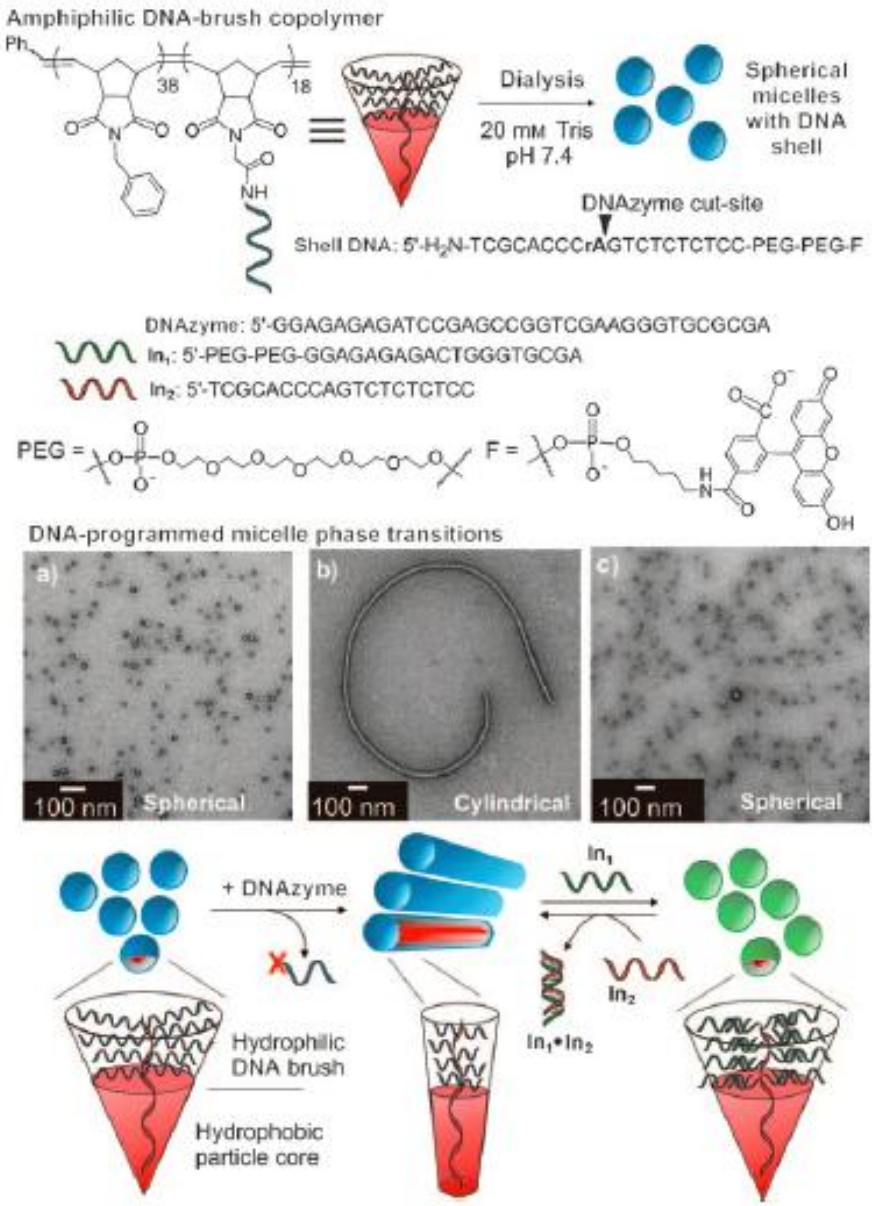

Figure 1.3. Spherical or cylindrical morphologies of DNA-brush copolymer assemblies. Amphiphilic DNA block copolymers are denoted as cone structures with hydrophobic block in red color. TEM images of (a) spherical micelles assembled from as-synthesized DNA-brush polymers; (b) cylindrical micelles obtained after the addition of DNAzyme to spherical micelles; (c) spherical micelles obtained after the addition of 19-base input DNA sequences to cylindrical morphologies. Figure reprint with permission from ref. [63].

1.3 Liposomes

1.3.1 DNA-mediated liposomes fusion. Lipid membrane fusion happening between cells, between intracellular compartments, between different intracellular compartments, is essential for many biological processes, for example, endo- and exocytosis whereby vesicles undergo fusion to deposit receptors, transporters, or adhesion molecules into membrane, or to release hormones, neurotransimitters into extracellular milieu. It is believed that most vesicle fusion processes are dependent on SNARE (soluble *N*-ethylmaleimide-sensitive fusion protein attachment protein receptor) protein complex, composed of recognition pairs on the vesicle and target membranes with the aid of many other proteins.[64-66] Although systems that use SNARE proteins or their synthetic surrogates provide valuable insights, due to the complexity of the fusion process and huge number of proteins involved, the precise physical mechanism and kinetics are not yet well studied.[67-69]

Recently, a new model system that makes use of DNA-lipid conjugates was developed to displace for the SNARE machinery.[70-72] This new system overcomes the shortcomings of SNARE system. Firstly, it is easy to tailor the length, sequence, and binding geometry of DNA which are difficult to track during SNARE-mediated fusion. Thus, it becomes possible to investigate the fusion process when vesicles and target membranes are brought into contact by DNA hybridization event. Furthermore, the DNA binding specificity of DNA-lipid conjugates can prevent the contact with false partners resulting from protein binding promiscuity. Compared to SNARE systems which require detergent dialysis, the DNA-lipid conjugates can

directly tag into lipid membranes.[73] The new system allows for the examination of DNA-mediated vesicle fusion mechanism.

In this new system, DNA sequences attached to a hydrophobic anchor are tethered to both vesicle and targeted membrane surfaces with high density of DNA-lipids, about 65 DNA per vesicle, which ensures DNA-lipids will not deplete during fusion. Moreover, it is important to note that only zippering orientation of DNA sequences can induce vesicle fusion. In Chapter 5, we applied a similar tethering method to functionalize lipid membranes and obtained modified lipid membranes with high DNA density. The DNA hybridization event brings membranes close together and initiates vesicle docking and fusion. The DNA-mediated vesicle fusion process is classified as four stages, docking-only, hemi-fusion-only, hemi-then-full-fusion, and full-fusion-only (Figure 1.4).[74] A large portion of vesicles participate docking-only process, and no contents transferred were observed at this phase. Following docking process, vesicles transfer some of their dyes incorporated into membranes to the targeted membranes, and also merge part of their inner and outer leaflets. During the last two stages, vesicles transfer all of remain contents across the target membrane and complete lipid mixing process simultaneously.

It was also revealed that during vesicle docking and fusion, all DNA-lipid conjugates attend the hybridization event. They migrate to junction sites and form duplex with the target membrane. In Chapter 3, the DNA hybridization event also caused the migration of DNA block copolymers to junction areas with fast traveling

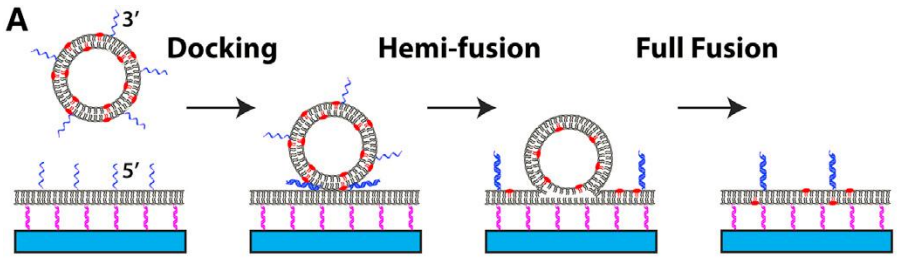

Figure 1.4. Schematic description for DNA-mediated vesicle fusion. Figure reprint with permission from ref. [74].

rate. Other studies also suggested that the density of DNA-lipid conjugates on surface dictates the lateral mobility of vesicles. The less DNA-lipid conjugates, the higher mobility of vesicles on surface.

The mechanistic model of DNA-mediated membrane fusion was successfully constructed by researchers and thereby provides insight into a few important questions: Can polymer vesicles undergo membrane fusion as well? Will they proceed the same pathway? It will be very interesting to see membrane fusion between polymer vesicles, between cell membranes and polymer vesicles. If so, it opens up the opportunities of using polymer vesicles as drug delivery vehicles.

1.3.2 DNA-mediated liposomes rupture. Researchers use supported lipid bilayers as a model to study cell membranes by taking advantage of their simple preparation.[75,76] Supported lipid bilayers can either be formed by Langmuir-Blodgett techniques, or fusion of unilamellar vesicles on pre-treated surfaces, including hydrophobic or piranha treated hydrophilic glass slides,[77] silica,[78] or TiO_2.[79] Although they are easy to handle and have planar geometry, the close distance between lower leaflet and substrate easily gives rise to troublesome interaction with contents incorporated into membranes. To overcome this limitation, methods have been applied to separate the bilayers from substrates, such as polymer cushioned membranes,[80] polymer tethered membranes,[81] or tethered lipid vesicles.[82]

Recently, a strategy based on DNA hybridization was developed for the preparation of tethered lipid bilayers on solid supports. In this strategy, one can adjust the distance between lipid membrane and solid surface by varying the length of

DNA sequences. The strategy includes two methods. For the first method, single-stranded DNA sequences were coupled to a solid surface, for instant, silica, by click chemistry to avoid direct exposure to lipid bilayers. Giant unilamellar vesicles which are tagged by DNA-lipid conjugates were incubated with DNA-functionalized surfaces and allowed to spread and rupture to form supported lipid bilayers. In the second method, supported lipid bilayers were first created on solid surfaces and further modified with DNA-lipid conjugates to obtain DNA-functionalized lipid membranes. Then giant unilamellar vesicles tethered by complementary DNA sequences were again incubated with solid surfaces and allowed to spread and rupture to supported lipid bilayers (Figure 1.5).[83] Both methods can be used to prepare supported lipid bilayers, however, there are essential differences between the two methods. In the first one, single-stranded DNA sequences were covalently linked on the solid surfaces, while DNA strands were tagged onto the surfaces in the second method. Thus, the supported lipid bilayers formed by the former are immobile, and are mobile and unstable by the latter. For the mobile supported lipid bilayers, if varied lengths of DNA sequences are used, lateral segregation was recorded by confocal microscopy. In Chapter 5, supported lipid bilayers were prepared by direct rupture of lipid vesicles. We demonstrated that the lipid bilayers possess lateral mobility and undergo phase segregation to form gold nanoparticle 2D assemblies.

The supported lipid bilayers formed by the two methods not only provide a soft lipid membrane platform with a designated distance from solid substrate, also have their promising applications. For the immobile lipid bilayers, it is useful for the

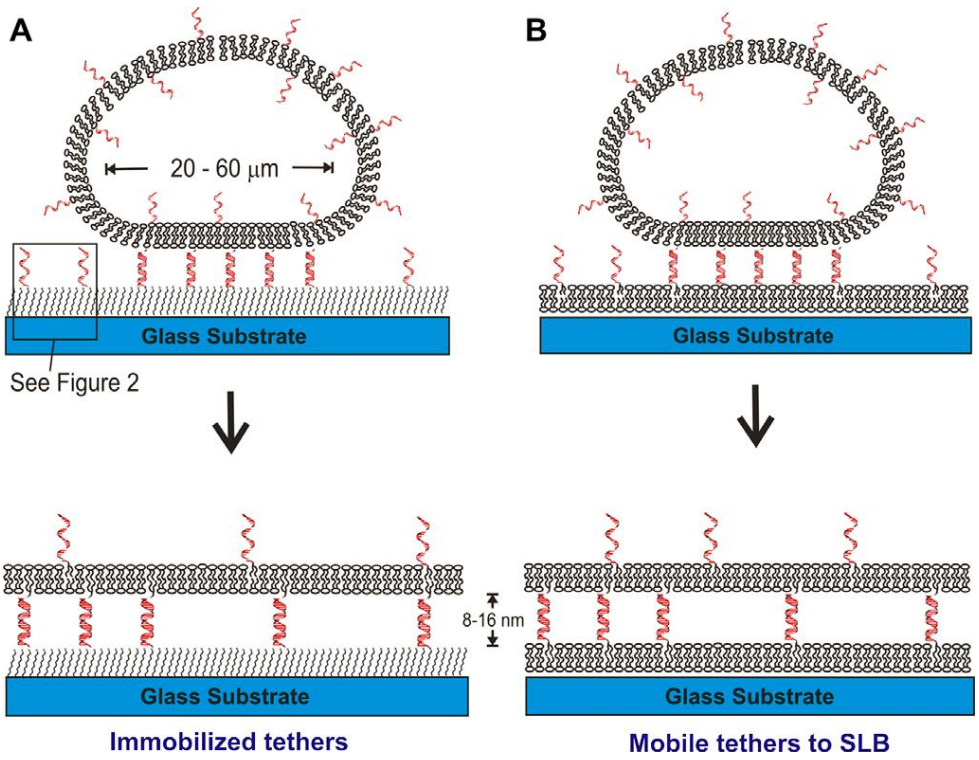

Figure 1.5. Schematic description of DNA-mediated lipid membrane formed on (A) alkyl-siloxane functionalized glass substrate; and (B) supported lipid bilayers. Figure reprint with permission from ref. [83].

doping of membrane proteins but keep them away from solid substrates. For the mobile lipid bilayers, their lateral segregation can be used as a model to study biological processes, such as the interactions occurring in cell junctions.

1.3.2 DNA liposome self-assemblies and their DNA melting properties. Due to sequence specificity, DNA sequences have been used as promising building blocks to construct new biomaterials and devices.[84-87] Various particles have been conjugated to DNA molecules and assemble into high-ordered superstructures.[88-92] Hydrophobic modification of DNA molecules using hydrophobic moieties, such as hydrocarbon chain and cholesterol, was found to be useful to functionalize liposome and further build their high-ordered assembly.

There are several strategies for encoding DNA molecules to membrane surfaces, and most of them involve couple DNA sequences to hydrophobic molecules that can spontaneously anchor into lipid membranes. So far, the most widely used molecule is cholesterol because they are commercially available. Thus, it can be prepared and performed in a wide range of laboratories. The stability of anchoring is influenced by the length of DNA, but detailed study is not reported. However, it was discovered that single cholesterol anchor is not sufficient to label liposome with DNA sequences longer than 30 bases, and a double cholesterol anchor will be needed to strengthen the tethering in lipid bilayers with DNA sequence hanging in solution.[93] DNA-modified liposomes show high stability over a week.

DNA hybridization can be used to direct self-assembly between two types of liposomes decorated by complementary sequences.[94] Self-assembly of

DNA-functionalized liposomes were formed by a broad range of sizes liposomes, spanning from nano-size (100 nm, LUV) to micron-size (> 5 μm, GUV). The cluster formation is reversible by increasing temperature above DNA melting temperature or reducing salt concentration in solution. It is challenging to proceed thermal melting of giant vesicles on microscope due to the restriction of temperature stage. However, the clustering regimes of LUV can be tracked by dynamic light scattering. The number of DNA on LUV affects the aggregation size as well as speed. For DNA density less than 2.5 per vesicle, aggregation is invisible. When DNA density increases up to 20 per vesicle, small aggregation is observed. If DNA density keeps increasing to 39 per vesicle or even higher, one can observe big clusters by eye. As cholesterol-DNA conjugates are mobile within lipid membranes, excess DNA conjugates can float outside adhesion plaque regions where are saturated by about 20 DNA strands per vesicle, and further collide with additional liposomes to create network structures. There is other work showing that it is possible to control association and dissociation of three populations of liposomes by utilizing designed DNA strands which opens up the opportunity to form complex and smart interaction liposome networks.[95]

The significant difference between DNA-mediated assembly of liposomes which are soft particles, and hard particles such as gold nanoparticles is the lateral mobility of DNA conjugates within fluid vesicle bilayers. In contrast to chemically fixed on gold nanoparticles surfaces, DNA strands are tethered and mobile on liposomes surfaces. In DNA-mediated self-assembly, DNA strands migrate to adhesion plaques

and form maximum DNA duplex structures with complementary sequences between adjacent liposome, resulting in a high local concentration of DNA strands, and also salt which is used to screen out the negative charge of DNA backbones. The local environment has a huge impact on the thermodynamic stability of DNA duplexes. Previous work demonstrated sharp melting transitions of DNA-functionalized liposomes aggregates which were connected by linker DNA strands (Figure 1.6).[96,97]

The concept of DNA-mediated self-assembly has been extended to between other soft materials besides liposomes, including connecting liposomes to layer-by-layer capsules,[98] to gas microbubbles for applications in medical theranostics,[99] and to oil-in-water microemulsions,[100] allowing the fabrication of multicompartment assemblies and multifunctional soft materials.

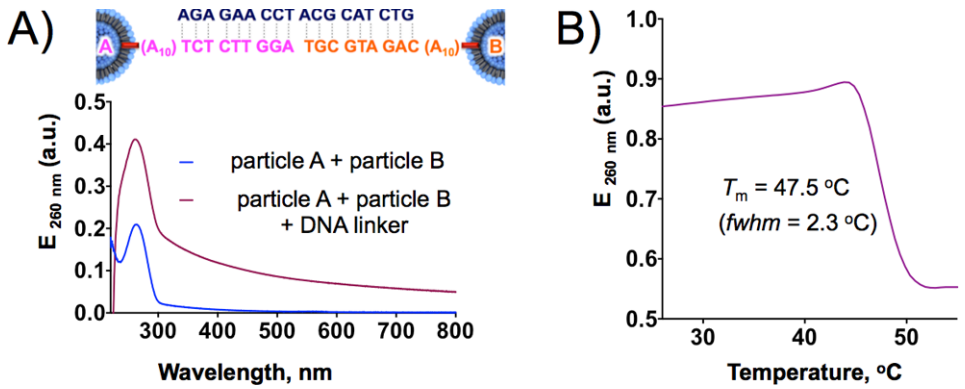

Figure 1.6. (a) Extinction spectra of DNA liposomes before (blue) and after (red) clustering in the presence of linker DNA. (b) Melting transition of DNA liposome clusters monitored as a change in extinction at 260 nm. Figure reprint with permission from ref. [97].

1.4 Thesis overview

This dissertation will focus on the self-assembly of nanomaterials with varying functionalities into hybrid nanocomposites with tunable structures and functions. The nanomaterials involved in this dissertation are gold nanoparticles, amphiphilic block copolymers including synthetic block copolymers and DNA block copolymers, and lipid molecules. The overall motivation of this work is to develop ways to control the structures of these hybrid materials in order to obtain desired functionalities and properties. It is critical to control over the assembly structure of amphiphilic block copolymers and nanoparticles for the fabrication of nanomaterials with controllable properties. Chapter 1 gives a brief overview of self-assembly formed by amphiliphilic block copolymers and nanoparticles, DNA block copolymers, and lipids, and their applications. Each subsequent chapter will focus on the synthesis and the self-assembly of these functional moieties. Chapter 2 focuses on the self-assembly of a prototypical amphiphilic block copolymer (PS-*b*-PAA) and mixed ligand gold nanoparticles with controllable nanoparticles locations. An in-depth study of interfacial energies is presented to explain the relation between nanoparticle spatial arrangement and nanoparticle surface chemistry. In Chapter 3 the synthesis of DNA block copolymer (PMA-*b*-DNA) and the self-assembly of PMA-*b*-DNA and PBD-*b*-PEO are presented. In this work mixed giant vesicles formed by two block copolymers show fast phase segregation driven by DNA hybridization event. Chapter 4 also presents the synthesis DNA block copolymer (PBD-*b*-PEO-*b*-DNA) and their mixed assemblies with PBD-*b*-PEO. Investigations

of DNA melting temperatures of different DNA percentages on assembly surfaces provide insight into how the phase behavior influences DNA binding properties. Chapter 5 focuses on the self-assembly of gold nanoparticles assisted by lipid bilayers. Since planar lipid bilayers possess lateral mobility, gold nanoparticles tethered on top of lipid bilayers by DNA hybridization are capable of migrating and linked by linker DNA to form 2D assembly.

1.5 References

(1) Bates, F. S.; Fredrickson, G. H. *Physics Today* **1999**, *52*, 32-38.

(2) Cameron, N. S.; Corbierre, M. K.; Eisenberg, A. *Can. J. Chem.* **1999**, *77*, 1311-1326.

(3) Mai, Y.; Eisenberg, A. *Chem. Soc. Rev.* **2012**, *41*, 5969-5985.

(4) Riess, G. *Prog. Polym. Sci.* **2003**, *28*, 1107-1170.

(5) Jain, S.; Bates, F. S. *Science* **2003**, *300*, 460-464.

(6) Discher, D. E.; Ahmed, F. *Annu. Rev. Biomed. Eng.* **2006**, *8*, 323-341.

(7) LoPresti, C.; Lomas, H.; Massignani, M.; Smart, T.; Battaglia, G. *J. Mater. Chem.* **2009**, *19*, 3576-3590.

(8) Menger, F. M.; Angelova, M. I. *Acc. Chem. Res.* **1998**, *31*, 789-797.

(9) Caruso, F. *Adv. Mater.* **2001**, *13*, 11-22.

(10) Shum, H. C.; Kim, J.-W.; Weitz, D. A. *J. Am. Chem. Soc.* **2008**, *130*, 9543-9549.

(11) Kabanov, A. V.; Batrakova, E. V.; Alakhov, V. Y. *J. Controlled Release* **2002**, *82*, 189-212.

(12) Harada, A.; Kataoka, K. *Prog. Polym. Sci.* **2006**, *31*, 949-982.

(13) Maysinger, D.; Lovrić, J.; Eisenberg, A.; Savić, R. *European Journal of Pharmaceutics and Biopharmaceutics* **2007**, *65*, 270-281.

(14) Bermudez, H.; Brannan, A. K.; Hammer, D. A.; Bates, F. S.; Discher, D. E.

Macromolecules **2002**, *35*, 8203-8208.

(15) Bermúdez, H.; Hammer, D. A.; Discher, D. E. *Langmuir* **2004**, *20*, 540-543.

(16) Blanazs, A.; Armes, S. P.; Ryan, A. J. *Macromol. Rapid Commun.* **2009**, *30*, 267-277.

(17) Meng, F.; Zhong, Z.; Feijen, J. *Biomacromolecules* **2009**, *10*, 197-209.

(18) Smith, A. E.; Xu, X.; McCormick, C. L. *Prog. Polym. Sci.* **2010**, *35*, 45-93.

(19) Tanner, P.; Baumann, P.; Enea, R.; Onaca, O.; Palivan, C.; Meier, W. *Acc. Chem. Res.* **2011**, *44*, 1039-1049.

(20) Opsteen, J. A.; Brinkhuis, R. P.; Teeuwen, R. L. M.; Lowik, D. W. P. M.; Hest, J. C. M. v. *Chem. Commun.* **2007**, 3136-3138.

(21) Ghoroghchian, P. P.; Frail, P. R.; Susumu, K.; Blessington, D.; Brannan, A. K.; Bates, F. S.; Chance, B.; Hammer, D. A.; Therien, M. J. *Proc. Natl. Acad. Sci. U. S. A.* **2005**, *102*, 2922-2927.

(22) Nikolic, M. S.; Olsson, C.; Salcher, A.; Kornowski, A.; Rank, A.; Schubert, R.; Frömsdorf, A.; Weller, H.; Förster, S. *Angew. Chem., Int. Ed.* **2009**, *48*, 2752-2754.

(23) Mai, Y.; Eisenberg, A. *J. Am. Chem. Soc.* **2010**, *132*, 10078-10084.

(24) Broz, P.; Driamov, S.; Ziegler, J.; Ben-Haim, N.; Marsch, S.; Meier, W.; Hunziker, P. *Nano Lett.* **2006**, *6*, 2349-2353.

(25) Choi, H.-J.; Montemagno, C. D. *Nano Lett.* **2005**, *5*, 2538-2542.

(26) Ahmed, F.; Pakunlu, R. I.; Brannan, A.; Bates, F.; Minko, T.; Discher, D. E. *J. Controlled Release* **2006**, *116*, 150-158.

(27) Hickey, R. J.; Haynes, A. S.; Kikkawa, J. M.; Park, S.-J. *J. Am. Chem. Soc.* **2011**, *133*, 1517-1525.

(28) Christian, D. A.; Cai, S.; Bowen, D. M.; Kim, Y.; Pajerowski, J. D.; Discher, D. E. *European Journal of Pharmaceutics and Biopharmaceutics* **2009**, *71*, 463-474.

(29) Lomas, H.; Canton, I.; MacNeil, S.; Du, J.; Armes, S. P.; Ryan, A. J.; Lewis, A. L.; Battaglia, G. *Adv. Mater.* **2007**, *19*, 4238-4243.

(30) Kinge, S.; Crego-Calama, M.; Reinhoudt, D. N. *ChemPhysChem* **2008**, *9*, 20-42.

(31) Balazs, A. C.; Emrick, T.; Russell, T. P. *Science* **2006**, *314*, 1107-1110.

(32) Hamley, I. W. *Angew. Chem., Int. Ed.* **2003**, *42*, 1692-1712.

(33) Bockstaller, M. R.; Mickiewicz, R. A.; Thomas, E. L. *Adv. Mater.* **2005**, *17*, 1331-1349.

(34) Shenhar, R.; Norsten, T. B.; Rotello, V. M. *Adv. Mater.* **2005**, *17*, 657-669.

(35) Kang, Y.; Taton, T. A. *Angew. Chem., Int. Ed.* **2005**, *44*, 409-412.

(36) Jancar, J.; Douglas, J. F.; Starr, F. W.; Kumar, S. K.; Cassagnau, P.; Lesser, A. J.; Sternstein, S. S.; Buehler, M. J. *Polymer* **2010**, *51*, 3321-3343.

(37) Bockstaller, M. R.; Lapetnikov, Y.; Margel, S.; Thomas, E. L. *J. Am. Chem. Soc.* **2003**, *125*, 5276-5277.

(38) Thompson, R. B.; Ginzburg, V. V.; Matsen, M. W.; Balazs, A. C. *Science* **2001**, *292*, 2469.

(39) Sun, Y.; Xia, Y. *Science* **2002**, *298*, 2176-2179.

(40) Gupta, A. K.; Gupta, M. *Biomaterials* **2005**, *26*, 3995-4021.

(41) Murray, C. B.; Kagan, C. R.; Bawendi, M. G. *Annual Review of Materials Science* **2000**, *30*, 545-610.

(42) Costioli, M. D.; Fisch, I.; Garret-Flaudy, F.; Hilbrig, F.; Freitag, R. *Biotechnol. Bioeng.* **2003**, *81*, 535-545.

(43) Tong, G.; Lawlor, J. M.; Tregear, G. W.; Haralambidis, J. *The Journal of Organic Chemistry* **1993**, *58*, 2223-2231.

(44) Lemaitre, M.; Bayard, B.; Lebleu, B. *Proceedings of the National Academy of Sciences* **1987**, *84*, 648-652.

(45) Leonetti, J.-P.; Degols, G.; Milhaud, P.; Gagnor, C.; Lemaitre, M.; Lebleu, B. *Nucleosides and Nucleotides* **1989**, *8*, 825-828.

(46) Takei, Y. G.; Aoki, T.; Sanui, K.; Ogata, N.; Okano, T.; Sakurai, Y. *Bioconjugate Chem.* **1993**, *4*, 42-46.

(47) Lee, K.; Povlich, L. K.; Kim, J. *Adv. Funct. Mater.* **2007**, *17*, 2580-2587.

(48) Oishi, M.; Hayama, T.; Akiyama, Y.; Takae, S.; Harada, A.; Yamasaki, Y.; Nagatsugi, F.; Sasaki, S.; Nagasaki, Y.; Kataoka, K. *Biomacromolecules* **2005**, *6*, 2449-2454.

(49) Oishi, M.; Nagasaki, Y.; Itaka, K.; Nishiyama, N.; Kataoka, K. *J. Am. Chem. Soc.* **2005**, *127*, 1624-1625.

(50) Isoda, K.; Kanayama, N.; Miyamoto, D.; Takarada, T.; Maeda, M. *Reactive and Functional Polymers* **2011**, *71*, 367-371.

(51) Gramlich, P. M. E.; Wirges, C. T.; Manetto, A.; Carell, T. *Angew. Chem., Int. Ed.* **2008**, *47*, 8350-8358.

(52) Li, Z.; Zhang, Y.; Fullhart, P.; Mirkin, C. A. *Nano Lett.* **2004**, *4*, 1055-1058.

(53) Storhoff, J. J.; Elghanian, R.; Mucic, R. C.; Mirkin, C. A.; Letsinger, R. L. *J. Am. Chem. Soc.* **1998**, *120*, 1959-1964.

(54) Alemdaroglu, F. E.; Ding, K.; Berger, R.; Herrmann, A. *Angew. Chem., Int. Ed.* **2006**, *45*, 4206-4210.

(55) Rush, A. M.; Thompson, M. P.; Tatro, E. T.; Gianneschi, N. C. *ACS Nano* **2013**, *7*, 1379-1387.

(56) Jin, R.; Wu, G.; Li, Z.; Mirkin, C. A.; Schatz, G. C. *J. Am. Chem. Soc.* **2003**, *125*, 1643-1654.

(57) Katz, E.; Willner, I. *Angew. Chem., Int. Ed.* **2004**, *43*, 6042-6108.

(58) Rosi, N. L.; Mirkin, C. A. *Chemical Reviews* **2005**, *105*, 1547-1562.

(59) Liu, J.; Cao, Z.; Lu, Y. *Chemical Reviews* **2009**, *109*, 1948-1998.

(60) Alemdaroglu, F. E.; Alemdaroglu, N. C.; Langguth, P.; Herrmann, A. *Adv. Mater.* **2008**, *20*, 899-902.

(61) Kwak, M.; Musser, A. J.; Lee, J.; Herrmann, A. *Chem. Commun.* **2010**, *46*, 4935-4937.

(62) Nagarajan, R. *Langmuir* **2002**, *18*, 31-38.

(63) Chien, M.-P.; Rush, A. M.; Thompson, M. P.; Gianneschi, N. C. *Angew. Chem., Int. Ed.* **2010**, *49*, 5076-5080.

(64) Brunger, A. T. *Q. Rev. Biophys.* **2005**, *38*, 1-47.

(65) Rizo, J.; Südhof, T. C. *Annu. Rev. Cell Dev. Biol.* **2012**, *28*, 279-308.

(66) Jahn, R.; Fasshauer, D. *Nature* **2012**, *490*, 201-207.

(67) Weber, T.; Zemelman, B. V.; McNew, J. A.; Westermann, B.; Gmachl, M.; Parlati,

F.; Söllner, T. H.; Rothman, J. E. *Cell*, *92*, 759-772.

(68) Domanska, M. K.; Kiessling, V.; Tamm, L. K. *Biophys. J.* **2010**, *99*, 2936-2946.

(69) Shi, L.; Shen, Q.-T.; Kiel, A.; Wang, J.; Wang, H.-W.; Melia, T. J.; Rothman, J. E.; Pincet, F. *Science* **2012**, *335*, 1355-1359.

(70) Chan, Y.-H. M.; van Lengerich, B.; Boxer, S. G. *Biointerphases* **2008**, *3*, FA17-FA21.

(71) Burin, A. L.; Armbruster, M. E.; Hariharan, M.; Lewis, F. D. *Proceedings of the National Academy of Sciences* **2009**, *106*, 989-994.

(72) Rawle, Robert J.; van Lengerich, B.; Chung, M.; Bendix, Poul M.; Boxer, Steven G. *Biophys. J.*, *101*, L37-L39.

(73) Chen, X.; Araç, D.; Wang, T.-M.; Gilpin, C. J.; Zimmerberg, J.; Rizo, J. *Biophys. J.*, *90*, 2062-2074.

(74) van Lengerich, B.; Rawle, Robert J.; Bendix, Poul M.; Boxer, Steven G. *Biophys. J.*, *105*, 409-419.

(75) Sackmann, E. *Science* **1996**, *271*, 43-48.

(76) Chan, Y.-H. M.; Boxer, S. G. *Curr. Opin. Chem. Biol.* **2007**, *11*, 581-587.

(77) Seu, K. J.; Pandey, A. P.; Haque, F.; Proctor, E. A.; Ribbe, A. E.; Hovis, J. S. *Biophys. J.*, *92*, 2445-2450.

(78) Richter, R. P.; Bérat, R.; Brisson, A. R. *Langmuir* **2006**, *22*, 3497-3505.

(79) Rossetti, F. F.; Bally, M.; Michel, R.; Textor, M.; Reviakine, I. *Langmuir* **2005**, *21*, 6443-6450.

(80) Renner, L.; Osaki, T.; Chiantia, S.; Schwille, P.; Pompe, T.; Werner, C. *The Journal of Physical Chemistry B* **2008**, *112*, 6373-6378.

(81) Koper, I. *Molecular BioSystems* **2007**, *3*, 651-657.

(82) Yoshina-Ishii, C.; Miller, G. P.; Kraft, M. L.; Kool, E. T.; Boxer, S. G. *J. Am. Chem. Soc.* **2005**, *127*, 1356-1357.

(83) Chung, M.; Lowe, R. D.; Chan, Y.-H. M.; Ganesan, P. V.; Boxer, S. G. *Journal of Structural Biology* **2009**, *168*, 190-199.

(84) Pinheiro, A. V.; Han, D.; Shih, W. M.; Yan, H. *Nat Nano* **2011**, *6*, 763-772.

(85) Seeman, N. C. *Nature* **2003**, *421*, 427-431.

(86) Aldaye, F. A.; Palmer, A. L.; Sleiman, H. F. *Science* **2008**, *321*, 1795-1799.

(87) Bath, J.; Turberfield, A. J. *Nat Nano* **2007**, *2*, 275-284.

(88) Geerts, N.; Eiser, E. *Soft Matter* **2010**, *6*, 4647-4660.

(89) Storhoff, J. J.; Mirkin, C. A. *Chemical Reviews* **1999**, *99*, 1849-1862.

(90) Kim, A. J.; Biancaniello, P. L.; Crocker, J. C. *Langmuir* **2006**, *22*, 1991-2001.

(91) Nykypanchuk, D.; Maye, M. M.; van der Lelie, D.; Gang, O. *Nature* **2008**, *451*, 549-552.

(92) Park, S. Y.; Lytton-Jean, A. K. R.; Lee, B.; Weigand, S.; Schatz, G. C.; Mirkin, C. A. *Nature* **2008**, *451*, 553-556.

(93) Pfeiffer, I.; Höök, F. *J. Am. Chem. Soc.* **2004**, *126*, 10224-10225.

(94) Beales, P. A.; Vanderlick, T. K. *The Journal of Physical Chemistry A* **2007**, *111*, 12372-12380.

(95) Hadorn, M.; Eggenberger Hotz, P. *PLoS ONE* **2010**, *5*, e9886.

(96) Dave, N.; Liu, J. *ACS Nano* **2011**, *5*, 1304-1312.

(97) Banga, R. J.; Chernyak, N.; Narayan, S. P.; Nguyen, S. T.; Mirkin, C. A. *J. Am. Chem. Soc.* **2014**, *136*, 9866-9869.

(98) Loew, M.; Kang, J.; Dähne, L.; Hendus-Altenburger, R.; Kaczmarek, O.; Liebscher, J.; Huster, D.; Ludwig, K.; Böttcher, C.; Herrmann, A.; Arbuzova, A. *Small* **2009**, *5*, 320-323.

(99) Lozano, M. M.; Starkel, C. D.; Longo, M. L. *Langmuir* **2010**, *26*, 8517-8524.

(100) Hadorn, M.; Boenzli, E.; Sørensen, K. T.; Fellermann, H.; Eggenberger Hotz, P.; Hanczyc, M. M. *Proceedings of the National Academy of Sciences* **2012**, *109*, 20320-20325.

CHAPTER 2. Controlling the Location of Nanoparticles in Colloidal Assemblies of Amphiphilic Polymers by Tuning Nanoparticle Surface Chemistry

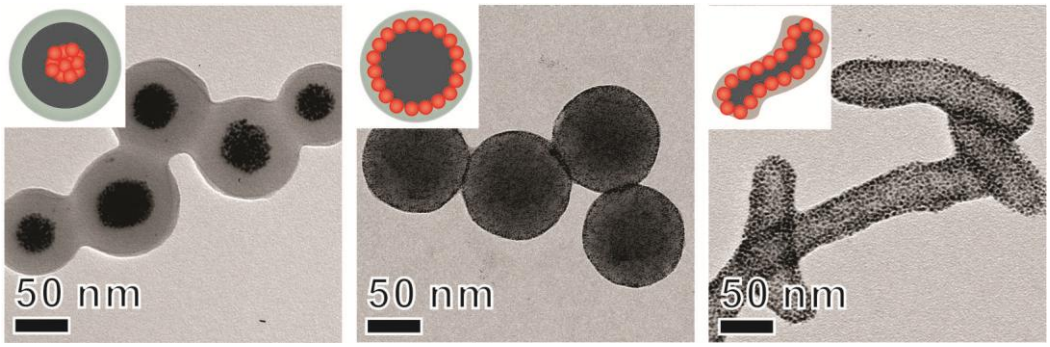

Controllable location of nanoparticles in colloidal block-copolymer assemblies can be achieved by using nanoparticles modified with mixed surface ligands. The binary self-assembly of amphiphilic polymers of polystyrene-b-poly(acrylic acid) (PS-b-PAA) and gold nanoparticles (AuNPs) modified with a hydrophobic ligand, dodecanethiol (DT), led to polymer micelles with nanoparticles segregated in the core of polymer micelles. On the other hand, AuNPs modified with mixed ligands of mercaptoundecanol (MUL) and DT were distributed at the PS−PAA interface, reducing the interfacial energy between the two polymers. This result was in good agreement with the prediction by the surface energy calculations. We also showed that the AuNPs with mixed ligands can decorate preformed polymer assemblies by the interfacial self-assembly. Furthermore, we demonstrated the compartmentalization of two different types of nanoparticles in colloidal polymer assemblies based on the strategy.

Reprinted with permission from Luo, Q.; Hickey, R.J.; Park, S.-J. Controlling the Location of Nanoparticles in Colloidal Assemblies of Amphiphilic Polymers by Tuning Nanoparticles Surface Chemistry. *ACS Macro. Lett.* 2013, 2, 107. Copyright 2013 American Chemical Society

2.1 Introduction

Colloidal self-assembly of amphiphilic block-copolymers and inorganic nanoparticles offers a way to create solution processable functional materials with useful chemical and mechanical properties of polymers and the unique sizedependent properties of nanoparticles for various applications including medical imaging and drug delivery.[1-4] Because the distribution of nanoparticles in the polymer matrixes is an important factor that determines the properties of such hybrid structures, it is of great interest to form polymer assemblies with controllable nanoparticle arrangements. A range of different types of nanoparticles (e.g., semiconducting,[5] magnetic,[6] and metallic nanoparticles[7]) have been encapsulated in various polymer assemblies. For example, Eisenberg and coworkers have demonstrated a strategy to incorporate polymer grafted nanoparticles in the membrane of polymer vesicles.[8] Taton and co-workers have fabricated nanoparticle-loaded polymer micelles where alkyl-terminated nanoparticles were uniformly embedded in the hydrophobic polymer core.[9,10] Using a similar method, we have shown that the arrangement of nanoparticles and the polymer morphology can be controlled by changing the initial solvent composition, polymer lengths, and nanoparticle weight fractions.[11] Unique cavity-like assemblies of hydrophobic nanoparticles were formed in A−B polymer assemblies where nanoparticles were arranged at the B−B interface.[12-14] We have also prepared polymer vesicles densely packed with magnetic nanoparticles and showed that the spatial arrangement of nanoparticles in the polymer matrix significantly affects the magnetic relaxation rate of surrounding water.[11]

This second chapter shows a simple method to control the location of gold nanoparticles (AuNPs) in colloidal polymer assemblies by tuning the nature of the

nanoparticle surface. For bulk and thin film composite systems, various factors affecting the binary self-assembly of block-copolymers and nanoparticles have been investigated including the size of the nanoparticles, the molecular weight of polymers, and the nanoparticle surface ligands.[15-17] For example, Kramer and coworkers have localized polymer-grafted AuNPs in different domains of lamellar assemblies of block-copolymers by changing the polymer composition grafted onto AuNPs.[18] Emrick and co-workers have shown that the location of nanoparticles in block-copolymer assemblies can be controlled by varying the ratio between hydrophobic and hydrophilic ligands on nanoparticles.[19] On the contrary, the ability to control the nanoparticle distribution in the solution-phase selfassembly is still quite limited. In this chapter, we show for the first time that the arrangement of nanoparticles in A−B polymer micelles can be controlled from the core of the polymer micelles to the A−B polymer interface by using mixed nanoparticle ligands. We also demonstrate that different types of nanoparticles can be compartmentalized in different locations of colloidal polymer assemblies using the approach.

2.2 Experimental Section

2.2.1 Materials. Gold (III) chloride trihydrate ($HAuCl_4 \bullet 3H_2O$, >99.9%), 1-dodecanethiol (DT, >98%), 11-mercapto-1-undecanol (MUL, >97%), Tetraoctylammonium bromide (TOAB, 98%), sodium borohydride ($NaBH_4$, 99%) were purchased from Sigma-Aldrich. Block copolymers of polystyrene-block-poly(acrylic acid) (PS-*b*-PAA), PS(26000)-*b*-PAA(1000) (PS_{250}-*b*-PAA_{14} Mw/Mn:1.18) and PS(15000)-*b*-PAA(3600) (PS_{144}-*b*-PAA_{49} Mw/Mn:1.2) were purchased from Polymer

Source, Inc. Carboxylate-modified microspheres (60 nm, 100 nm, and 200 nm) were purchased from Invitrogen. All solvents were purchased from Fischer Scientific. Deionized water (Millipore Milli-Q grade) with resistivity of 17.9 MΩ was used in all experiments.

2.2.2 Synthesis of DT-stabilized Gold Nanoparticles (AuNPs). AuNPs were synthesized by the Brust method,[20] and then modified by a ligand exchange reaction.[19,21] For the Brust method, typically, 34.5 mg (0.1 mmol) of $HAuCl_4 \bullet 3H_2O$ were dissolved in 3 mL of water, and 0.2187 g (0.4 mmol) of TOAB were dissolved in 7 mL of toluene, separately. The two solutions were mixed and stirred until gold precursors were transferred to the toluene phase and the water phase became clear and colorless. A 0.1 mmol portion of DT was added to the mixture and then the mixture was left stirring for 20 min. Then, the reducing agent, $NaBH_4$ (1 mmol in 200 μL of water) was quickly added to the mixture. After the addition of $NaBH_4$, the solution was allowed to stir for 3 hrs, and then the toluene phase was collected (~7 mL). Synthesized nanoparticles were precipitated by adding an excess amount of ethanol (35 mL) to the solution and collected by a gentle centrifugation (8,000 rpm for 10 min). The supernatant was decanted and the nanoparticle precipitate was redissolved in toluene. The nanoparticles were washed one more time in order to remove excess ligands. Finally, the nanoparticles were redispersed into 5 mL of dichloromethane (DCM) for the ligand exchange reaction.

2.2.3 Synthesis of MUL-stabilized AuNPs. AuNPs functionalized with MUL were synthesized, following the procedure described above but using MUL instead of DT. 20 mg of MUL was dissolved in 1 mL of toluene, and the solution was added to the mixture of gold precursor and TOAB. The mixture was left stirring for 20 min. Then,

the reducing agent $NaBH_4$ (1 mmol in 200 μL of water) was quickly added to the mixture. After the addition of $NaBH_4$, the solution was allowed to stir for 3 hrs. Nanoparticles were collected by a gentle centrifugation (8,000 rpm for 5 min), and redispersed in 5 mL of ethanol. The particles were precipitated by adding an excess amount of toluene (35 mL) and collected by a gentle centrifugation (8,000 rpm for 10 min). The supernatant was decanted and the nanoparticle precipitate was redissolved in ethanol. The nanoparticles were washed one more time in order to remove excess ligands.

2.2.4 Ligand Exchange. AuNPs with mixed surface ligands of DT and MUL were prepared by the ligand exchange reaction. First, a solution of MUL in DCM (1 mL) was added to the 5 mL DCM solution of DT-stabilized AuNPs. The amount of MUL in the 1 mL solution was varied according to the desired molar ratio on the AuNP surface and presented in Table 2.1. For example, for a 50 % molar ratio of MUL, 4.5 mg of MUL in 1 mL of DCM was added to the DT-stabilized AuNPs. The solution was magnetically stirred at room temperature for 48 h. For high MUL% AuNPs, 1 mL of ethanol was added to the reaction vial after stirring for a day. After the ligand exchange, the nanoparticle solution was concentrated by air flow until the volume was reduced to about 3-4 mL, and nanoparticles were precipitated by adding hexanes (35 mL) and collected by centrifugation (8,000 rpm for 10 min). The precipitates were washed one more time by DCM and hexanes to remove unbound ligands. The nanoparticles were then dispersed in chloroform or ethanol.

Table 2.1. The composition of surface ligands on AuNPs.

MUL concentration (g/L) used for ligand exchange	MUL% by NMR
1.71	25%
2.40	33%
4.82	50%
9.02	60%[a]
17.3	80%[a]

[a]Some precipitates were observed in $CDCl_3$ solutions of AuNPs with 60% and 80% MUL. Because supernatants were used for NMR measurements, the actual MUL percent of the samples can be slightly larger than the values determined by NMR.

2.2.5 Self-assembly of AuNPs and PS-*b*-PAA. The assemblies of AuNPs and PS_{250}-*b*-PAA_{14} were prepared by a reported literature procedure.[11] In a typical experiment, 500 μL of a PS_{250}-*b*-PAA_{14} solution (4 μM) in N,N-dimethylformamide (DMF) was mixed with 50 μL of AuNPs (1.7 μM) in chloroform (for 0%, 25%, 33%, and 50% MUL particles) or ethanol (for 50%, 60%, 80%, and 100% MUL particles) solution. In all experiments, the volume fraction of AuNPs, which is the volume of AuNPs divided by the total volume of particles and block-copolymers, was kept constant (0.06); the concentration of AuNPs was estimated by using the extinction coefficient of $3.61 \times 106\ M^{-1}cm^{-1}$ reported for 3.5 nm particles.5 Additional DMF (1 mL) was added to the solution while stirring, and then 300 μL of water (17.9 MΩ) was slowly added to the solution at the rate of 10 μL/30 s for 15 min in order to induce the self-assembly of AuNPs and block-copolymers. The solution was stirred for about 15 h. Next, 1.5 mL of water was added over 15 min and then dialyzed against water (17.9 MΩ) with the minimum of three water changes over 24 hrs.

2.2.6 Self-assembly of AuNPs and Pre-formed Worm-like Polymer Templates. PS_{96}-*b*-PAA_{48} was dissolved in water at 2 mg/mL concentration by applying sonication. Then, ethanol solution of MUL-stabilized AuNPs (15 μM, 100 μL) was mixed with 10 μL of the polymer solution. The volume fraction of AuNPs was 0.38. Water was slowly added to the solution at the rate of 10 μL/30 s for 30 min. The solution was stirred for about 15 h. Then, 1.5 mL of water was added to the solution over 15 min, and then dialyzed against water (17.9 MΩ) with a minimum of three water changes over 24 hrs.

2.2.7 Self-Assembly of AuNPs and Commercial Microspheres. Concentrated polymer bead solutions were diluted to 2 mg/mL, and then the interfacial assembly of

nanoparticles to the beads was formed by following the same procedure described above for worm-like micelles.

2.2.8 Co-assembly of AuNPs and Magnetic NPs. The tertiary-assembly of two different types of nanoparticles and a polymer was formed using a procedure similar to the one described above for binary assemblies of AuNPs and a polymer. For core/shell type assemblies, 50 μL THF solution of magnetic nanoparticles (4.5 nm in diameter, 1.5 mg/mL) was mixed with 500 μL of PS_{144}-*b*-PAA_{49} solution (8 μM) in DMF. Then 50 μL of AuNPs (1.3 μM, 80 % MUL) in ethanol was added to the mixture. Then, the assembly of the three components was induced by following the sample procedure used for the binary assembly described above. For simple micelles, a 50 μL THF solution of magnetic nanoparticles (15.7 nm in diameter, 3.0 mg/mL) was mixed with 500 μL of PS_{144}-*b*-PAA_{49} solution (22 μM) in THF. Then 150 μL of AuNPs (0.3 μM, 100 % MUL) in ethanol was slowly added (10 μL/30 s) to the mixture while stirring. Then, the assembly of the three components was induced by following the sample procedure used for the binary assembly described above.

2.2.9 Preparation of Self-Assembled Monolayers (SAMs) on Au. The gold thin films were prepared by thermal evaporation (base pressure 10-6 Torr). Ti (~4 nm) and Au (~80 nm) were evaporated onto glass slides without breaking the vacuum. After cooling down, the slides were transferred into centrifuge tubes containing 30 mL of ethanolic solution of DT and MUL at varying ratios. The total ligand concentration was 3 mM. Slides were placed in the ethanolic solutions for 2 days, removed from solutions, washed with ethanol, and dried under a nitrogen flow before analyses.

2.2.10 Contact Angle Measurements. Contact angles of water and formamide were taken on the prepared SAMs on gold. At least six measurements were carried out at different locations on each slide.

2.2.11 Instrumentation. Transmission electron microscopy (TEM) images and scanning transmission electron microscopy (STEM) images were taken on FEI-Tecnai T12 and JEOL 2010F using acceleration voltages of 120 kV and 200 kV, respectively. Energy-dispersive X-ray spectroscopy (EDS) results were collected using JEOL 2010F. Dynamic light scattering (DLS) data were taken with a Malvern Zetasizer Nano Series. A Rame-Hart Automated Goniometer was used to perform contact angle measurements. UV-vis absorption spectra were taken with an Agilent 8453 spectrometer. ^{1}H NMR spectra were collected with Bruker DMX500, using $CDCl_3$ as solvent. The final molar ratio of DT to MUL on mixed ligand AuNPs was determined by ^{1}H-NMR. The broad CH_3 peak at δ 0.90 ppm and broad -CH_2- peak which is next to -OH centered at δ 3.50 ppm were used for DT and MUL, respectively.

2.3 Results and Discussion

2.3.1. Self-assembly of PS_{250}-*b*-PAA_{14} and AuNPs with varying surface ligands. Figure 2.2 presents TEM images of binary assemblies of PS-*b*-PAA and AuNPs with varying surface ligands. The AuNPs immobilized with 100% DT segregated into the PS core of polymer micelles due to the favorable enthalphic interaction between the hydrophobic nanoparticles and the PS block as well as the attractive interaction between AuNPs (Figure 2.2 b). As the fraction of MUL increases to 25% or 33%, the nanoparticle aggregates moved toward the PS−PAA interface, forming Janus-type

particles (Figure 2.2 c). The asymmetric assembly formed at the MUL % range is reminiscent of the report by Chen and co-workers where single gold nanoparticles are eccentrically embedded in polymer micelles when nanoparticles and polymers are self-assembled in the presence of hydrophobic and hydrophilic thiols.[22] A further increase of the MUL % over 50 (50%, 60%, 80%, 100%) led to AuNPs distributed at the PS−PAA interface (Figure 2.2 d). Note that TEM images are two-dimensional projections of three-dimensional objects. Therefore, the dark contrast at the edges of polymer assemblies indicates the selective accumulation of nanoparticles at the PS−PAA interface.

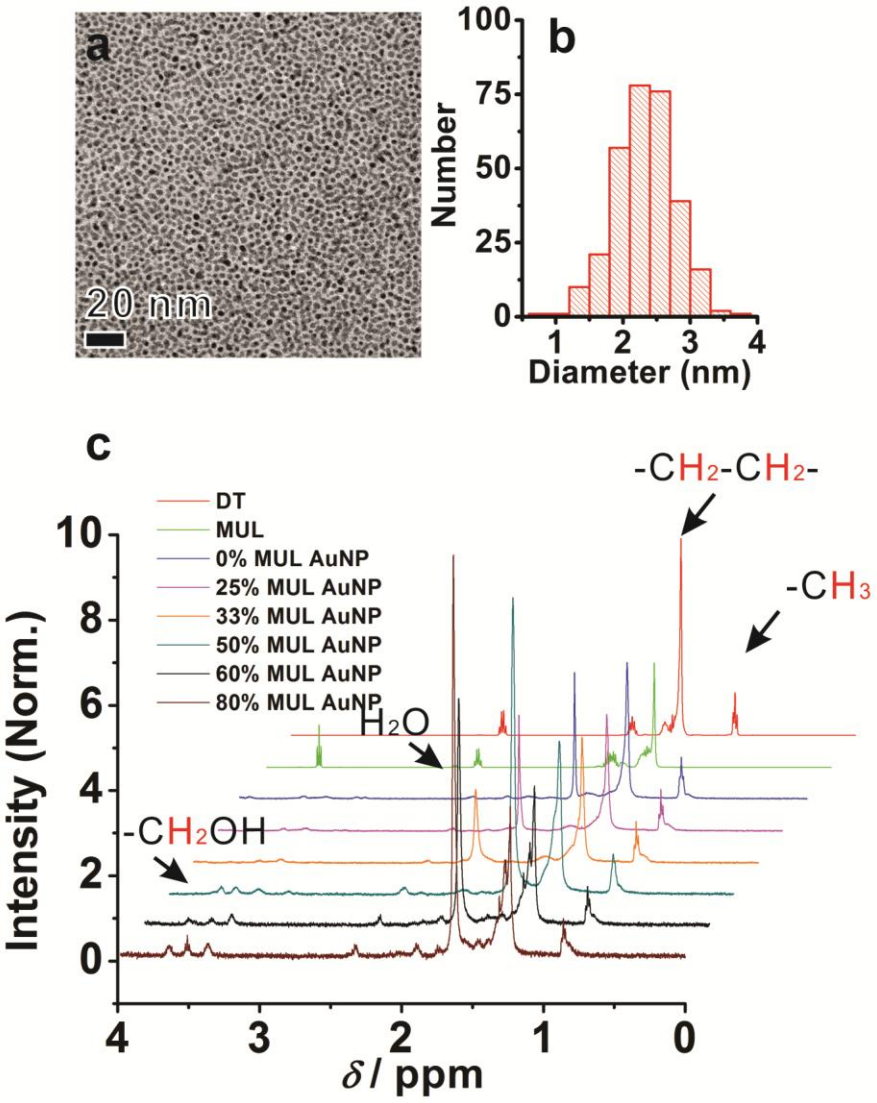

Figure 2.1. TEM image (a) of AuNPs (50% MUL) and their size histogram (b). ^{1}H NMR spectra of AuNPs with different MUL% (c).

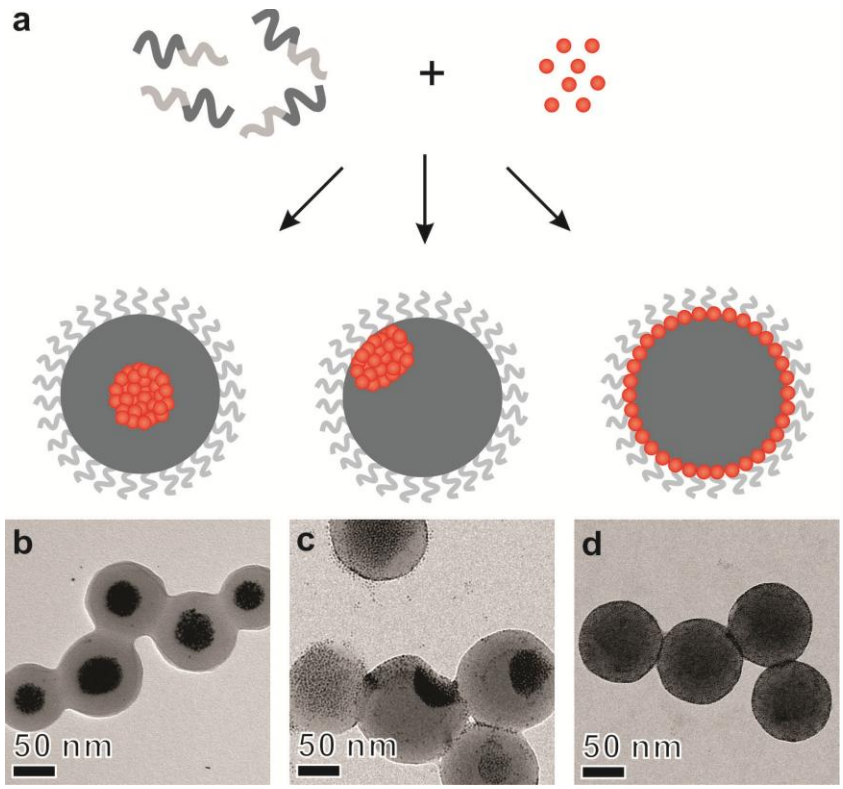

Figure 2.2. (a) Pictorial description of the self-assembly of PS_{250}-*b*-PAA_{14} and AuNPs with varying surface ligands. Light gray lines, dark gray lines, and red spheres represent PAA, PS, and AuNP, respectively. (b) A TEM image of coassemblies prepared with AuNPs modified with 100% DT. (c) A TEM image of coassemblies prepared with AuNPs modified with 75% DT and 25% MUL. (d) A TEM image of coassemblies prepared with AuNPs modified with 20% DT and 80% MUL. Note that the PAA layer is not visible in TEM images.

2.3.2 Theoretical Calculation of Interfacial self-assembly Structure.

Understanding the wetting properties of nanoparticles and polymers is important for the rational design of polymer nanocomposites.[16,23,24] The spatial arrangements of nanoparticles with varying surface ligands in polymer assemblies can be explained by the interfacial energies between two polymer blocks, A and B, and nanoparticles. Nanoparticles can locate at the A−B interface of two polymers if the criterion of

$$\left|\sigma_{A/NP} - \sigma_{B/NP}\right| < \sigma_{A/B} \quad (1)$$

is satisfied, where $\sigma_{A/NP}$, $\sigma_{B/NP}$, and $\sigma_{A/B}$ are the interfacial energies of A−AuNP, B−AuNP, and A−B pairs, respectively.[16,24,25] The interfacial energy, $\sigma 1/2$, between two interacting components, 1 and 2, is defined as

$$\sigma_{1/2} = (\sqrt{\gamma_1} - \sqrt{\gamma_2})^2 \quad (2)$$

where γ is the surface energy.[26] Surface energy can be estimated by measuring contact angle, θ

$$\frac{\gamma_L}{\sqrt{\gamma_L^D}}(1 + \cos\theta) = 2\sqrt{\gamma_S^D} + 2\sqrt{\gamma_S^P}\sqrt{\frac{\gamma_L^P}{\gamma_L^D}} \quad (3)$$

where γ_L is the surface energy of liquids and γ_S is the surface energy of solids.[26] The γ_L^D and γ_S^D denote dispersion components, and γ_L^P and γ_S^P denote polar components. From contact angle measurements with a polar and a nonpolar liquid with known surface energies, γ_S^P and γ_S^D can be obtained from the slope and the intercept of eq 3.

We used these relationships to predict the molar ratio of MUL and DT that induces the interfacial assembly of AuNPs. To estimate the interfacial energies between modified AuNPs and two polymer blocks, PS and PAA, gold thin films coated with DT and MUL were used as model systems for ligand-modified AuNPs (Table 2.2). Water and

formamide were used as test solvents for contact angle measurements (Table 2.3). The ligand-modified gold films were prepared by immersing freshly deposited gold films into ethanolic solutions of DT or DT/MUL mixtures (3 mM) for two days at room temperature. The surface energies of modified Au films were estimated from the contact angle measurements for varying molar ratios of DT and MUL (Table 2.4). As expected, the surface energy gradually increased as the percentage of MUL increased (Figure 2.3), which is consistent with previous reports.[27,28] The $\sigma_{PS/NP}$ and $\sigma_{PAA/NP}$ values were then calculated from the surface energies using eq 2. As plotted in Figure 2.4, the $|\sigma_{PS/NP} - \sigma_{PAA/NP}|$ value decreases with increasing MUL percentage and becomes smaller than $\sigma_{PS/PAA}$ (3.43 mJ/m^2) at about 61% MUL (Table 2.5). Eventually, the $|\sigma_{PS/NP} - \sigma_{PAA/NP}|$ becomes negative for 100% MUL, and the absolute value of $|\sigma_{PS/NP} - \sigma_{PAA/NP}|$ becomes closer to $\sigma_{PS/PAA}$. Therefore, the minimum value of $|\sigma_{PS/NP} - \sigma_{PAA/NP}|$ is found at an MUL % between 65% and 100%. These data indicate that NPs with MUL % larger than 65% can reside at the PS−PAA interface, reducing the interfacial energy between PS and PAA. It also indicates that the ideal MUL % for interfacial assembly should be larger than 65% and smaller than 100%.

This prediction is in a good agreement with the experimental data presented in Figure 2.2. Among four different MUL % (50%, 60%, 80%, 100%) that showed the interfacial assembly, the nanoparticle distribution was most even at 80% MUL (Figure 2.2 d and Figure 2.5). This result is consistent with the prediction that the most effective MUL % for reducing the PS−PAA interfacial energy is in between 65% and 100% (Figure 2.4). However, it is worth noting that the interfacial assembly of nanoparticles was found over a wider range of MUL % than predicted. This is partly

due to the fact that the surface energy of modified AuNPs can be different from that of modified gold films, as reported by Stellacci and co-workers.[27] Moreover, the two ligands on AuNPs can phase segregate to maximize the interaction between PS and DT and the interaction between PAA and MUL rather than forming homogeneously mixed monolayers. Also, note that the prediction by the interfacial energy calculation does not consider the distribution in ligand compositions, while the actual ligand composition is distributed about the measured average values with fractions of nanoparticles with more or less MUL % than the average value. Nonetheless, the interfacial energy calculation presented in Figure 2.4 provides a useful guidance for the solution-phase interfacial assemblies of nanoparticles and amphiphilic polymers.

Table 2.2. Contact angles of SAMs of DT and MUL at different ratios.

	This work		Literature[28]	
MUL%	Water	Formamide	Water	Hexadecane
0	88 °	74 °	105 °	44 °
25	85 °	67 °	90 °	29 °
50	73 °	60 °	74 °	22 °
75	49 °	45 °	51 °	8 °
100	25 °	25 °	0 °	0 °

Table 2.3. Surface energies of liquids used for contact angle measurements.[29]

	γ_L (mJ/m^2)	γ_L^D (mJ/m^2)	γ_L^P (mJ/m^2)
Water	72.8	21.8	51
Formamide	58.2	39.5	18.7
Hexadecane	27.6	27.6	0

Table 2.4. Surface energies of SAMs of DT and MUL at different ratios.

MUL%	This work			Literature[28]		
	[a]γ_S^D (mJ/m^2)	[b]γ_S^P (mJ/m^2)	γ_S (mJ/m^2)	[a]γ_S^D (mJ/m^2)	[b]γ_S^P (mJ/m^2)	γ_S (mJ/m^2)
0	17.84	6.47	24.31	20.39	0.59	20.98
25	22.63	5.95	28.58	24.22	3.48	27.70
50	19.07	14.15	33.22	25.54	10.19	35.74
75	14.08	36.12	50.20	27.33	23.70	51.03
100	14.89	51.65	66.54	27.6	45.69	73.29

[a]Values are obtained from the intercepts of the extrapolation of equation (1). [b]Values are from the slopes of equation (1).

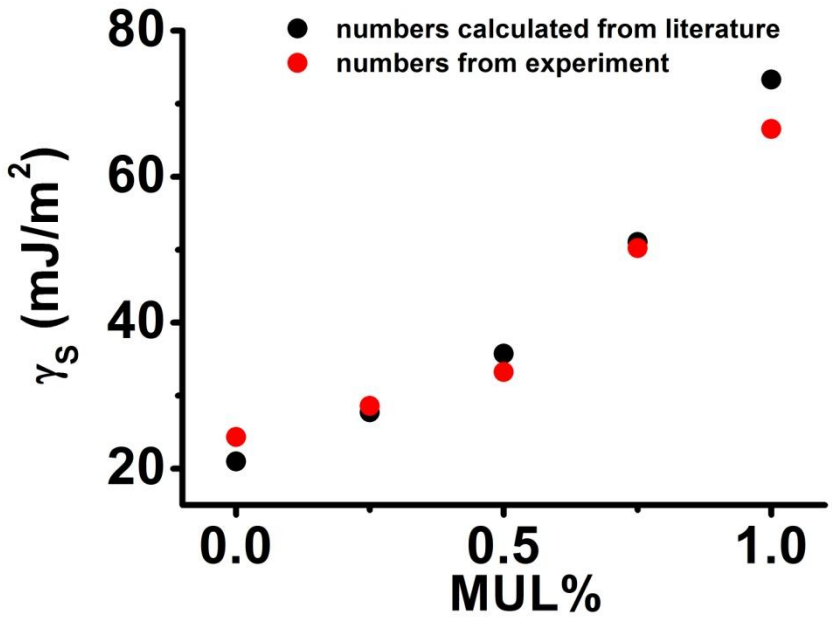

Figure 2.3. Surface energies of SAMs of DT and MUL at different MUL percents. The literature values 28 are plotted along with the data measured in this work.

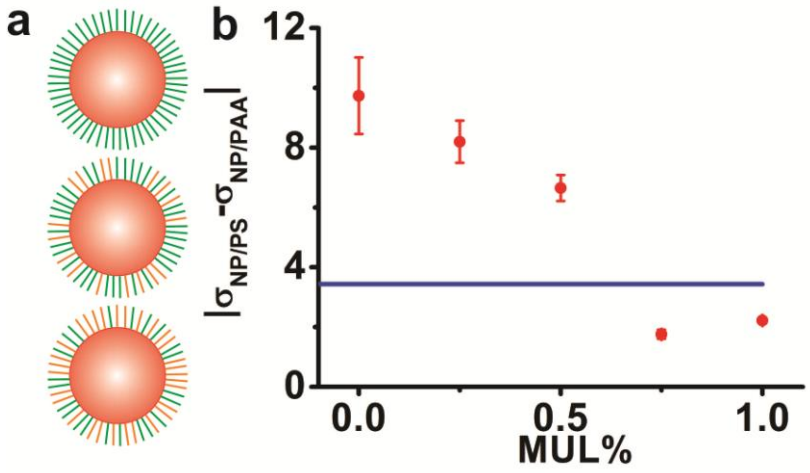

Figure 2.4. (a) Pictorial description of nanoparticles modified with two different ligands at different ratios. Green lines and orange lines represent two different ligands. (b) The $|\sigma_{PS/NP} - \sigma_{PAA/NP}|$ values at varying MUL % on nanoparticle surfaces. The blue line indicates the interfacial energy between PS and PAA.

Table 2.5. Interfacial energies of SAMs of DT and MUL at different ratios.

MUL %	This work			Literature[28]		
	$\sigma_{NP/PS}$ (mJ/m^2)	$\sigma_{NP/PAA}$ (mJ/m^2)	$\lvert\sigma_{NP/PS}$-$\sigma_{NP/PAA}\rvert$	$\sigma_{NP/PS}$ (mJ/m^2)	$\sigma_{NP/PAA}$ (mJ/m^2)	$\lvert\sigma_{NP/PS}$-$\sigma_{NP/PAA}\rvert$
0	2.90	12.64	9.74	4.22	15.25	11.03
25	1.66	9.85	8.20	1.88	10.38	8.51
50	0.76	7.41	6.65	0.43	6.29	5.86
75	0.20	1.96	1.76	0.26	1.80	1.54
100	2.32	0.11	2.21	3.72	0.01	3.71
[a]$\sigma_{PS/PAA}$ (mJ/m^2)			3.43			

[a]The surface energy values[30,31] of γ_{PS}=44 mJ/m^2, γ_{PAA} =72 mJ/m^2 were used for the calculation.

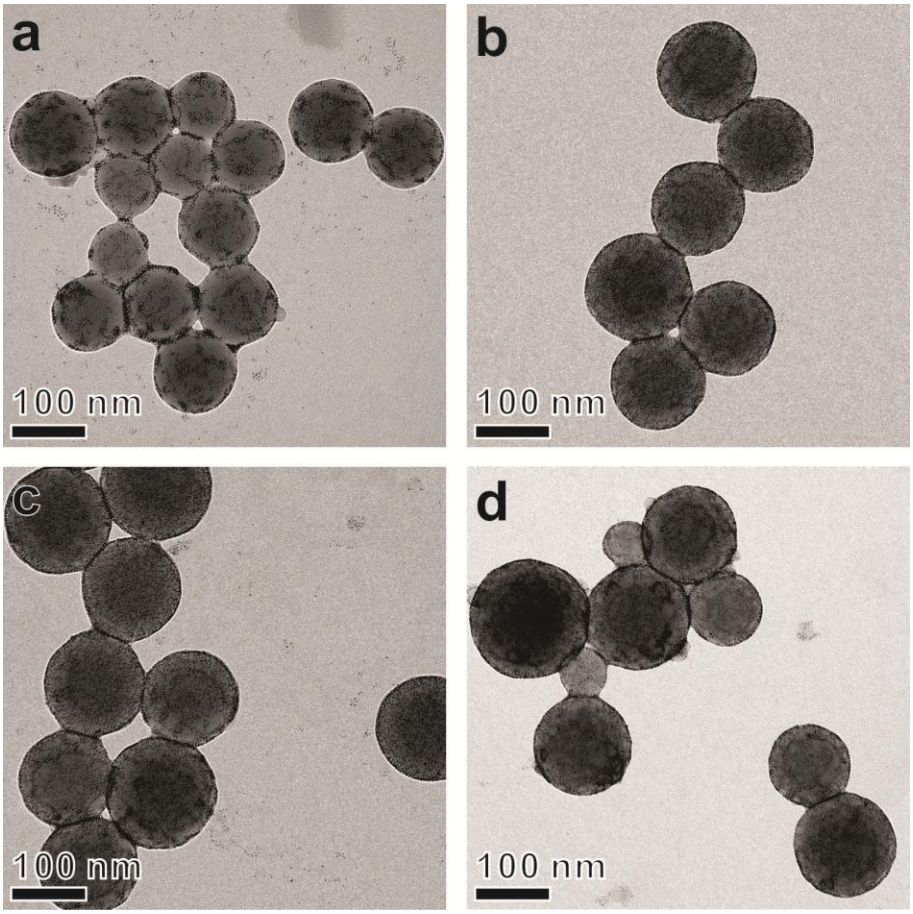

Figure 2.5. TEM images of AuNPs and block copolymer assemblies formed with AuNPs modified with 50% MUL (a), 60% MUL (b), 80% MUL (c), and 100% MUL (d).

2.3.3 EDS Measurements and Size Distributions of Interfacial self-assembly Structures. The EDS measurements were consistent with the TEM observations (Figure 2.6). The Au intensity profile of the assemblies formed with 100% DT showed a Gaussian-shape curve indicating that AuNPs concentrated in the center of polymer micelles (Figure 2.6 a). The assemblies with 80% MUL, on the other hand, showed high intensities at the edges of the micelle, confirming the assembly of nanoparticles at the PS−PAA interface (Figure 2.6 b). On the basis of the size of the assemblies (Figure 2.6 c,d), it is likely that the assemblies formed at 80% MUL adopt the compound micelle structure,[32,33] which is composed of a micelle containing reverse micelles in the core. Because varying numbers of reverse micelles can be incorporated in compound micelles, they typically show broad size distributions.[32] However, the interfacial assemblies prepared with 80% MUL AuNPs were fairly uniform and showed a narrow size distribution with the standard deviation of 8% from TEM measurements (Figure 2.6 d). This result indicates that the incorporation of amphiphilic AuNPs regulates the characteristic length scale and overall size of polymer assemblies, as shown for polymer melts and larger colloidal polymer particles.[34] It is interesting to note that the size distribution becomes broader when the MUL % was increased to 100% or decreased to 50% (Figure 2.6 e). For 100% MUL, polymer assemblies might be preformed before nanoparticles start associating with polymers at the PS−PAA interface or in the PAA block because of the hydrophilic nature of the NPs, resulting in a broader size distribution.

2.3.4 Mixed-ligand AuNPs Decorated Preformed Polymer Assemblies. The result of 100% MUL suggests that nanoparticle decorated polymer assemblies can be prepared from preformed polymer assemblies (Figure 2.8). This approach provides a

simple way to decorate various types of polymeric nanostructures with inorganic nanoparticles and is particularly useful for nonspherical assemblies that are difficult to prepare using the simultaneous self-assembly of amphiphilic polymers and nanoparticles. To test the feasibility of the approach, rod-like micelles were first prepared by dispersing PS_{96}-*b*-PAA_{48} in water by sonication. An ethanol solution of AuNPs immobilized with 100% MUL (2.7 μM, 100 μL) was then slowly added to the aqueous solution of micelles (2 mg/mL, 15 μM, 10 μL) while stirring the solution. The self-assembly was induced by the slow water addition (1.8 mL) followed by dialysis. This procedure led to rod-like micelles densely coated with AuNPs, as revealed by TEM (Figure 2.8 a,b). As another example, commercial carboxylic acid modified polystyrene beads were used for the interfacial assembly. As shown in Figure 2.8 d and 2.9, polystyrene beads uniformly coated with nanoparticles were formed by the same procedure.

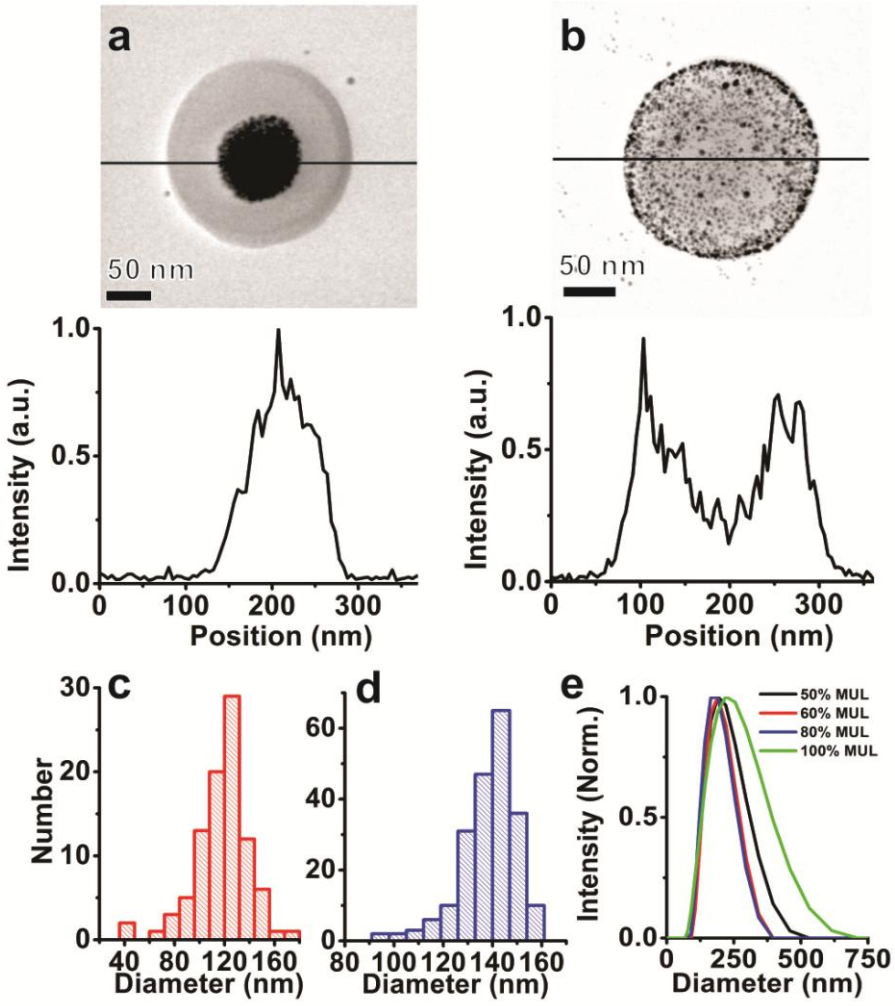

Figure 2.6. (a,b) STEM images and EDS line scans of the assemblies prepared with 100% DT (a) and 80% MUL (b). The EDS line profile (gold Lα line) is an average of multiple scans. (c,d) Size distribution histograms of the assemblies prepared with 100% DT (c) and the assemblies prepared with 80% MUL (d) obtained from TEM images. (e) DLS data for assemblies prepared with 50%, 60%, 80%, and 100% MUL.

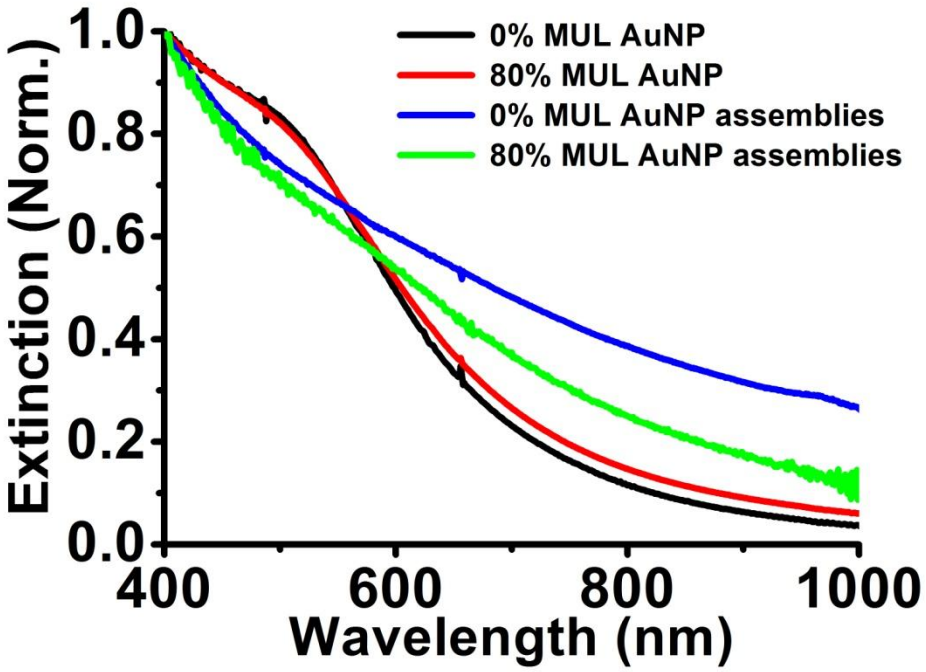

Figure 2.7. UV-vis spectra of polymer assemblies with AuNPs.

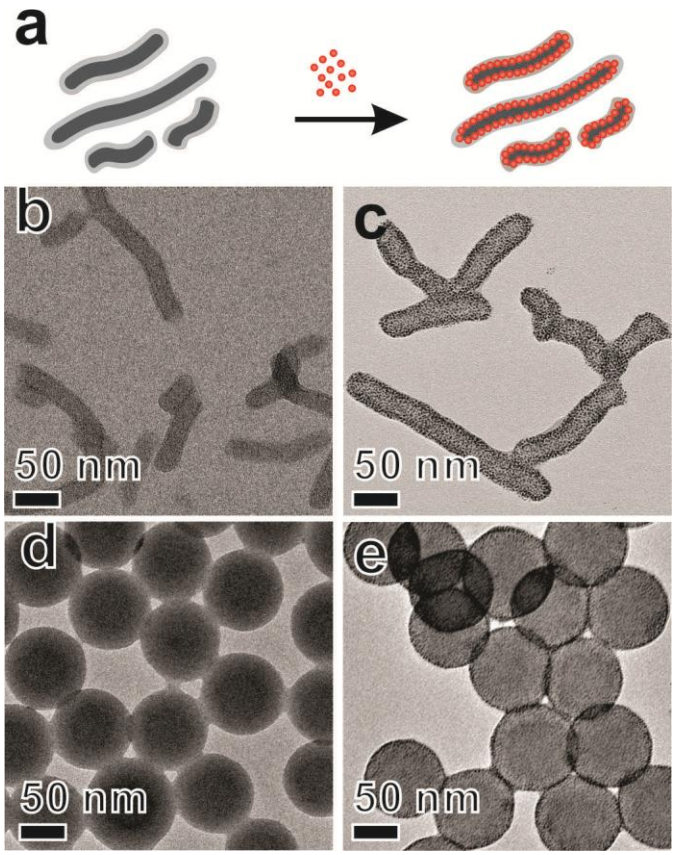

Figure 2.8. (a) Schematic description for the formation of rod-like micelles decorated with AuNPs. (b,c) Rod-like micelles of PAA_{96}−PS_{48} (b) before and (c) after the nanoparticle assembly. (d,e) Commercial carboxylic acid terminated polystyrene beads (100 nm) (d) before and (e) after the nanoparticle assembly.

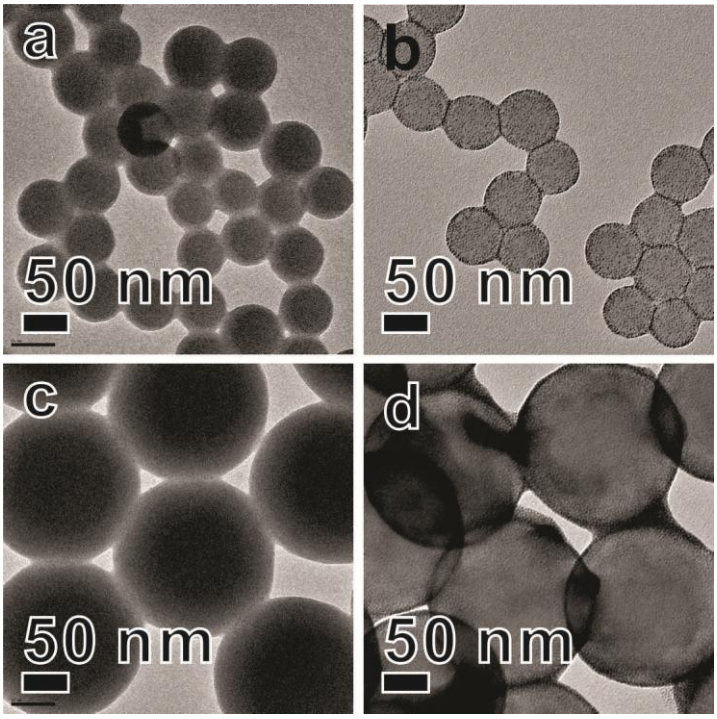

Figure 2.9. (a,c) Commercial polystyrene beads of 60 nm (a) and 200 nm (c) diameters. (b,d) Commercial polystyrene beads of 60 nm (a) and 200 nm (c) diameters decorated with AuNPs with 100% MUL.

2.3.5 The Fabrication of Multicomponent assemblies. With these capabilities, we fabricated multicomponent assemblies where gold and iron oxide nanoparticles are embedded in different locations of polymer assemblies (Figure 2.10). We have previously shown that iron oxide nanoparticles stabilized with oleic acids can form unique radial arrays at the PS−PS interface in compound micelles of PS-*b*-PAA (Figure 2.10 b).[11,35] The ternary self-assembly of iron oxide nanoparticles, AuNPs (80% MUL or 100% MUL), and PS-*b*-PAA resulted in layered assemblies with AuNPs located at the PS−PAA interface and iron oxide nanoparticles located in between the polymer core and polymer shell[11] of compound micelles (Figure 2.10 a,d). For a typical experiment, magnetic NPs were first mixed with PS_{144}-*b*-PAA_{49} (2 μM, 20 μL) in DMF and then mixed with AuNPs (4.7 μM, 10 μL) in ethanol, followed by the slow water addition and dialysis. The distance between two nanoparticle layers can be potentially controlled by varying the molecular weight of polymers or nanoparticle volume fractions.[13] The EDS data confirmed that iron oxide nanoparticles and AuNPs are arranged at two different radial positions of polymer assemblies (Figure 2.10 d). The distribution of iron oxide nanoparticles can be controlled by using a different initial cosolvent for nanoparticles and polymers as we previously reported.[11] When THF was used instead of DMF, iron oxide nanoparticles are embedded throughout the PS matrix rather than forming shell-like assemblies as previously reported (Figure 2.10 e).[10,11] Figure 2.10 f presents the coassemblies of AuNPs and iron oxide nanoparticles prepared in the condition that favors the uniform distribution of iron oxide nanoparticles. It is apparent from TEM images and EDS line scans that iron oxide nanoparticles are embedded in the PS core, while AuNPs are located at the PS−PAA interface.

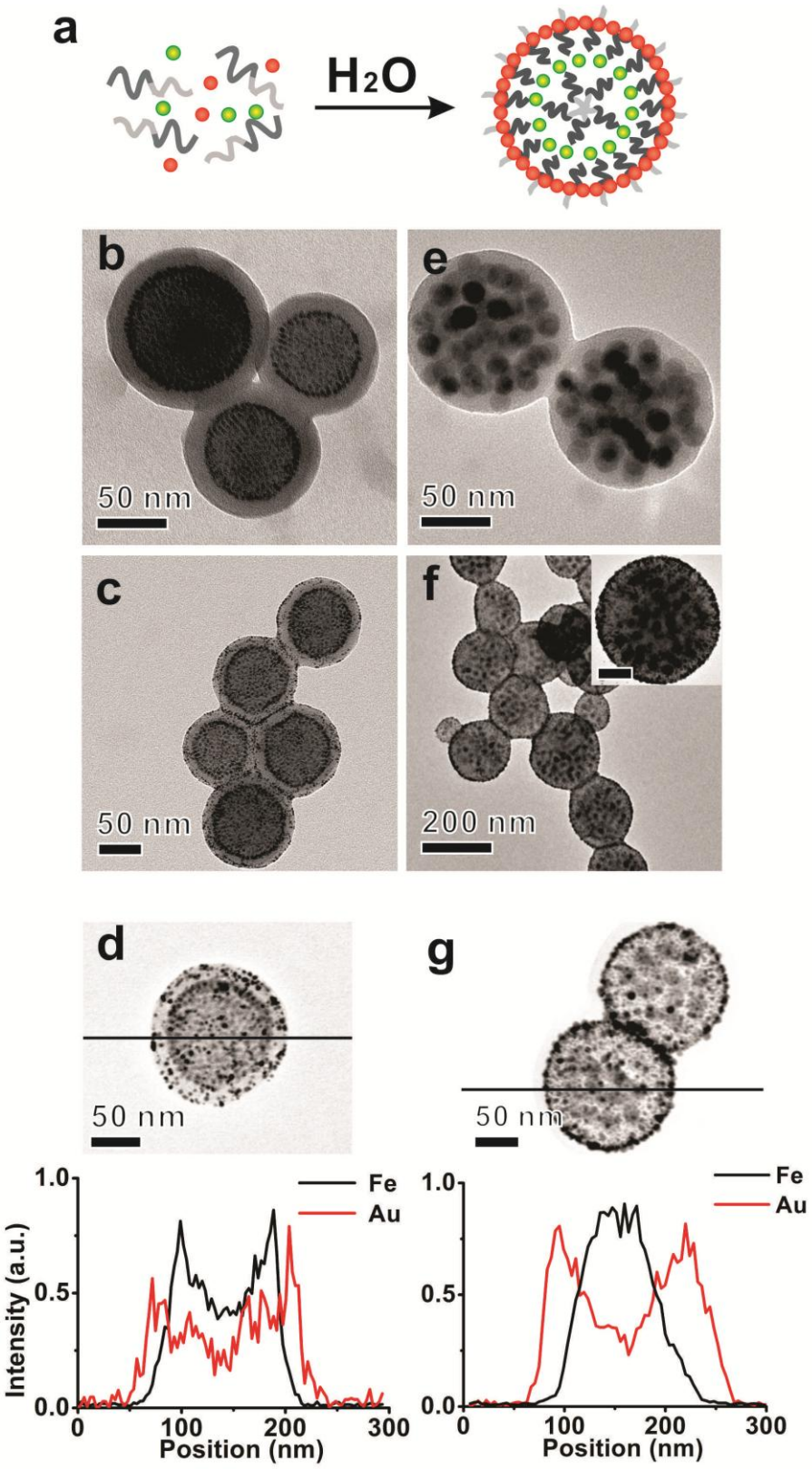
a
H2O
b
50 nm
e
50 nm
c
50 nm
f
200 nm
d
50 nm
g
50 nm
Intensity (a.u.)
1.0
0.5
0.0
0
100
200
300
Position (nm)
Fe
Au

Figure 2.10. (a) Pictorial description for the formation of multicomponent layered assemblies of AuNPs and magnetic nanoparticles. Red dots and green dots represent AuNPs and iron oxide nanoparticles, respectively. (b) Compound micelles with 4.5 nm magnetic nanoparticles arranged in between the polymer core and polymer shell. (c) Compound micelles with 4.5 nm iron oxide nanoparticles arranged in between the polymer core and polymer shell and AuNPs (80% MUL) at the PS−PAA interface. (d) An STEM image and EDS Au intensity (L_α line) and Fe intensity (K_α line) profiles of the assemblies shown in (c). (e) Polymer micelles encapsulated with 15.7 nm magnetic nanoparticles in the PS domain. (f) Polymer micelles encapsulated with 15.7 nm magnetic nanoparticles in the PS domain and AuNPs (100% MUL) at the PS−PAA interface. The inset shows a higher magnification TEM image (scale bar: 50 nm). (g) An STEM image and the EDS Au intensity (L_α line) and Fe intensity (K_α line) profiles of the assemblies shown in (f).

2.4 Conclusions

In summary, we demonstrated a strategy to control the location of nanoparticles in colloidal solution-phase assemblies of amphiphilic polymers. Depending on the ratio between hydrophobic and hydrophilic surface ligands, particles either localized at the interface between PS and PAA blocks or aggregated in the center of the assemblies. Uniform interfacial assemblies of AuNPs were obtained with AuNPs modified with 80% MUL and 20% DT, which is in good agreement with the prediction by interfacial energy calculations. Compared to the hollow nanoparticle capsules fabricated by the interfacial assembly at the oil/water interface of emersions,[36] the binary assembly of nanoparticles and polymers reported here results in more stable nanoparticle capsules supported by polymer templates. On the basis of the approach, we fabricated multifunctional assemblies where iron oxide nanoparticles and AuNPs are compartmentalized at different locations of polymer matrixes. Furthermore, we demonstrated that MUL-modified AuNPs can decorate preformed assemblies of amphiphilic polymers. This approach can be potentially useful for functionalizing polymer particles with targeting molecules or drugs for biomedical applications.

2.5 References

(1) Gao, X.; Cui, Y.; Levenson, R. M.; Chung, L. W. K.; Nie, S. *Nat Biotech* **2004**, *22*, 969-976.

(2) Euliss, L. E.; Grancharov, S. G.; O'Brien, S.; Deming, T. J.; Stucky, G. D.; Murray, C. B.; Held, G. A. *Nano Lett.* **2003**, *3*, 1489-1493.

(3) Berret, J.-F.; Schonbeck, N.; Gazeau, F.; El Kharrat, D.; Sandre, O.; Vacher, A.; Airiau, M. *J. Am. Chem. Soc.* **2006**, *128*, 1755-1761.

(4) Sanson, C.; Diou, O.; Thévenot, J.; Ibarboure, E.; Soum, A.; Brûlet, A.; Miraux, S.; Thiaudière, E.; Tan, S.; Brisson, A.; Dupuis, V.; Sandre, O.; Lecommandoux, S. b. *ACS Nano* **2011**, *5*, 1122-1140.

(5) Mueller, W.; Koynov, K.; Fischer, K.; Hartmann, S.; Pierrat, S.; Basché, T.; Maskos, M. *Macromolecules* **2008**, *42*, 357-361.

(6) Krack, M.; Hohenberg, H.; Kornowski, A.; Lindner, P.; Weller, H.; Förster, S. *J. Am. Chem. Soc.* **2008**, *130*, 7315-7320.

(7) Binder, W. H.; Sachsenhofer, R.; Farnik, D.; Blaas, D. *Phys. Chem. Chem. Phys.* **2007**, *9*, 6435-6441.

(8) Mai, Y.; Eisenberg, A. *J. Am. Chem. Soc.* **2010**, *132*, 10078-10084.

(9) Kang, Y.; Taton, T. A. *Angew. Chem., Int. Ed.* **2005**, *44*, 409-412.

(10) Kim, B.-S.; Qiu, J.-M.; Wang, J.-P.; Taton, T. A. *Nano Lett.* **2005**, *5*, 1987-1991.

(11) Hickey, R. J.; Haynes, A. S.; Kikkawa, J. M.; Park, S.-J. *J. Am. Chem. Soc.* **2011**, *133*, 1517-1525.

(12) Sanchez-Gaytan, B. L.; Cui, W.; Kim, Y.; Mendez-Polanco, M. A.; Duncan, T. V.; Fryd, M.; Wayland, B. B.; Park, S.-J. *Angew. Chem., Int. Ed.* **2007**, *46*, 9235-9238.

(13) Sanchez-Gaytan, B. L.; Li, S.; Kamps, A. C.; Hickey, R. J.; Clarke, N.; Fryd, M.; Wayland, B. B.; Park, S.-J. *J. Phys. Chem. C* **2011**, *115*, 7836-7842.

(14) Kamps, A. C.; Sanchez-Gaytan, B. L.; Hickey, R. J.; Clarke, N.; Fryd, M.; Park, S.-J. *Langmuir* **2010**, *26*, 14345-14350.

(15) Bockstaller, M. R.; Mickiewicz, R. A.; Thomas, E. L. *Adv. Mater.* **2005**, *17*, 1331-1349.

(16) Chung, H.-J.; Kim, J.; Ohno, K.; Composto, R. J. *ACS Macro Letters* **2011**, *1*, 252-256.

(17) Bockstaller, M. R.; Lapetnikov, Y.; Margel, S.; Thomas, E. L. *J. Am. Chem. Soc.* **2003**, *125*, 5276-5277.

(18) Chiu, J. J.; Kim, B. J.; Kramer, E. J.; Pine, D. J. *J. Am. Chem. Soc.* **2005**, *127*, 5036-5037.

(19) Li, Q.; He, J.; Glogowski, E.; Li, X.; Wang, J.; Emrick, T.; Russell, T. P. *Adv. Mater.* **2008**, *20*, 1462-1466.

(20) Brust, M.; Walker, M.; Bethell, D.; Schiffrin, D. J.; Whyman, R. *J. Chem. Soc., Chem. Commun.* **1994**, 801-802.

(21) Glogowski, E.; He, J.; Russell, T. P.; Emrick, T. *Chem. Commun.* **2005**, 4050-4052.

(22) Chen, T.; Yang, M.; Wang, X.; Tan, L. H.; Chen, H. *J. Am. Chem. Soc.* **2008**, *130*, 11858-11859.

(23) Kim, D. H.; Wei, A.; Won, Y.-Y. *ACS Applied Materials & Interfaces* **2012**, *4*, 1872-1877.

(24) Chung, H.-j.; Ohno, K.; Fukuda, T.; Composto, R. J. *Nano Lett.* **2005**, *5*, 1878-1882.

(25) Pieranski, P. *Phys. Rev. Lett.* **1980**, *45*, 569-572.

(26) Israelachvili, J. N. *Intermolecular and Surface Forces, Third Edition*; Academic Press: Burlington, MA, 2011.

(27) Kuna, J. J.; Voitchovsky, K.; Singh, C.; Jiang, H.; Mwenifumbo, S.; Ghorai, P. K.; Stevens, M. M.; Glotzer, S. C.; Stellacci, F. *Nat. Mater.* **2009**, *8*, 837-842.

(28) Laibinis, P. E.; Fox, M. A.; Folkers, J. P.; Whitesides, G. M. *Langmuir* **1991**, *7*, 3167-3173.

(29) Dann, J. R. *J. Colloid Interf. Sci.* **1970**, *32*, 321-331.

(30) Mittal, K. L.; VSP - An imprint of BRILL, p 105-121.

(31) Ishimuro, Y.; Ueberreiter, K. *Colloid Polym. Sci.* **1980**, *258*, 928-931.

(32) Zhang, L.; Eisenberg, A. *J. Am. Chem. Soc.* **1996**, *118*, 3168-3181.

(33) Yu, Y.; Eisenberg, A. *J. Am. Chem. Soc.* **1997**, *119*, 8383-8384.

(34) Kim, B. J.; Fredrickson, G. H.; Hawker, C. J.; Kramer, E. J. *Langmuir* **2007**, *23*, 7804-7809.

(35) Hickey, R. J.; Sanchez-Gaytan, B. L.; Cui, W.; Composto, R. J.; Fryd, M.; Wayland, B. B.; Park, S.-J. *Small* **2010**, *6*, 48-51.

(36) Lin, Y.; Skaff, H.; Emrick, T.; Dinsmore, A. D.; Russell, T. P. *Science* **2003**, *299*, 226-229.

Chapter 3. DNA Rafts on hybrid DNA block copolymer assemblies induced by DNA hybridization

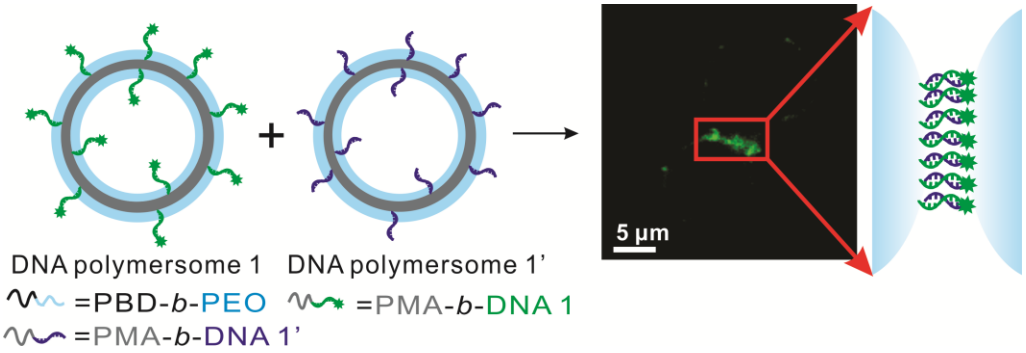

We report the DNA-induced phase segregation and DNA-raft formation in DNA block copolymer assemblies. DNA diblock copolymer of polymethylacrylate-block-DNA (PMA-b-DNA) was synthesized and assembled with a prototypical amphiphilic block polymer of poly(butadiene)-block-poly(ethylene oxide) (PBD-b-PEO). The binary self-assembly of PMA-b-DNA and PBD-b-PEO resulted in giant polymersomes where DNA is uniformly distributed in the hydrophilic PEO shell. When giant polymersomes were connected through specific DNA interactions, DNA block-copolymers appear to concentrate at the junction area, forming DNA-rafts within polymersomes. These results demonstrate that DNA hybridization induces effective phase segregation in polymer assemblies to form multiple DNA linkages.

3.1 Introduction

There has been tremendous effort and interest in nanostructures made of dense DNA shells without the gold particle which maintain sharp melting transitions.[1-4] In particular, amphiphilic DNA block copolymers have been utilized to fabricate nanoscale or mesoscale assemblies composed of a polymer core and a densely packed DNA shell. As a consequence of the high DNA density on polymer assemblies, they show similar molecular recognition properties to DNA-modified gold particles.[5] In addition, DNA block copolymer assemblies have several advantages over DNA-modified gold particles. Firstly, it does not contain gold nanoparticles which are costly to prepare and can be potentially toxic at high dose. Secondly, functional molecules or nanoparticles can be readily incorporated into the polymer core of DNA block copolymer micelles.[4] Capitalizing on these attributes, DNA block copolymers have been actively studied for various applications including drug delivery[6] and gene therapy.[7-10] For example, Hermann and co-workers have demonstrated that DNA-*block*-poly(propylene oxide) (DNA-*b*-PPO) micelles can be used as an effective chemotherapeutic drug delivery vehicle where anticancer drugs are loaded in the polymer core.[9]

Another unique property of DNA block copolymer micelles is that block copolymer strands composing the assemblies can undergo strand rearrangement and exchange. Gianneschi *et a*l utilized this aspect to induce the morphology change of DNA block copolymer assemblies.[11] Another important possibility arising from the strand rearrangement is the phase segregation and domain formation in mixed assemblies, which has not been previously explored. Phase segregation is a common phenomenon found in cell membranes where different membrane components are segregated to form domains

called membrane rafts.[12] The raft formation is known to play a critical role in cellular functions such as signal transduction pathways, cell adhesion and migration, and synaptic transmission, etc.[13]

In this chapter, we fabricated hybrid giant vesicles from DNA diblock copolymers of polymethylacrylate-*block*-DNA (PMA-*b*-DNA) using a prototypical block copolymer of poly(butadiene)-*block*-poly(ethylene oxide) (PBD-*b*-PEO) as a matrix polymer. We demonstrated that the hybrid vesicles undergo efficient phase segregation upon the introduction of complementary DNA. The full phase segregation occurred at time scales which is comparable to that shown in lipid membranes (from minutes to hours). Note that for polymers, it was shown to take days to months to fully develop large scale domain phase segregation.[14,15] The hybridization-induced phase segregation led to high density DNA rafts on the vesicle surface, and we are going to study their DNA binding properties at varied DNA sequence concentrations on hybrid assembly surfaces in the next chapter.

3.2 Experimental Section

3.2.1 Materials. Tetrahydrofuran (THF) was purified by distillation over Na/benzophenone under argon. Other common solvents such as acetone, methanol, isopropanol, chloroform, and dichloromethane were used as received. 1,3-butadiene (BD) was purchased from Aldrich and purified by distillation over calcium hydride. Ethylene oxide (EO) was purchased from Pfaltz&Bauer and dried with calcium hydride and distilled prior to use. *sec*-Butyllithium was purchased from Aldrich and used as received. The concentration of butyllithium was determined by diphenylacetic acid titration.

Potassium naphthalenide solution was prepared by adding freshly cut potassium metal to a stirring naphthalene solution (THF) under nitrogen flow. The dark green solution was allowed to stir at room temperature for at least 2 h before use. Methyl acrylate was purchased from Sigma and purified through an alumina neutral column to remove inhibitors. The initiator (4,4'-azobis(4-cyanovaleric acid) (V-501)), RAFT agent (4-cyano-4-[(dodecylsulfanylthiocarbonyl)sulfanyl] pentanoic acid (RAFT-2.0)), *N*,*N*-diisopropylethylamine and 1-[Bis(dimethylamino)methylene]-1H-1,2,3-triazolo[4,5-b]pyridinium 3-oxid hexafluorophosphate (HATU) were purchased from Sigma and used as received. Oligonucleotides (DNA 1: 5'-A10-ATCCTTATCAATATT-FAM-3'; DNA 1': 5'-AATATTGATAAGGAT-T10-3') were purchased from Trilink, Inc.

3.2.2 Synthesis of PBD. PBD-OH was synthesized by anionic polymerization.[16] Typically, *sec*-butyllithium (3.5 mL, 1.16 M, 4.06 mmol) was added into 30 mL anhydrous THF in a 250 mL dry flask under an inert atmosphere. The flask was cooled to about -65 ℃ using dry ice/isopropanol bath and a deep yellow color was observed for the solution. BD monomer (16 mL, 189 mmol) was added *via* cannula to the reaction flask. The solution was slightly warmed up to -60 ℃ where the solution color became yellowish orange. The reaction was kept stirring at -60 ℃ for about 5 h. EO was then added to the solution using cannula (2 mL). Upon the addition of EO, the solution became colorless within a minute. The solution was warmed up to room temperature by removing the cooling bath and stirred overnight. The reaction was then quenched by adding acidic methanol (200 mL). The solution was stirred overnight, filtered through filter paper, and concentrated by a rotary evaporator. The crude product of PBD-OH was

dissolved in hexane and filtered through filter paper to remove residual inorganic salts prior to the second block polymerization.

3.2.3 Synthesis of PBD-*b*-PEO. Typically, synthesized PBD-OH (3.86 g, 1.23 mmol) was dissolved in 15 mL anhydrous THF in a 250 mL dry flask. The PBD-OH solution was slowly titrated with freshly prepared potassium naphthalenide solution at room temperature until a light green-brown color appeared and the solution became cloudy. EO (2.2 mL, 44 mmol) was added to the solution *via* cannula. The green-brown color disappeared within a minute. The reaction mixture was warmed up to 40-45 ℃ and stirred for 24 h. The reaction flask was allowed to cool down to room temperature and then acidic methanol (200 mL) was added to the mixture to quench the reaction. The solution was kept stirring overnight, filtered by filter paper, and concentrated on a rotary evaporator. The crude product was redissolved in chloroform and washed several times by extraction with distilled water. The chloroform solution was dried over anhydrous Na_2SO_4 and concentrated on a rotary evaporator. The gel-like product was heated to 70 ℃ in a vacuum oven to remove residual solvents and naphthalene.

Scheme 3.1. Synthesis of PBD-*b*-PEO.

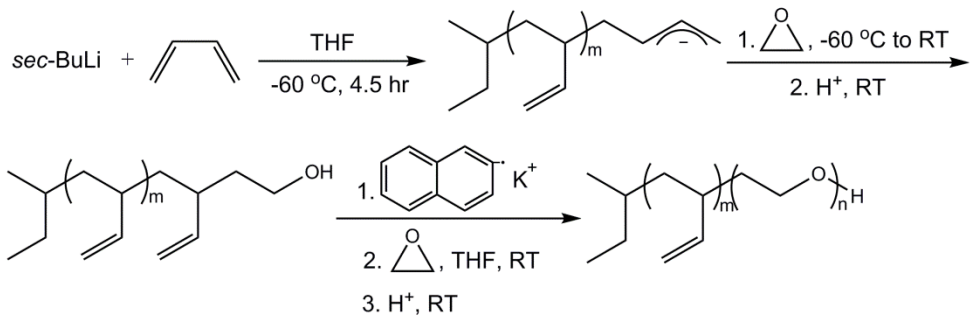

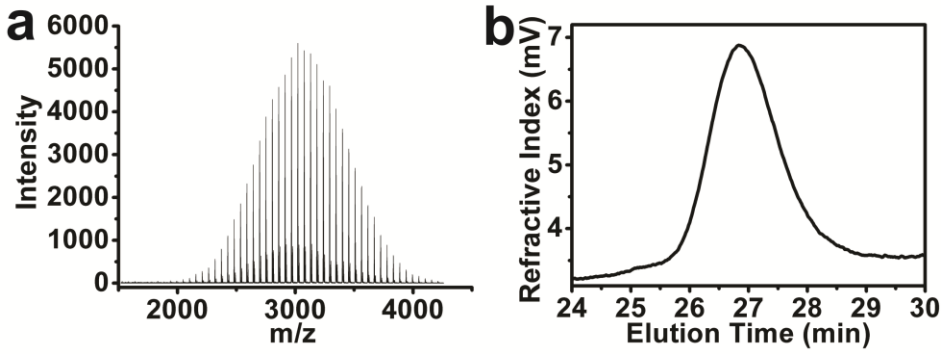

Figure 3.1. MALDI-TOF (a) and GPC spectra (RID trace) (b) of PBD_{52}-OH.

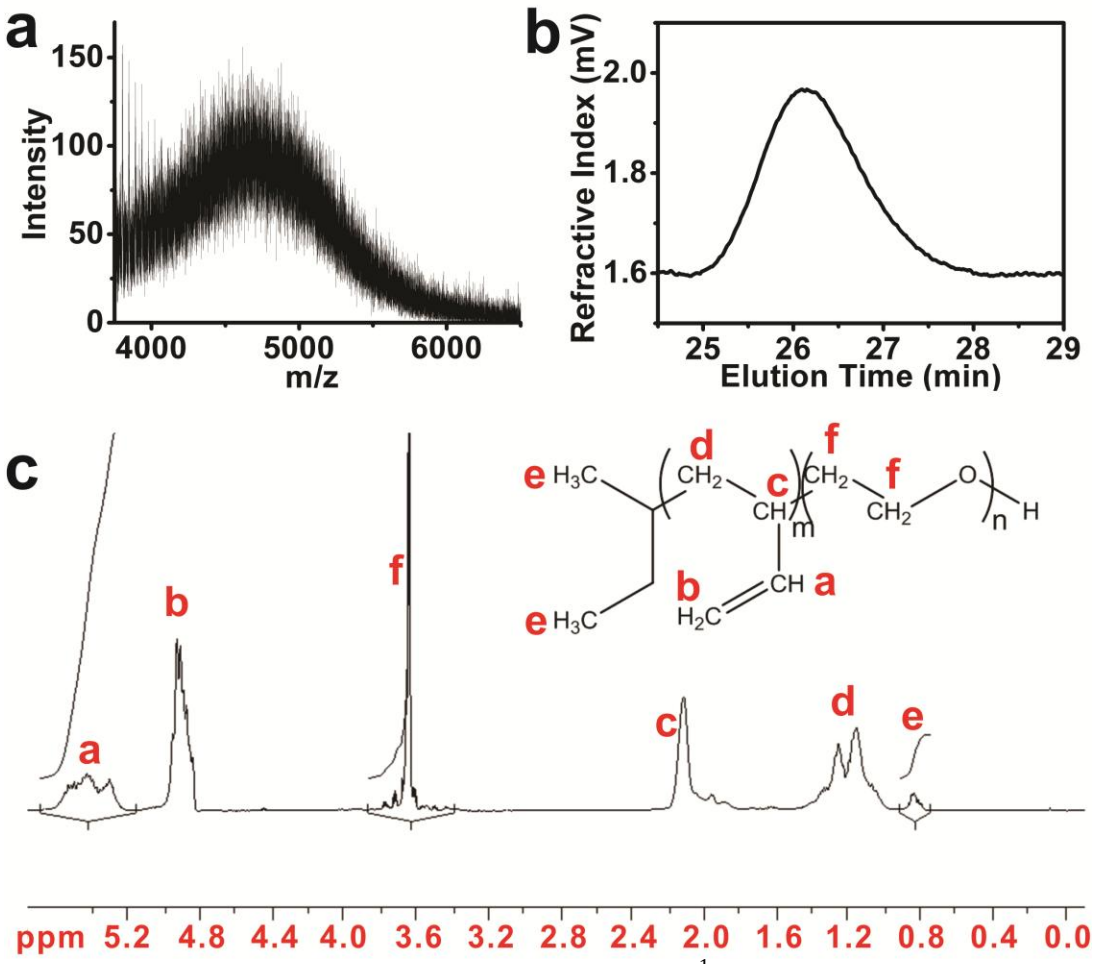

Figure 3.2. MALDI-TOF (a), GPC (RID trace) (a), and ^{1}H NMR spectra (b) of PBD_{52}-*b*-PEO_{32}.

3.2.4 Synthesis of PMA. Acetone solutions of MA (2 mL, 22 mmol), RAFT-2.0 (0.1 M, 2.5 mL) and initiator V-501 (0.02 M, 2.5 mL), and pyrene acrylate (0.075 g) were mixed in a Schlenk flask. Three freeze-pump-thaw cycles were applied to the reaction flask to remove oxygen. The reaction flask was heated at 75 ℃ for 6 h and then cooled down to room temperature. The reaction was stopped by introducing air to flask. The crude product was purified by precipitating in cold methanol using dry ice/acetone bath.

Scheme 3.2. Synthesis of PMA.

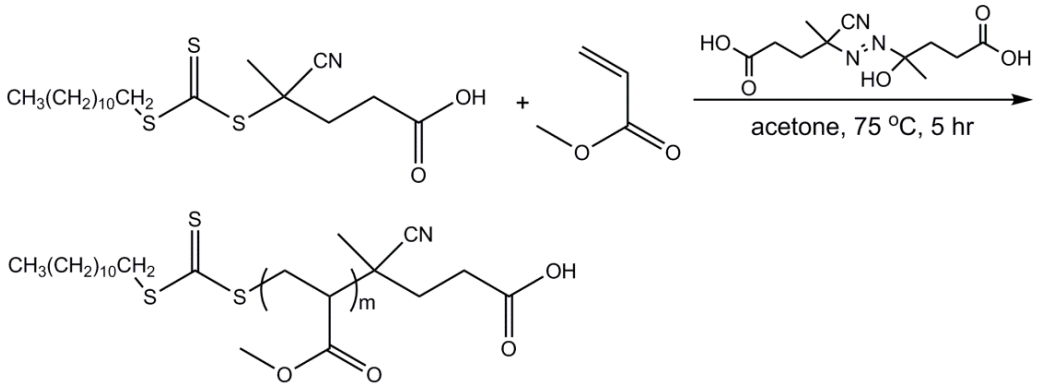

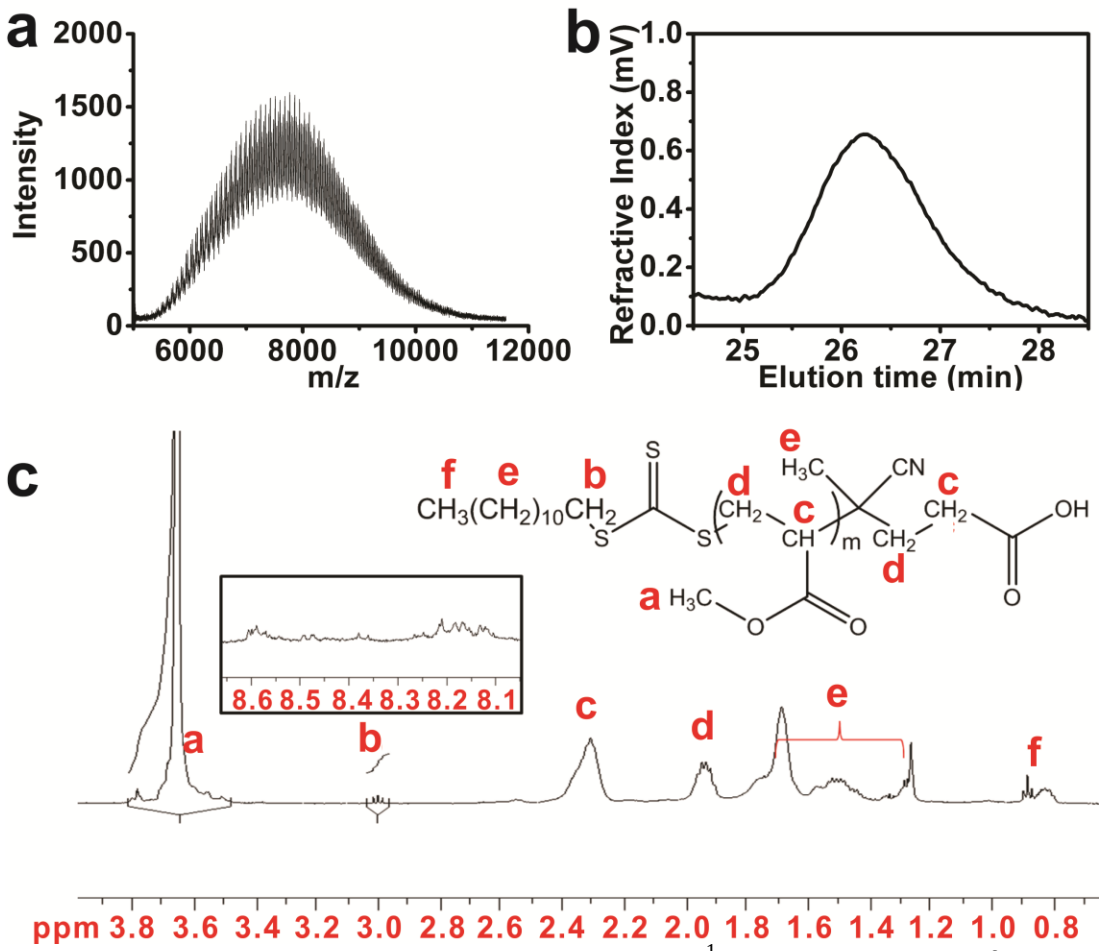

Figure 3.3. MALDI-TOF (a), GPC (RID trace) (b), and ^{1}H NMR spectra (c) of PMA_{82}.

3.2.5 Synthesis of PMA-*b*-DNA. PMA(0.264 g, 34 μmol) was dissolve in 500 μL of anhy-drous DMF. *N*,*N*-diisopropylethylamine (48 μL, 280 μmol) and HATU (13 mg, 34 μmol) were added to the solution.[10] The solution was vortexed for 10min to preactivate coupling reaction. 5'-amino-modified DNA on CPG solid support (ca. 1 μmol, MMT deprotected) was added to the activated solution. The mixture was kept on shaker at room temperature overnight. The CPG beads were washed with about 200 mL of DMF to remove unbound PMA homopolymers. The DNA block copolymer was cleaved from beads via treating in about 1 mL of concentrated ammonia at 65 ℃ for 2 h and ammonia was evaporated afterwards. The CPG beads were filtered off and subsequently washed with about 4 mL of H_2O. The resulting crude DNA block copolymers and unbound single strand DNAs were isolated by PAGE gel electrophoresis.

3.2.6 Purification of PMA-*b*-DNA. Gel electrophoresis was performed using Bio-Rad Criterion 15% TBE PAGE precast gels. Crude product solutions (1 mL) were concentrated down to 100 μL, separated into ten 10 μL portions, and loaded onto each lane of the gel loading well. The gel was run in 1×Tris/boric acid/EDTA (TBE) buffer at 200 V for 60 min. The lowest electrophoresis mobility band was cut with a razor blade and crushed mechanically in a centrifuge tube. Water (5 mL) was added to the tube which was then placed on a shaker overnight at room temperature to extract DNA block copolymers from gel pieces. The DNA block copolymer solution was dialyzed against water using dialysis tubing (10-12 kDa MWCO) for 2 days to remove salts.

3.2.7 Preparation of PBD-*b*-PEO and PMA-*b*-DNA hybrid assemblies. Polymersomes were prepared by film hydration method. Fifty microlitters PBD_{52}-*b*-PEO_{32} $CHCl_3$ solution (4 mg/mL) was mixed with 10 μL PMA-*b*-DNA (2.928E-6 M)

DMSO solution. The solution was first dried under nitrogen and flowed by evaporation of DMSO and $CHCl_3$ residue under vacuum > 6 h. Addition of 500 μL 0.1 M PBS buffer (100 mM NaCl, 10 mM phosphate buffer pH=7.17) and heating at 50 ℃ for 12 h led to the formation of mixed giant vesicles.

3.2.8 Preparation of DNA polymersome aggregates. In a typical experiment, 100 μL polymersome solution was combined with 100 μL polymersome solution functionalized with complementary DNA sequences. The mixture was incubated at 55 ℃ for 5 min then allowed to cool down to room temperature overnight prior to measurement.

3.2.9 Control experiments. In a typical experiment, 100 μL polymersome solution was combined with 100 μL polymersome solution functionalized with complementary DNA sequences in water. The mixture was incubated at 55 ℃ for 5 min then allowed to cool down to room temperature overnight prior to measurement.

In a typical experiment, 100 μL polymersome solution was combined with 100 μL polymersome solution functionalized with non-complementary DNA sequences in 0.1 M PBS buffer. The mixture was incubated at 55 ℃ for 5 min then allowed to cool down to room temperature overnight prior to measurement.

In a typical experiment, 100 μL polymersome solution was combined with complementary DNA sequences (5.86 nmol) in 0.1 M PBS. The mixture was incubated at 55 ℃ for 5 min then allowed to cool down to room temperature overnight prior to measurement.

Hybridization of DNA polymersomes with plain complementary DNA. In a typical experiment, 100 μL polymersome solution was combined with 100 μL hybrid micelle

solution functionalized with complementary DNA sequences in 0.1 M PBS. The mixture was incubated at 55 ℃ for 5 min then allowed to cool down to room temperature overnight prior to measurement.

3.2.10 Measurements and instrumentation. Dynamic light scattering (DLS) data were taken with a Malvern Zetasizer Nano Series. ^{1}H NMR spectra were collected with Bruker DMX500, using $CDCl_3$. All fluorescent spectra were collected with a Jobin Yvon Horiba Fluorolog3 spectrometer. A Quantum Northwest TLC50 temperature controller was used for temperature dependent fluorescence experiments. Matrix-assisted laser desorption ionization time-of-flight mass spectrometry (MALDI-TOF/TOF MS) spectra were obtained on a Bruker Flex Series MALDI-TOF/TOF MS. GPC measurements were carried out at 30 ℃ at a flow rate of 1.0 mL/min on a Perkin-Elmer Series 10 high-performance liquid chromatography system equipped with two AM gel columns (500 Å, 5 μm; 1000 Å, 5 μm), a Perkin-Elmer 785 UV-vis detector (254 nm), and a Varian star 4090 refractive index (RI) detector calibrated against poly(methyl methacrylate) (PMMA) standards in THF. Optical images of polymersomes were obtained with 488 nm excitation (argon ion laser) and an 40 x objective lens (water immersion 40 x/1.15 NA) using an Olympus Fluoview FV1000 confocal laser scanning microscope equipped with an inverted IX81 microscope.

3.3 Results and discussion

3.3.1 Synthesis of PBD-*b*-PEO. Amphiphilic block copolymer poly(butadiene)-*block*-poly(ethylene oxide) (PBD-*b*-PEO) were synthesized by anionic polymerization following a previously reported procedures. The purified block copolymer was

characterized by MALDI-TOF mass spectroscopy (Figure 3.2a), gel permeation chromatography (GPC, Figure 3.2b) and ^{1}H NMR spectroscopy (Figure 3.2c). The repeating unit numbers of the two blocks were calculated by the ratios between starting material *sec*-butyllithium (δ 0.8 ppm) and PBD, PEO integrals (δ 5.4 ppm, δ 3.6 ppm) on ^{1}H NMR spectrum, respectively (Figure 3.2c). The block copolymer was determined to be PBD_{52}-*b*-PEO_{32}.

3.3.2 Synthesis and purification of PMA-b-DNA. An amphiphilic DNA block copolymer, PMA-*b*-DNA was synthesized through the coupling of carboxylic acid terminated polymethylacrylate (PMA, Mn=7800 kg mol^{-1}) to 5'-amine-modified 25 base oligonucleotide strands (DNA 1: 5'-A10-ATCCTTATCAATATT-FAM-3') attached on solid supports (Figure 3.4a).[10] A green fluorescent dye (6-FAM) was attached at the 3' end of DNA to monitor the presence of DNA. Typically, pyrene acrylate dyes were incorporated into PMA at a ratio of one pyrene molecule per polymer chain to track the presence of PMA (Figure 3.3c). The gel electrophoresis data show that DNA block copolymers were successfully synthesized and purified from the crude product of DNA block copolymers and unbound free DNA (Figure 3.4b); as DNA block copolymers form nanoscale assemblies in water, they remain in the loading well while unconjugated free DNA strands move along the electric field. The successful conjugation was also confirmed by the coexistence of the fingerprint-like absorption peaks of pyrene and the absorption peak of FAM at 494 nm as well as the DNA peak at 260 nm (Figure 3.4c). Based on the absorbance at 494 nm of 6-FAM and 335 nm of pyrene, the molar ratio of the two dye molecules was calculated to be 0.88 to 1, which is close to the predesigned 1:1 ratio. Due to the amphiphilic nature, PMA-*b*-DNA spontaneously form micelles in

water after gel purification. The diameter of the polymer micelles was determined to be 14 nm with the polydispersity index of 0.28 by dynamic light scattering (DLS) (Figure 3.4d).

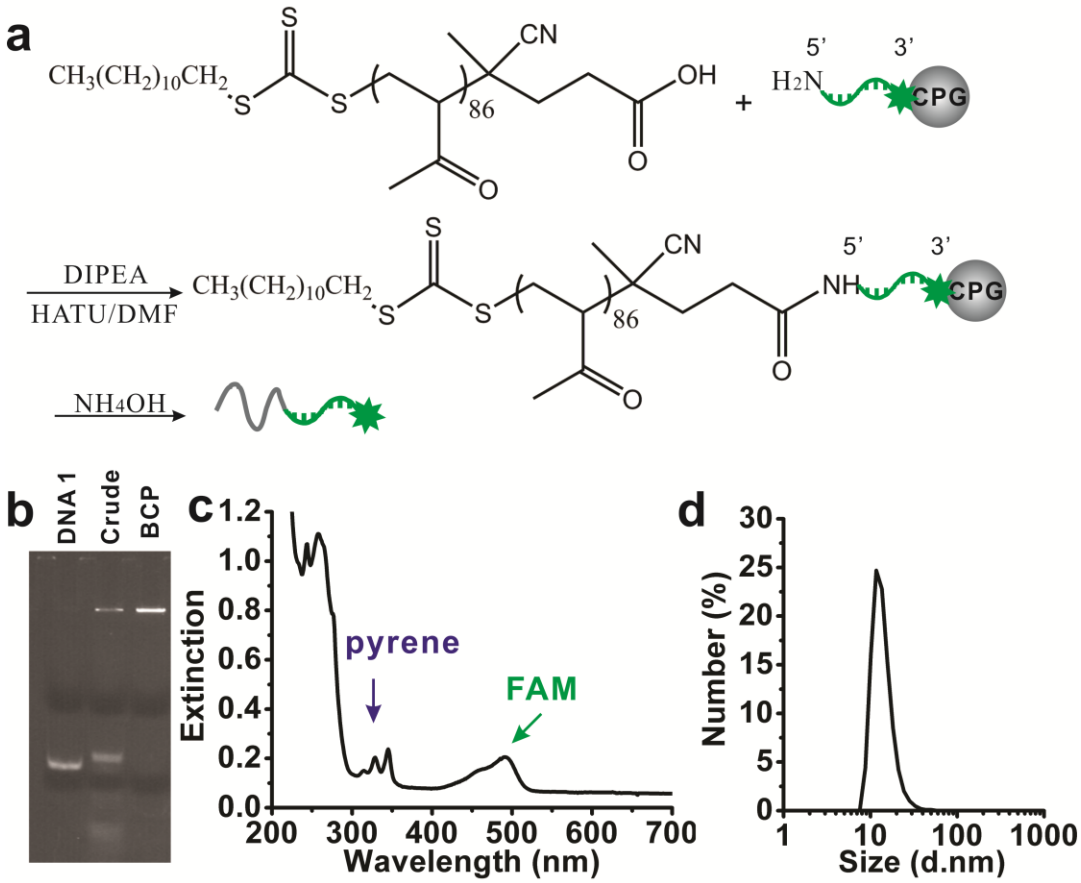

Figure 3.4. (a) Synthesis of PMA-*b*-DNA. (b) PAGE analysis. Lane 1: DNA 1 sequence. Lane 2: crude product containing PMA-*b*-DNA conjugate (top) and unbound DNAs (lower bands). Lane 3: purified PMA-*b*-DNA block copolymer (BCP), purified via gel electrophoresis. (b) Extinction spectrum of purified PMA-*b*-DNA in water. (c) DLS data for purified PMA-*b*-DNA self-assembled into small micelles in water.

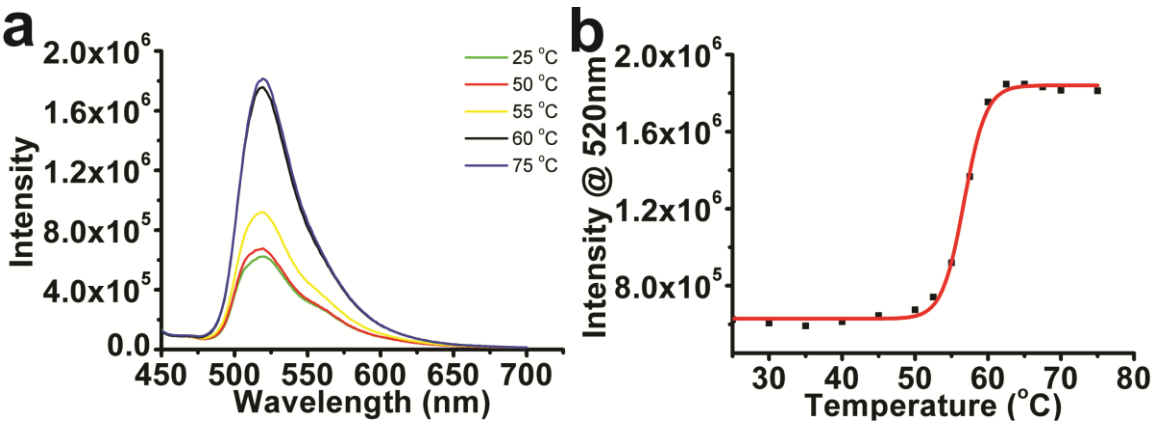

Figure 3.5. Photoluminescence spectra of PMA-*b*-DNA with plain complementary DNA sequence at different temperatures. Melting profiles (b) of the same solution in (a) by monitoring the fluorescence intensity at 520 nm with increasing temperature.

3.3.3 Fabrication of hybrid giant polymersome from PMA-*b*-DNA and PBD-*b*-PEO (DNA polymersome). Giant DNA polymersomes were prepared by the film hydration of PMA-*b*-DNA and PBD-*b*-PEO (Scheme 3.3). PBD-*b*-PEO diblock copolymers can self-assemble into various structures, such as spherical micelles, bilayers and cylinders in water, depending on the relative block ratio.[17] In this study, PBD_{52}-*b*-PEO_{32} with the weight fraction of PEO (w_{PEO}) of 0.33 was used for the hybrid self-assembly, as PBD_{52}-*b*-PEO_{32} readily form giant vesicles by the film hydration method (Figure 3.6a). In typical experiments, PMA-*b*-DNA and PBD_{52}-*b*-PEO_{32} were mixed at a molar ratio of 1: 1600 in $CHCl_3$/DMSO mixture (5$CHCl_3$:1DMSO). The solution (60 uL) was placed on the bottom of a glass vial and dried by the stream of N_2 gas, which generated a thin film of mixed polymers on the bottom of the vial. The film was further dried under vacuum overnight, and then hydrated in 500 uL of 0.1 M phosphate buffered saline (PBS) solution (100 mM NaCl, 10 mM phosphate, pH=7.17). The 12 hour incubation in the buffer produced suspensions of giant vesicles of two polymers. Figure 3.7a,b presents confocal microscope images (Figure 3.6b) of the assemblies formed with 0.062% DNA block copolymer, showing well-defined giant vesicles composed of the hydrophobic inner layer of PBD and PMA and the hydrophilic corona of PEO and DNA (Scheme 3.3). Green fluorescence from vesicles indicates that DNA block copolymers are incorporated into the vesicle membranes. Z-stack images of DNA giant polymersomes obtained by immobilizing them onto a micropipette (Figure 3.7c,d) showed uniform distribution of FAM-labeled DNA on the polymersome surface (Figure 3.7d).

Scheme 3.3. Schematic Description of the Self-Assembly of polymethylacrylate-*block*-DNA (PMA-*b*-DNA) and PBD-*b*-PEO into DNA Polymersome.

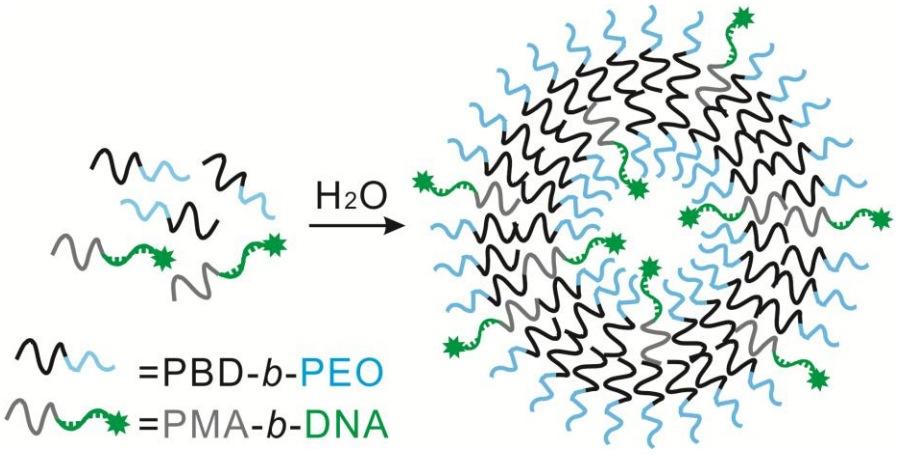

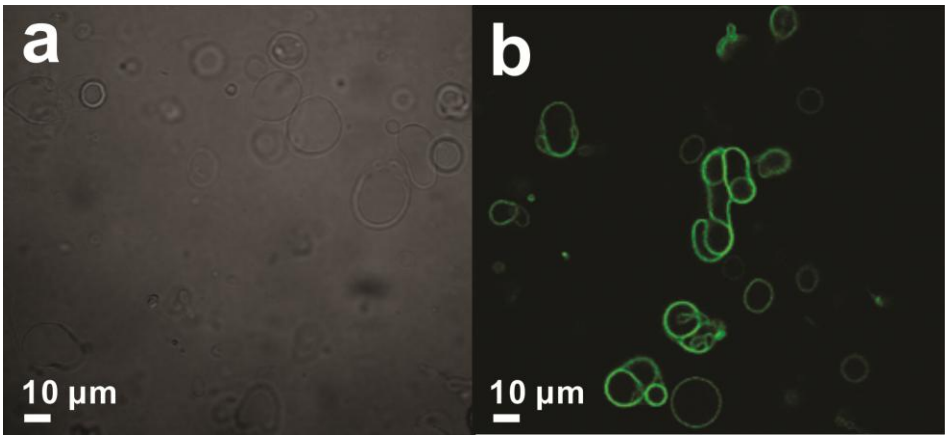

Figure 3.6. (a) Transmission image of polymersomes formed by PBD_{52}-*b*-PEO_{32}. (b) Confocal laser scanning fluorescence image of PBD_{52}-*b*-PEO_{32} and PMA_{82}-*b*-DNA hybrid polymersomes.

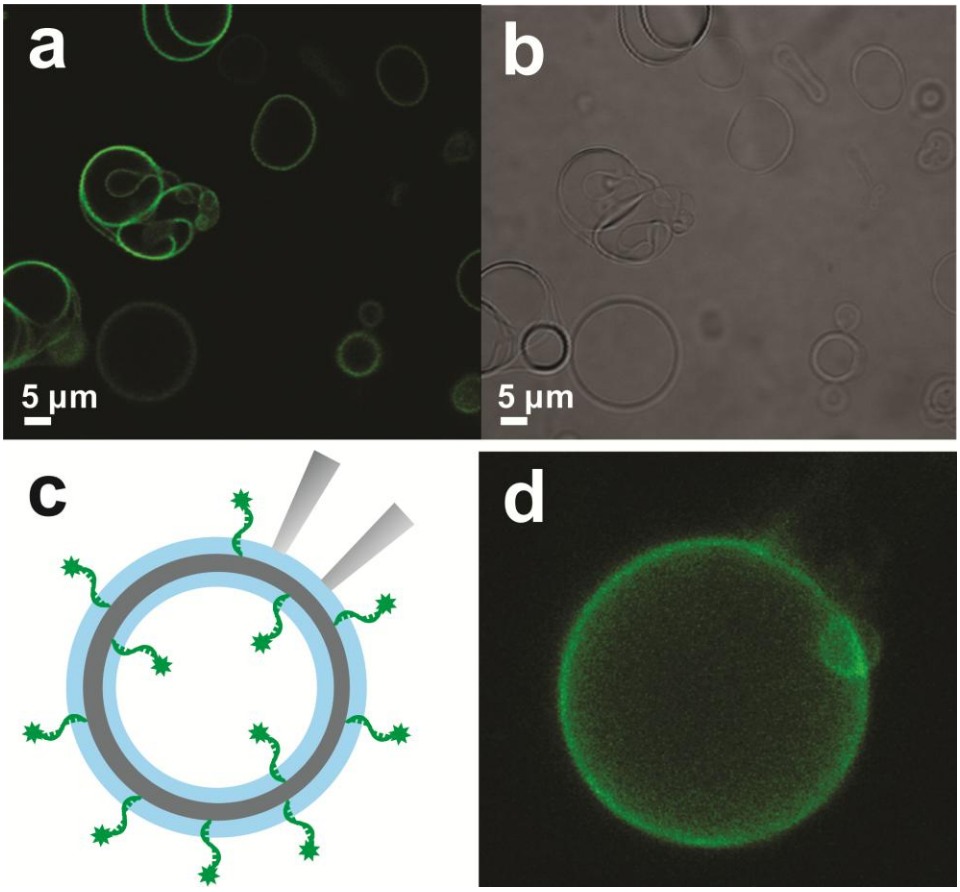

Figure 3.7. (a) Confocal laser scanning fluorescence and (b) transmission images of PBD_{52}-*b*-PEO_{32} and PMA-*b*-DNA hy-brid polymersome (excitation wavelength 488 nm). (c) A pictorial description of DNA polymersome immobilized onto a micropipette. (d) DNA polymersome imaged by z-stacking confocal microscopy during aspiration in micropipette.

3.3.4 Clustering and Phase segregation induced by the self-assemblies of DNA polymersomes.

Two sets of giant DNA polymersomes (polymersome 1 and polymersome 1') were prepared using complementary DNA strands, DNA 1 and DNA 1' (Scheme 3.4). The two sets of giant DNA polymersomes were mixed together in 0.1 M PBS buffer to induce the hybridization of DNA 1 and DNA 1' and the aggregation of giant DNA polymersomes. Optical microscope images taken after 16 hour incubation showed that the giant polymersomes are clustered up as expected (Figure 3.8a, Figure 3.9a,b). In our control experiment where polymersomes 1 and 1' were mixed in water did not show any polymersome clustering (Figure 3.10a,b). Yet, in another control experiment where non-complementary polymersomes were mixed in a 0.1 M PBS buffer, again no clustering was found (Figure 3.10c,d). To further confirm the duplex formation at the junction, we introduced ethidium bromide ethidium bromide to the polymersome clusters. The orange fluorescence observed at the junction area (Figure 3.9b, Figure 3.9c,d) confirms that the polymersome clusters are indeed formed through specific DNA interactions.

Scheme 3.4. Schematic description of the self-assembly of DNA polymersomes.

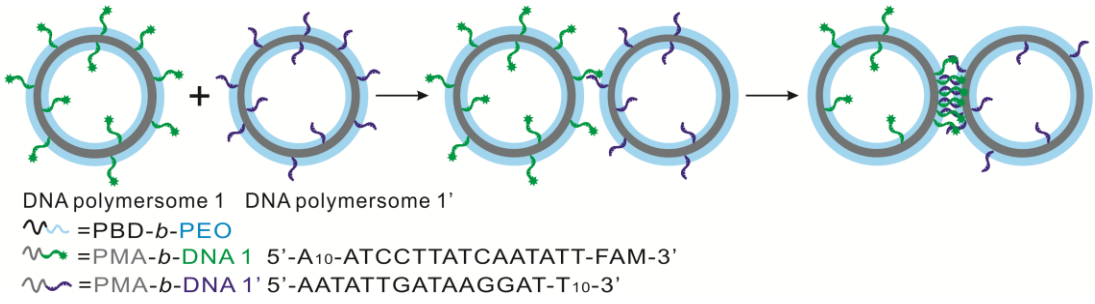

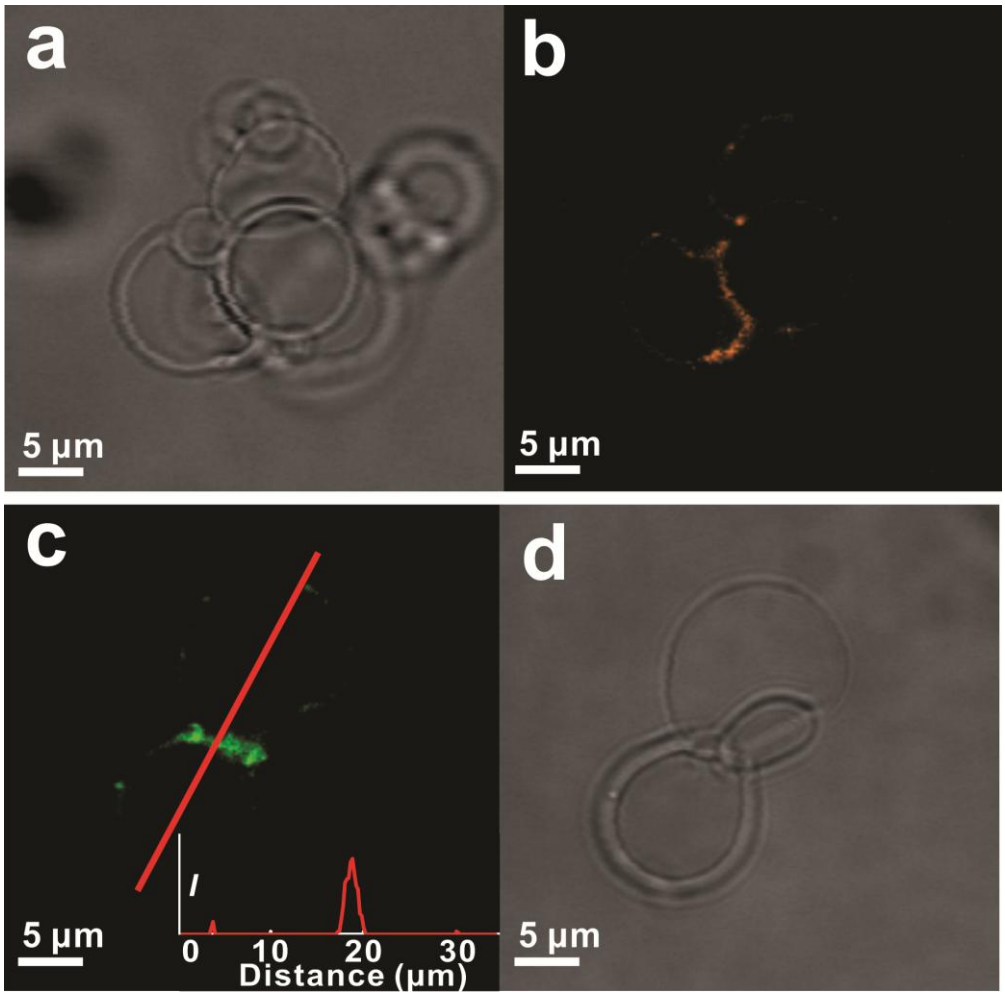

Figure 3.8. (a) Transmission and (b) confocal laser scanning images of phase-separated polymersome clusters (excitation wavelength 515 nm). (c) Confocal laser scanning fluores-cence and (d) Transmission images of phase-separated polymersome clusters resulting from specific DNA hybridization. Inset: An intensity line profile through the junction area and unbound region.

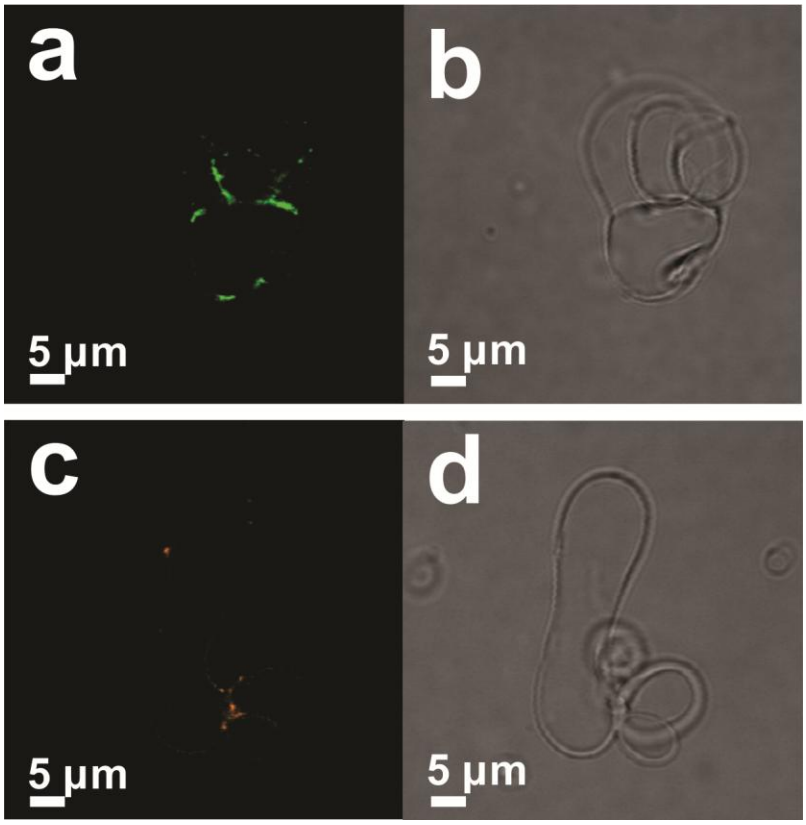

Figure 3.9. (a) Confocal laser scanning fluorescence and (b) Transmission images of phased-spearated polymersome cluster resulting from DNA specific hybridization. (c) Confocal laser scanning fluorescence and (d) Transmission images of phase-separated polymersome cluster stained with ethidium bromide.

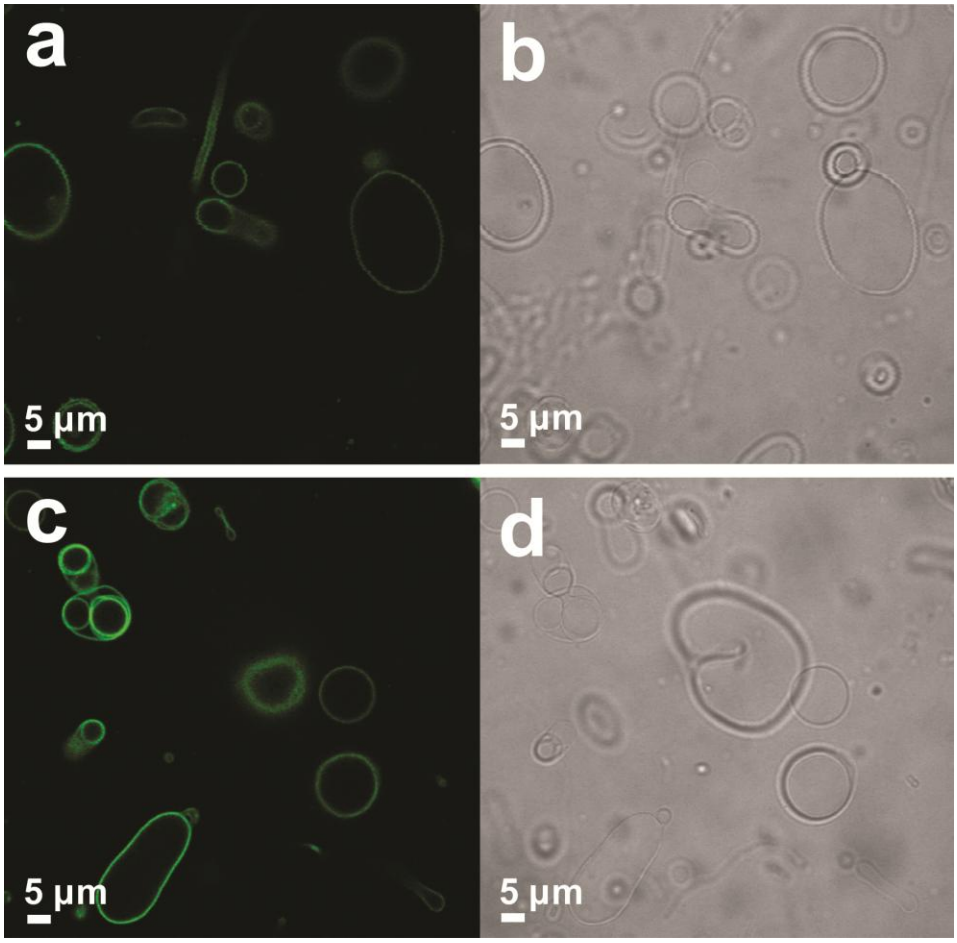

Figure 3.10. (a) Confocal laser scanning fluorescence and (b) Transmission images of complementary hybrid polymersomes mixed in low salt solution. (c) Confocal laser scanning fluorescence and (d) Transmission images of non-complementary hybrid polymersomes mixed in buffer (100 mM NaCl, 10 mM phosphate buffer pH=7.17).

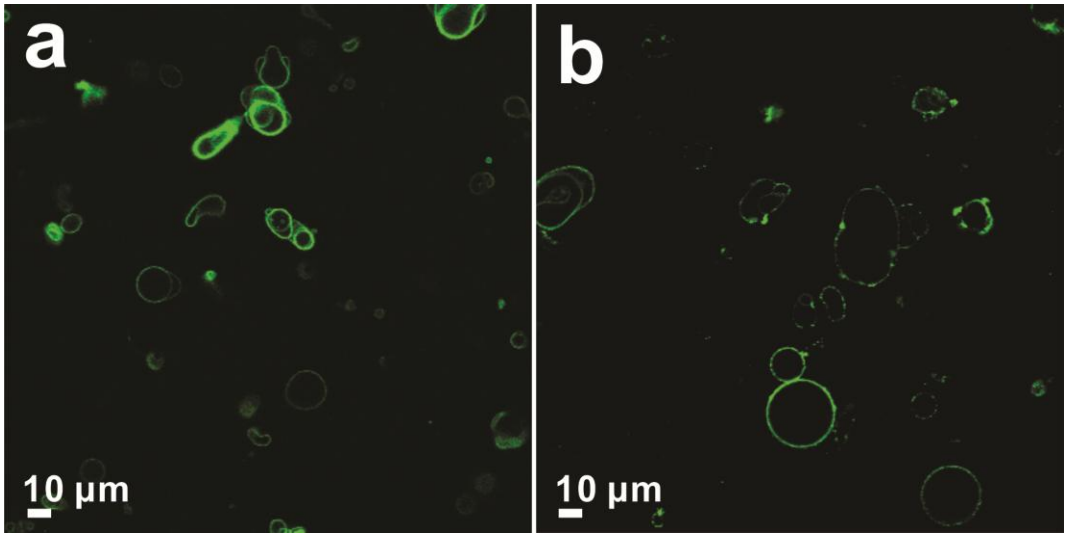

Figure 3.11. (a) Confocal laser scanning fluorescence of hybrid polymersomes mixed with plain complementary DNA. (b) Confocal laser scanning fluorescence image of hybrid polymersomes mixed with complementary DNA hybrid micelles.

3.3.5 Fluorescence intensity studies of DNA rafts on DNA polymersomes, non-junction sites and isolated DNA polymersomes.

Calculation of DNA polymersomes fluorescence intensity. In DNA polymersomes confocal images (Figure 3.12), hybrid polymersomes which are on the focus plane were chosen to analyze. In the two images (Figure 3.12a,d), 2 lines were drawn to create its intensity line profile. Peaks at about 3μm and 18 μm were chosen and averaged as the intensity of hybrid polymersomes (I=29.3).

Calculation of phase-segregation DNA polymersomes fluorescence intensity. In the self-assembly of DNA polymersomes confocal image (Figure 3.13), 10 lines were drawn in different locations to create their intensity line profiles. Peaks at about 20 μm were chosen and averaged as the intensity of junction sites (I=65.8). Peaks at about 5μm and 30 μm were chosen and averaged as the intensity of non-junction sites (I=5.9).

Interestingly, fluorescent microscope images reveal that FAM fluorescence from DNA is localized at the junction between polymersomes (Figure 3.8c,d, Figure 3.9a,b). The intensity line profiles show that the fluorescence intensity at the junction is about eleven times higher than that on the other area (Figure 3.8e, Figure 3.13) and is about two times higher than that on isolated polymersomes (Figure 3.12) by comparing peak intensities on intensity line profiles. This result indicates that polymer strands in the giant vesicles are mobile and DNA block copolymers accumulate at the junction area, creating DNA rafts on polymersome surfaces.

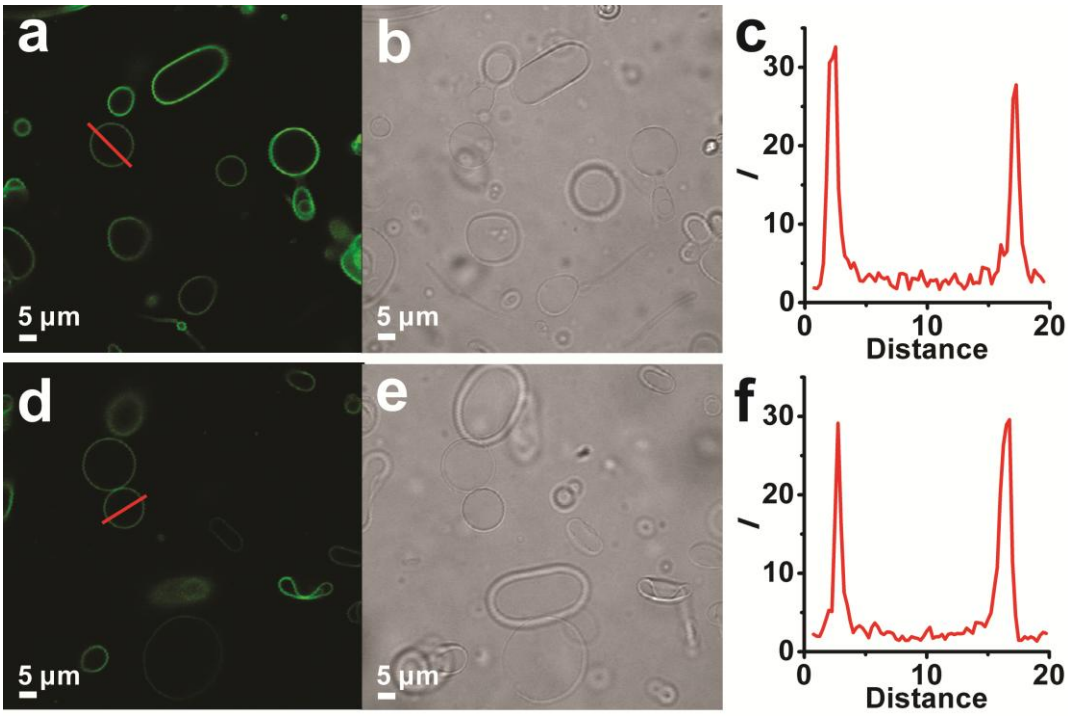

Figure 3.12. (a,d) Confocal laser scanning fluorescence and (b,e) Transmission images and (c,f) intensity line profiles of PBD_{52}-*b*-PEO_{32} and PMA_{82}-*b*-DNA hybrid polymersomes.

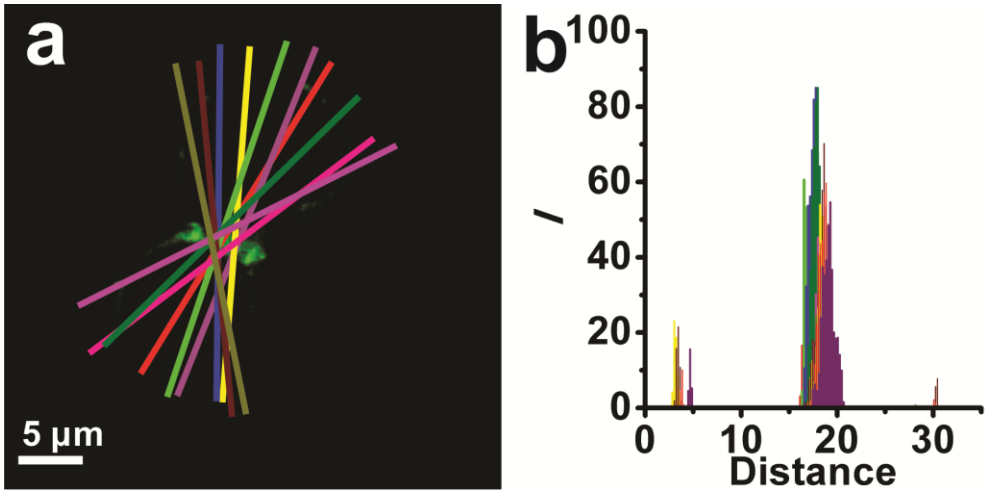

Figure 3.13. (a) Confocal laser scanning fluorescence of phase-separated polymersome cluster resulting from DNA specific hybridization and corresponding intensity line profiles (b).

3.3.6 Fast responsive time scale of DNA polymersomes. It is interesting to note that the full phase segregation occurred at a relatively short time frame. The phase segregation and domain coalescence is fast for liposomes; the phase segregation in liposomes typically takes minutes to hours.[18-20] For polymersomes, the phase segregation is much slower due to the entanglement of large molecular weight polymers. For example, Discher and coworkers reported that segregated polymer domains were developed after 40 hr incubation of micron-sized polymersomes made of PBD-*b*-PEO and poly(butadiene)-*block*-poly(acrylic acid) (PBD-*b*-PAA) in a solution containing cross-bridging polyvalent cations.[14] In another example, nanometer-sized hybrid polymersomes made of PBD-*b*-PEO and poly(2-(diisopropylamino)ethyl methacrylate)-*block*-poly((2-methacryloyloxy)ethyl phosphorylcholine) (PDPA-*b*-PMPC) showed the evolution of surface patterns over the time-scale of more than a month.[15] The DNA polymersomes in this work showed full phase segregation at a time scale comparable to the responsive time shown for liposomes. We attribute the fast phase separation occurred for DNA polymersomes studied here to the thermodynamic drive of forming multiple DNA linkages between conjoined polymersomes. In other words, the DNA segregation occurs to maximize the number of DNA binding and the cooperative DNA inter-actions promote the phase segregation.

3.4 Conclusions

In summary, we have fabricated mixed assemblies of DNA block copolymers (PMA-*b*-DNA) and a prototypical block copolymer of PBD-*b*-PEO. Binary self-assembly of PBD-*b*-PEO and PMA-*b*-DNA at low DNA block copolymer content adopt the morphology of PBD-*b*-PEO and form giant polymersomes, where DNA block copolymers are uniformly distributed in the membrane. Note that DNA block copolymer alone typically forms small micelles in water due to the highly charged DNA backbone.[21] Mixed assembly reported here provides a way to form various types of DNA block copolymer assemblies that are difficult to make on their own. Interestingly, when the hybrid giant polymersomes with complementary DNA strands were mixed together in buffer to induce clustering of polymersomes, DNA block copolyemrs segregated from the matrix polymer of PBD-*b*-PEO to the binding area, forming DNA rafts at the junction between polymersomes. The phase segregation occurred at relatively short time frame. Phase segregation in polymersomes typically takes much longer period (days to months) than lipids due to the entanglement of long polymer strands. The efficient phase segregation observed here was attributed to the thermodynamic drive of forming multiple DNA linkages between polymersomes. This phase segregation has important consequences in DNA melting properties of mixed assemblies, which will be discussed in Chapter 4. We believe that this work is the first to demonstrate the efficient DNA-induced phase segregation in mixed polymer assemblies.

3.5 References

(1) Cutler, J. I.; Auyeung, E.; Mirkin, C. A. *J. Am. Chem. Soc.* **2012**, *134*, 1376-1391.

(2) Banga, R. J.; Chernyak, N.; Narayan, S. P.; Nguyen, S. T.; Mirkin, C. A. *J. Am. Chem. Soc.* **2014**, *136*, 9866-9869.

(3) Cutler, J. I.; Zhang, K.; Zheng, D.; Auyeung, E.; Prigodich, A. E.; Mirkin, C. A. *J. Am. Chem. Soc.* **2011**, *133*, 9254-9257.

(4) Chen, X.-J.; Sanchez-Gaytan, B. L.; Hayik, S. E. N.; Fryd, M.; Wayland, B. B.; Park, S.-J. *Small* **2010**, *6*, 2256-2260.

(5) Li, Z.; Zhang, Y.; Fullhart, P.; Mirkin, C. A. *Nano Lett.* **2004**, *4*, 1055-1058.

(6) Schnitzler, T.; Herrmann, A. *Acc. Chem. Res.* **2012**, *45*, 1419-1430.

(7) Liu, H.; Zhu, Z.; Kang, H.; Wu, Y.; Sefan, K.; Tan, W. *Chemistry – A European Journal* **2010**, *16*, 3791-3797.

(8) Kwak, M.; Musser, A. J.; Lee, J.; Herrmann, A. *Chem. Commun.* **2010**, *46*, 4935-4937.

(9) Alemdaroglu, F. E.; Alemdaroglu, N. C.; Langguth, P.; Herrmann, A. *Adv. Mater.* **2008**, *20*, 899-902.

(10) Rush, A. M.; Thompson, M. P.; Tatro, E. T.; Gianneschi, N. C. *ACS Nano* **2013**, *7*, 1379-1387.

(11) Chien, M.-P.; Rush, A. M.; Thompson, M. P.; Gianneschi, N. C. *Angew. Chem., Int. Ed.* **2010**, *49*, 5076-5080.

(12) Pike, L. J. *J. Lipid Res.* **2006**, *47*, 1597-1598.

(13) Munro, S. *Cell* **2003**, *115*, 377-388.

(14) Christian, D. A.; Tian, A.; Ellenbroek, W. G.; Levental, I.; Rajagopal, K.; Janmey, P. A.; Liu, A. J.; Baumgart, T.; Discher, D. E. *Nat. Mater.* **2009**, *8*, 843-849.

(15) LoPresti, C.; Massignani, M.; Fernyhough, C.; Blanazs, A.; Ryan, A. J.; Madsen, J.; Warren, N. J.; Armes, S. P.; Lewis, A. L.; Chirasatitsin, S.; Engler, A. J.; Battaglia, G. *ACS Nano* **2011**, *5*, 1775-1784.

(16) Hillmyer, M. A.; Bates, F. S. *Macromolecules* **1996**, *29*, 6994-7002.

(17) Jain, S.; Bates, F. S. *Science* **2003**, *300*, 460-464.

(18) Veatch, S. L.; Keller, S. L. *Biophys. J.* **2003**, *85*, 3074-3083.

(19) Beales, P. A.; Nam, J.; Vanderlick, T. K. *Soft Matter* **2011**, *7*, 1747-1755.

(20) Hadorn, M.; Eggenberger Hotz, P. *PLoS ONE* **2010**, *5*, e9886.

(21) Fuks, G.; Mayap Talom, R.; Gauffre, F. *Chem. Soc. Rev.* **2011**, *40*, 2475-2493.

Chapter 4. DNA binding studies of DNA Rafts on hybrid DNA block copolymer assemblies induced by DNA hybridization

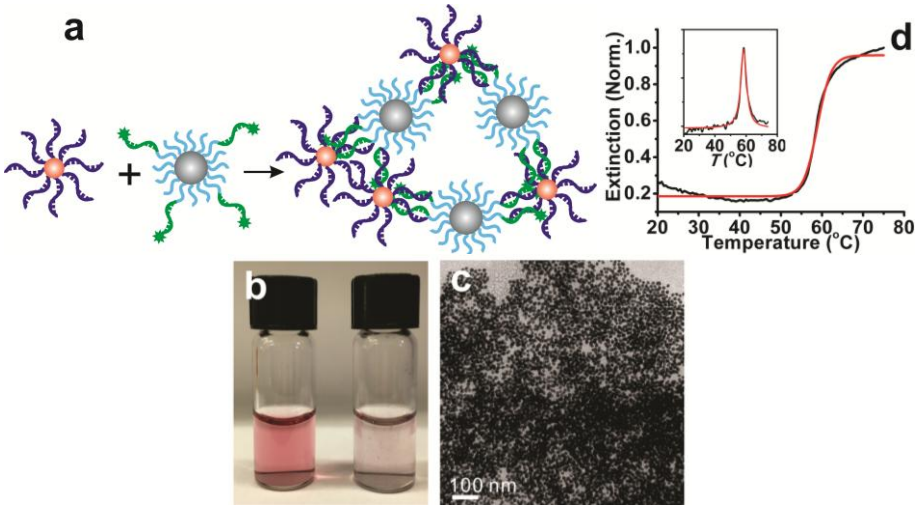

We report the DNA-induced phase segregation and DNA-raft formation in DNA block copolymer assemblies in Chapter 3. Here, DNA triblock copolymer of PBD-b-PEO-b-DNA were synthesized and assembled with a prototypical amphiphilic polymer of poly(butadiene)-block-poly(ethylene oxide) (PBD-b-PEO). The binary self-assembly of PBD-b-PEO-b-DNA and PBD-b-PEO resulted in small assemblies where DNA where DNA strands are hanging outside assembly shell instead of being buried inside the PEO layer. We show the phase segregation has important implications in DNA melting properties, as mixed block copolymer assemblies with low DNA content can still exhibit useful DNA melting properties that are characteristic of DNA nanostructures with high DNA density.

4.1 Introduction

Gold nanoparticles (AuNPs) modified with a dense layer of oligonucleotides[1] have been extensively studied for many applications ranging from materials syntheses[2] to diagnostics and drug delivery.[3-7] The most attractive characteristic of DNA-modified gold particles is their unique DNA melting properties such as sharp melting transitions and high binding constants. Thorough and systematic studies have been carried out to define and evaluate relevant parameters contributing to the unusual melting properties, such as the size of the nanoparticles, the surface density of DNA, the dielectric constant of surrounding medium, etc. These unique properties originate from the cooperative interaction of densely packed DNA strands, and thus they are independent of the core composition.[8]

Recently, significant research has been focused on spherical nucleic acids with cores composed of soft materials, including DNA liposomes and DNA block coopolymer amphiphiles. Liposomes are attractive as they show well-established applications in chemical cargo loading and releasing[9,10] and drug delivery.[11-13] Large DNA-functionalized liposomes have been utilized in the context of DNA-mediated material assemblies,[14-16] while small DNA-functionalized liposomes not only show sharp melting transitions,[17] but also reveal the ability of rapidly entering multiple cell lines and effectively knocking down gene expression via antisense pathways.[18] On the other hand, DNA block copolymer amphiphiles as a novel class of DNA hybrid materials have been thoroughly explored for their potential in drug delivery[19] and gene therapy,[20,21] showing superior chemistry processibilty, functionality and stability to lipid molecules. Tailorable and desired material properties for designated applications can be achieved through

appropriate selection of synthetic polymers and DNA sequences. More importantly, it is well known that the manipulation of block lengths, solvent compositions and other self-assembly parameters have led to the formation of various morphologies of amphiphilic block copolymer assemblies, such as spherical micelles, bilayers and cylinders.[22] The introduction of organic polymers to hydrophilic DNA sequences results in a wide range of amphiphilic structures, for example, micellar structure with hydrophobic core and hydrophilic DNA corona, or vesicular structure with hydrophobic wall and hydrophilic DNA corona, which cannot be obtained by only DNA sequences.

In last chapter, we demonstrated that the hybrid polymersomes undergo efficient phase segregation upon the introduction of complementary DNA polymersomes. The DNA raft formation shown in last chapter is advantageous, as it indicates that the useful DNA binding properties of DNA block copolymer micelles such as sharp melting transition[8] might occur in the hybrid assemblies with low DNA content. In this chapter, we studied their DNA binding properties at these particular sites on hybrid assembly surfaces with varied DNA concentrations. To examine how the phase behavior affects DNA binding properties, we prepared two new sets of hybrid assemblies from DNA triblock copolymers of poly(butadiene)-*block*-poly(ethylene oxide)-*block*-DNA (PBD-*b*-PEO-*b*-DNA) and polystyrene-*block*-poly(ethylene oxide)-*block*-DNA (PS-*b*-PEO-*b*-DNA), which contain low glass temperature polymer PBD and high glass temperature polymer PS, respectively. This new design allows for the formation of hybrid assemblies where DNA strands are not buried inside the PEG layer which can destabilize DNA duplexes.[23]

4.2 Experimental Section

4.2.1 Materials. Tetrahydrofuran (THF) was purified by distillation over Na/benzophenone under argon. Other common solvents such as acetone, methanol, isopropanol, chloroform, and dichloromethane were used as received. *N*,*N*-diisopropylethylamine, sodium hydride, 4-bromomethylbenzoic acid and 1-[Bis(dimethylamino)methylene]-1H-1,2,3-triazolo[4,5-b]pyridinium 3-oxid hexafluorophosphate (HATU) were purchased from Sigma and used as received. PBD_{46}-*b*-PEO_{30} and PS_{48}-*b*-PEO_{45} were purchased from Polymer Sources (Montreal, Canada). Oligonucleotides (DNA 2: 5'-ATCCTTATCAATATT-FAM-3'; DNA 2': 5'-A10-AATATTGATAAGGAT-3') were purchased from Trilink, Inc.

4.2.2 Synthesis of PBD-*b*-PEO-*b*-DNA. PBD-*b*-PEO-*b*-DNA was synthesized by coupling PBD-*b*-PEO and amine-terminated DNA, following a previously reported method.[24] Typically, PBD_{46}-*b*-PEO_{30} (0.129 g, 34 μmol) was dissolved in 500 μL of anhydrous DMF. *N*,*N*-diisopropylethylamine (48 μL, 280 μmol) and HATU (13 mg, 34 μmol) were added to the solution. The solution was vortexed for 10 min to preactivate the COOH group. 5'-amino-modified DNA on CPG solid support (ca. 1 μmol, MMT-deprotected) was added to the solution. The mixture was kept on a shaker at room temperature overnight. Then, the CPG beads were washed with about 200 mL of DMF to remove unbound PBD-*b*-PEO. Synthesized DNA block copolymers were cleaved from the beads by immersing the beads in about 1 mL of concentrated ammonia at 65 ℃. After 2 h reaction, ammonia was evaporated by loosening the vial cap. The CPG beads were filtered and subsequently washed with about 4 mL of water. DNA block copolymers and unbound single strand DNAs were collected and separated by PAGE.

4.2.3 Synthesis of PS-*b*-PEO-COOH. PS-b-PEO-COOH was prepared by converting the hydroxyl end group of PS48-b-PEO45-OH to carboxylic acid, following a literature procedure.[25] Sodium hydride (15 mg) was dissolved in a mixture of THF (2 mL) and DMF (1 mL) and cooled to 0 ℃. 4-bromomethylbenzoic acid (17 mg) dissolved in 1 mL of THF was added dropwise to the mixture. Subsequently, PS-*b*-PEO-OH (0.5 g) dissolved in THF (2 mL) was added dropwise to the mixture. The reaction mixture was then warmed up to room temperature and stirred for 3 days. The reaction was quenched by 10% HCl (0.5 mL) in an ice bath and then the reacted polymer was extracted with dichloromethane (100 mL). The organic phase was washed with saturated $NaHCO_3$ (500 mL) and water (500 mL) to remove unreacted bromomethylbenzoic acid. The dichloromethane solution was dried over anhydrous Na_2SO_4 and concentrated on a rotary evaporator.

Scheme 4.1. Synthesis of PS-*b*-PEO-COOH.

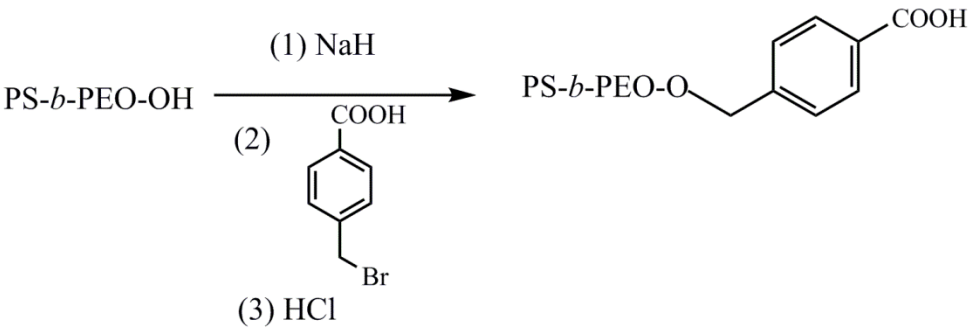

4.2.4 Synthesis of PS-*b*-PEO-*b*-DNA. PS-*b*-PEO-*b*-DNA was synthesized by coupling PS-*b*-PEO-COOH and amine-terminated DNA, following a previously reported method. Typically, PS-*b*-PEO (0.4 g) was dissolved in 500 μL of anhydrous DMF. *N*,*N*-diisopropylethylamine (48 μL, 280 μmol) and HATU (13 mg, 34 μmol) were added to the solution. The solution was vortexed for 10 min to preactivate the COOH group. 5'-amino-modified DNA on CPG solid support (ca. 1 μmol, MMT-deprotected) was added to the solution. The mixture was kept on a shaker at room temperature overnight. Then, the CPG beads were washed with about 200 mL of DMF to remove unbound PS-*b*-PEO. Synthesized DNA block copolymers were cleaved from the beads by immersing the beads in about 1 mL of concentrated ammonia at 65 ℃. After 2 h reaction, ammonia was evaporated by loosening the vial cap. The CPG beads were filtered and subsequently washed with about 4 mL of water. DNA block copolymers and unbound single strand DNAs were collected and separated by PAGE.

4.2.5 Purification of PBD-*b*-PEO-*b*-DNA and PS-*b*-PEO-*b*-DNA. Gel electrophoresis was performed using Bio-Rad Criterion 15% TBE PAGE precast gels. Crude product solutions (1 mL) were concentrated down to 100 μL, separated into ten 10 μL portions, and loaded onto each lane of the gel loading well. The gel was run in 1×Tris/boric acid/EDTA (TBE) buffer at 200 V for 60 min. The lowest electrophoresis mobility band was cut with a razor blade and crushed mechanically in a centrifuge tube. Water (5 mL) was added to the tube which was then placed on a shaker overnight at room temperature to extract DNA block copolymers from gel pieces. The DNA block copolymer solution was dialyzed against water using dialysis tubing (10-12 kDa MWCO) for 2 days to remove salts.

4.2.6 Preparation of PBD-*b*-PEO-*b*-DNA and PBD-*b*-PEO hybrid assemblies. Mixed small micelles were prepared by passing the assemblies formed by the film hydration method described in last chapter, and through the membrane extrusion filter. Typically, 100 μL of PBD-*b*-PEO-*b*-DNA (DMSO, 4.0 μM) solution was mixed with 35 μL of PBD_{46}-*b*-PEO_{30} solution ($CHCl_3$, 0.4 mg/mL) for mixed assemblies with 10 mol% DNA block copolymer content or with 38 μL of PBD_{46}-*b*-PEO_{30} solution ($CHCl_3$, 0.04 mg/mL) for mixed assemblies with 50 mol% DNA block copolymer contents. The mixture was placed into a glass vial and the solvent was evaporated under vacuum for at least 6 h. Then, 100 μL of 0.1 M PBS buffer (100 mM NaCl, 10 mM phosphate buffer pH=7.17) was added to the polymer film in the vial. The solution was vortexed, frozen and thawed 5 times before the extrusion. Finally, the sample was extruded 38 times through Whatman Nucleopore track-etch membrane with pore size of 400 nm.

4.2.7 Preparation of PS-*b*-PEO-*b*-DNA and PS-*b*-PEO hybrid assemblies. Mixed small micelles were prepared by passing the assemblies formed by the film hydration method described in last chapter, and through the membrane extrusion filter. Typically, 145 μL of PS-*b*-PEO-*b*-DNA (DMSO, 3.0 μM) solution was mixed with 35 μL of PS_{48}-*b*-PEO_{46} solution ($CHCl_3$, 0.74 mg/mL) for mixed assemblies with 10 mol% DNA block copolymer content or with 38 μL of PS_{48}-*b*-PEO_{46} solution ($CHCl_3$, 0.074 mg/mL) for mixed assemblies with 50 mol% DNA block copolymer contents. The mixture was placed into a glass vial and the solvent was evaporated under vacuum for at least 6 h. Then, 100 μL of 0.1 M PBS buffer (100 mM NaCl, 10 mM phosphate buffer pH=7.17) was added to the polymer film in the vial. The solution was vortexed, frozen

and thawed 5 times before the extrusion. Finally, the sample was extruded 38 times through Whatman Nucleopore track-etch membrane with pore size of 400 nm.

4.2.8 Synthesis of DNA-functionalized gold nanoparticles. DNA-functionalized gold nanoparticles were synthesized by following a literature procedure.[26] In a typical experiment, 1.5 mL of 57.55 nM citrate stabilized gold nanoparticle solution was mixed with 47.5 μL of 380 μM thiolated-DNA sequence, and 3453 μL of Mili-Q water was used to bring up the solution to 5 mL in total volume. The finally concentrations of gold nanoparticles and DNA sequences were 17 nM and 3.61 μM, respectively. The mixture was put on a shaker to shake overnight. Phosphate buffer saline (PBS, 1 M NaCl, 100 mM phosphate, pH = 7.17) was gradually added to the mixture to increase its salt concentration. Generally, 55.56 μL of PBS buffer was added to the solution every 20 min for 10 times. Eventually, nanoparticles were dispersed in 0.1 M PBS buffer (100 mM, 10 mM phosphate buffer, pH = 7.17). The solution was sat on a shaker for 2 days. The unconjugated DNA sequences were removed by centrifugation later on. The solution was centrifuged at a speed of 17K for 20 min. The supernatant was discarded and nanoparticles were collected and redispersed in 0.1 M PBS (100 mM NaCl, 10 mM phosphate buffer, pH = 7.17). The centrifuge cycle was repeated for twice. DNA-functionalized gold nanoparticles were dispersed and kept in 0.1 M PBS buffer.

4.2.9 Preparation of DNA hybrid assemblies and gold nanoparticles aggregates. To prepare DNA hybrid assemblies and gold nanoparticles aggregates, 3.2 nM DNA functionalized AuNPs were mixed with each DNA mole percent small micelle solution (100 μL) at a total volume approximate 1 mL. The solutions were frozen in dry ice for 3 min, and thawed to facilitate hybridization prior to thermal denaturation experiments.

For annealing studies, each of the macroscopic gold aggregates was heated at 50 ℃ for 16 h and then cooled down to room temperature before measurements were taken.

4.2.10 DNA melting studies of hybrid assemblies and nanoparticles aggregates. Melting studies were monitored in a quartz cuvette equipped with stir bar by UV-vis spectroscopy. We chose surface plasmon peak of gold nanoparticles at 520 nm which is sensitive to nanoparticle aggregation to monitor the hybridization and dehybridization processes.

4.2.11 Control experiments. For DNA binding studies of hybrid assemblies and nanoparticles aggregates without pre-annealing, 3.2 nM DNA functionalized AuNPs were mixed with each DNA mole percent small micelle solution (100 μL) at a total volume approximate 1 mL. The solutions were frozen in dry ice for 3 min, and thawed to facilitate hybridization prior to thermal denaturation experiments.

For DNA binding studies of plain dsDNA with annealing, 3.05 nmol plain ssDNA (5’ ATC CTT ATC AAT ATT 3’) was mixed with equal amount of ssDNA (5’ AAT ATT GAT AAG GAT 3’) in 1 mL of 0.1 M PBS. The solutions were frozen in dry ice for 3 min, and thawed to facilitate hybridization. The solution was heated at 50 ℃ for 16 h and then cooled down to room temperature prior to thermal denaturation experiments.

4.2.12 Measurements and instrumentation.

Dynamic light scattering (DLS) data were taken with a Malvern Zetasizer Nano Series. UV-vis absorption spectra were obtained with an Agilent 8453 spectrometer. Transmission electron microscopy (TEM) images were taken on FEI-Tecnai T12 using acceleration voltage of 120 kV.

4.3 Results and discussion

4.3.1 Synthesis and purification of PBD-*b*-PEO-*b*-DNA and PS-*b*-PEO-*b*-DNA.

The DNA triblock copolymer, PBD-*b*-PEO-*b*-DNA was synthesized with DNA 2 (5'-ATCCTTATCAATATT-FAM-3') and PBD-*b*-PEO (Mn: 3800 kg mol^{-1}, w_{PEO}: 0.34), following the same procedure used for DNA diblock copolymers. The synthesized polymers were purified by the gel electrophoresis (Figure 4.1a). The purified DNA triblock copolymers showed distinct DNA absorption peak at 260 nm and 6-FAM peak at 480 nm (Figure 4.1b), as expected. The DNA triblock copolymers spontaneously form big aggregates when cleaved from CPG beads, showing a broad peak at 343.8 nm in diameter with polydispersity index (PDI) of 0.54 (Figure 4.1c). And PS-*b*-PEO-*b*-DNA (Mn: 7000 kg mol^{-1}, w_{PEO}: 0.29) was synthesized and purified by PAGE using the same method. The triblock copolymer formed small aggregates in water with 35.7 nm in diameter and 0.20 of PDI (Figure 4.2).

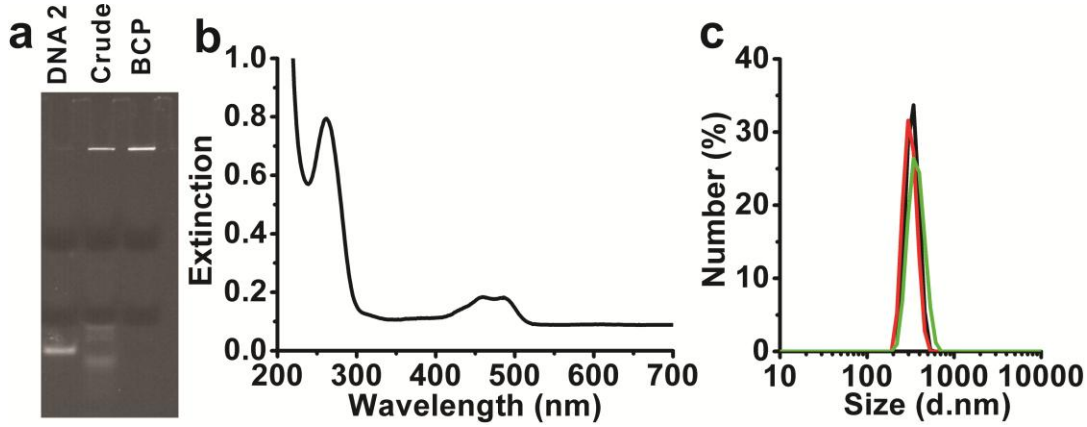

Figure 4.1. (a) PAGE analysis. Lane 1: DNA 1 sequence. Lane 2: crude product containing PBD-*b*-PEO-*b*-DNA conjugate (top) and unbound DNAs (lower bands). Lane 3: purified PBD-*b*-PEO-*b*-DNA block copolymer (BCP), purified via gel electrophoresis. (b) Extinction spectrum of purified PBD-*b*-PEO-*b*-DNA in water. (c) DLS data for purified PBD-*b*-PEO-*b*-DNA self-assembled into big aggregates in water.

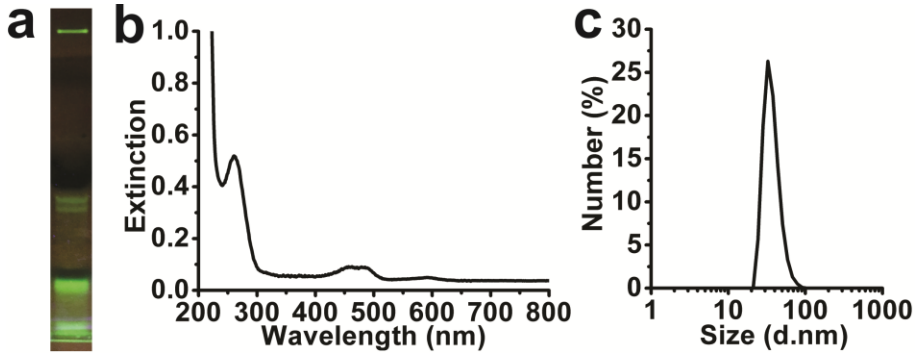

Figure 4.2. (a) PAGE analyses of crude product of PS-*b*-PEO-*b*-DNA. The higher band in the loading well corresponds to PS-*b*-PEO-*b*-DNA and lower bands are for unbound DNA. (b) Extinction spectrum of purified PS-*b*-PEO-*b*-DNA in water. (c) DLS data of purified PS-*b*-PEO-*b*-DNA micelles in water.

4.3.2 Characterization of DNA hybrid assemblies. To prepare hybrid assemblies, PBD-*b*-PEO-*b*-DNA was mixed with PBD_{46}-*b*-PEO_{30} at varying molar ratios (100 mol%, 50 mol%, 10 mol% of PBD-*b*-PEO-*b*-DNA) in small amount of $CHCl_3$/DMSO mixture (4$CHCl_3$:1DMSO). Suspensions of hybrid polymer assemblies were prepared following the procedure described in chapter 3 for diblock copolymers. The polymer suspensions were extruded through a polycarbonate membrane filter with 400 nm pores to obtain uniform nanoscale hybrid assemblies for DNA melting studies. Transmission electron microscopy (TEM) images showed that spherical assemblies were formed by the procedure (Figure 4.3). The diameters of the assemblies were determined to be 62 nm, 63 nm, 65 nm (PDI: 0.22, 0.23, 0.24) for 100%, 50%, 10%, respectively, by DLS (Figure 4.4). The mixed assemblies of PS-*b*-PEO-*b*-DNA and PS_{48}-*b*-PEO_{46} were prepared by the same method. The diameters of assemblies were determined to be 170 nm, 145 nm, 267 nm (PDI: 0.16, 0.20, 0.26) for 100%, 50%, 10 %, respectively (Figure 4.5). The mixed assemblies made from PS are larger than those made from PBD, since the molecular weight of PS-*b*-PEO is slightly higher than that of PBD-*b*-PEO.

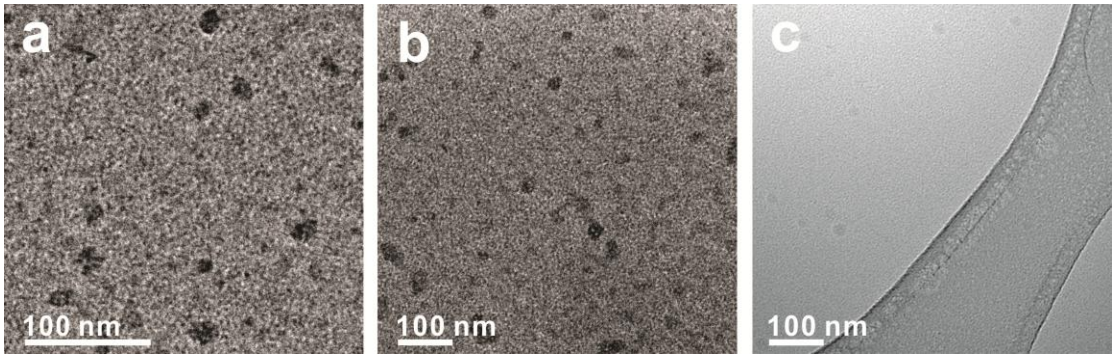

Figure 4.3. (a and b) A TEM image of assemblies composed of PBD-*b*-PEO and PBD-*b*-PEO-*b*-DNA (100 mol% and 50 mol% DNA block copolymer, respectively) in 0.1 M PBS buffer (100 mM NaCl, 10 mM phosphate buffer pH=7.17). (c) Cryo-TEM image of PBD-*b*-PEO and PBD-*b*-PEO-*b*-DNA mixed assemblies with 10 mol% DNA density in 0.1 M PBS buffer.

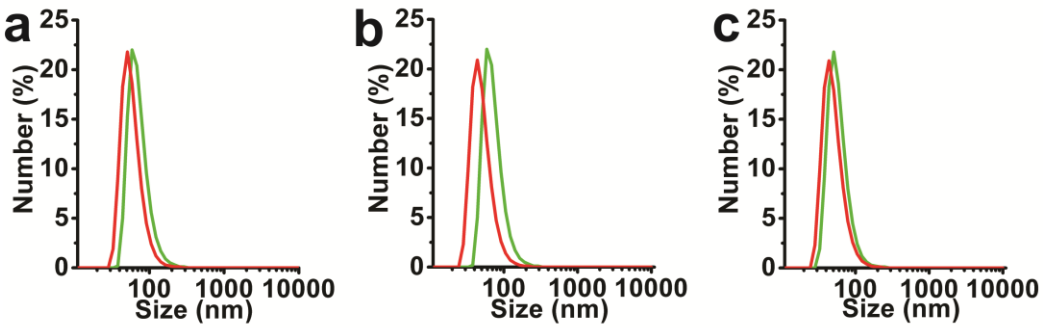

Figure 4.4. DLS data for hybrid assemblies made of PBD-*b*-PEO and PBD-*b*-PEO-*b*-DNA with 100 mol% (a), 50 mol% (b), and 10 mol% (c) DNA block copolymer content. Different colors represent data collected for different batches of hybrid assemblies.

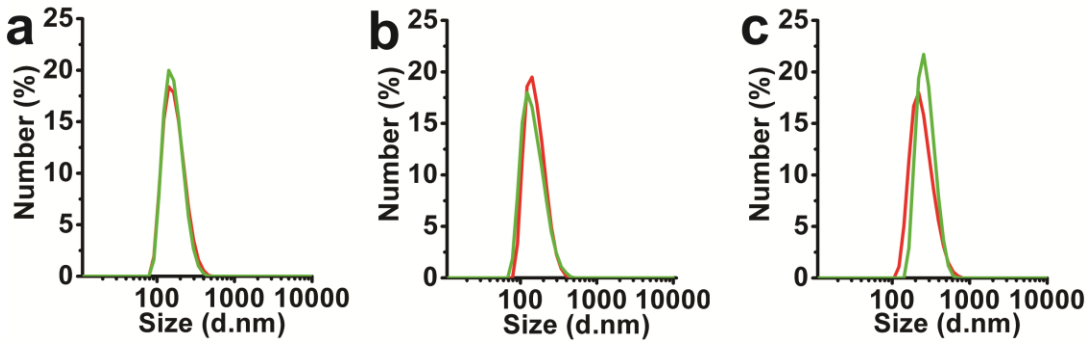

Figure 4.5. DLS data for hybrid assemblies made of PS-*b*-PEO and PS-*b*-PEO-*b*-DNA with 100 mol% (a), 50 mol% (b), and 10 mol% (c) DNA block copolymer content. Different colors represent data collected for different batches of hybrid assemblies.

Table 4.1. DLS data of DNA triblock copolymer hybrid assemblies.

	DNA mol%	PDI	d. nm (Number)
PBD-*b*-PEO-*b*-	100	0.217	61.6
DNA	50	0.234	63.8
	10	0.243	65.2
PS-*b*-PEO-*b*-DNA	100	0.158	170.9
	50	0.199	145.2
	10	0.262	267.3

4.3.3 DNA melting properties of hybrid assemblies with pre-annealing. To investigate the melting properties of hybrid DNA assemblies, AuNPs modified with DNA 2' (5'-A10-AATATTGATAAGGAT-3') were mixed with DNA triblock copolymer assemblies in 0.1 M PBS buffer, as illustrated in Scheme 4.1. The mixtures were then incubated at 50 ℃ for 16 hr to facilitate the polymer strand migration and DNA duplex formation. The DNA hybridization connects nanoparticles with PBD-*b*-PEO-*b*-DNA polymer assemblies or PS-*b*-PEO-*b*-DNA assemblies with high DNA concentration on surfaces (100 mol% and 50 mol%) together into macroscopic aggregates (Figure 4.6). This assembly process causes a red-shift and broadening of 520 nm (SPR) band of gold nanoparticles and corresponding red to purple color change (Figure 4.7). The melting curves were obtained by monitoring the extinction of gold nanoparticles at 520 nm (Figure 4.7). A sharp melting transition was observed for the assemblies made of 100 mol% PBD-*b*-PEO-*b*-DNA (FWHM: 1.9 ℃), as expected, due to the cooperative interaction of densely packed DNA strands (Figure 4.7a, Figure 4.8a).[27] Hybrid assemblies containing 50 mol% (Figure 4.7b, Figure 4.8b) or 10 mol% DNA block copolymers (Figure 4.7c, Figure 4.8c) showed only slight broadening in the transition with narrow FWHM values of 2.4 ℃ and 4.1 ℃, respectively. And the sample with 10 mol% DNA of PS-*b*-PEO-*b*-DNA showed much broader melting transition (FWHM: 7.7 ℃) (Figure 4.7d, Figure 4.8d). The melting curve of plain dsDNA is given for comparison, which showed a much broader melting transition (FWHM: 9.8 ℃) (Figure 4.10). We attribute the sharp melting transitions with reduced concentration of PBD-*b*-PEO-*b*-DNA on surface to the mobility of PBD polymer strands and the phase segregation described in Chapter 3. During the annealing process, PBD-*b*-PEO-*b*-DNA

strands are segregated and form locally concentrated DNA rafts at the binding sites, which allows for the cooperative binding even at low DNA contents. By contrast, assemblies made from PS-*b*-PEO-*b*-DNA with high DNA mole percentages (50% and 100%) can form network aggregates with gold nanoparticles and show sharp melting transitions (Table 4.2), however, low percentage DNA can barely produce aggregates and broad melting transition was observed (Figure 4.7d). We believe that PS is high *Tg* polymer and not mobile at the annealing temperature (50 ℃). Thus low DNA concentration 10 mol% was not sufficient to have high DNA local concentration at binding areas resulting in a broad melting transition. It is also important to note that the melting temperature of 10 mol% PS-*b*-PEO-*b*-DNA is much lower than those of other mixed assemblies, indicating the hybridization is weak between assemblies and nanoparticles due to low DNA concentration at binding areas.

Scheme 4.2. Schematic description of DNA-induced self-assembly of DNA triblock copolymer micelles and DNA-modified gold nanoparticles.

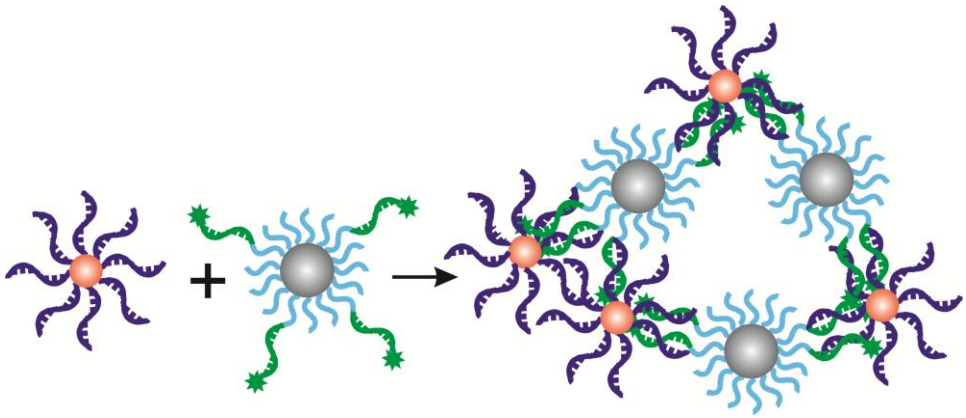

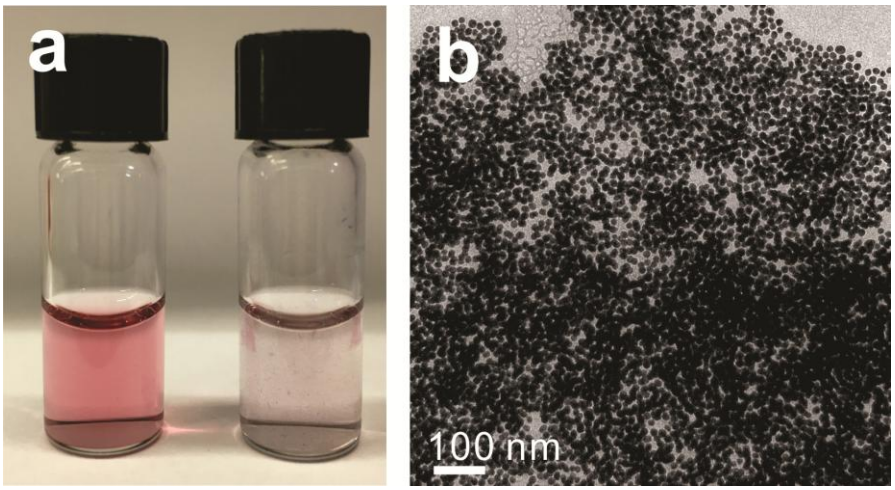

Figure 4.6. (a) A picture of dispersed nanoparticles (left) and nanoparticle aggregates (right). (b) A TEM image of nanoparticle networks.

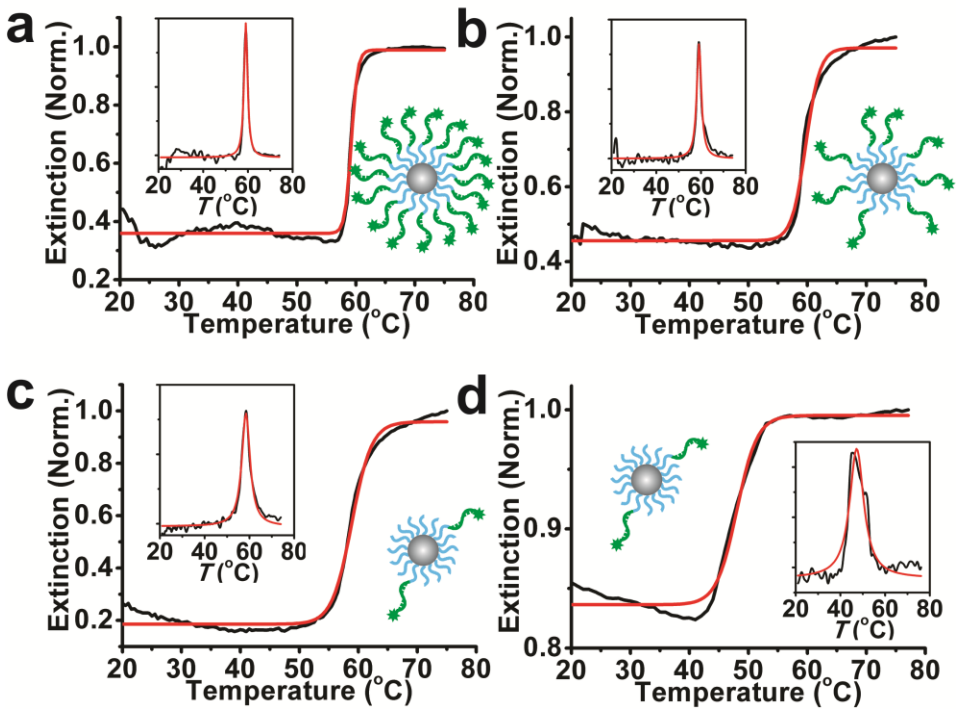

Figure 4.7. DNA Melting transitions of aggregates formed from DNA-modified gold nanoparticles and DNA micelles with (a) 100 mol%, (b) 50 mol%, and (c) 10 mol% DNA triblock copolymer content, and 10 mol% PS-*b*-PEO-*b*-DNA (d), obtained by monitoring the extinction at 520 nm. The insets show the first derivatives of the melting curves. The black and the red curves are experimental data and fitted curves, respectively.

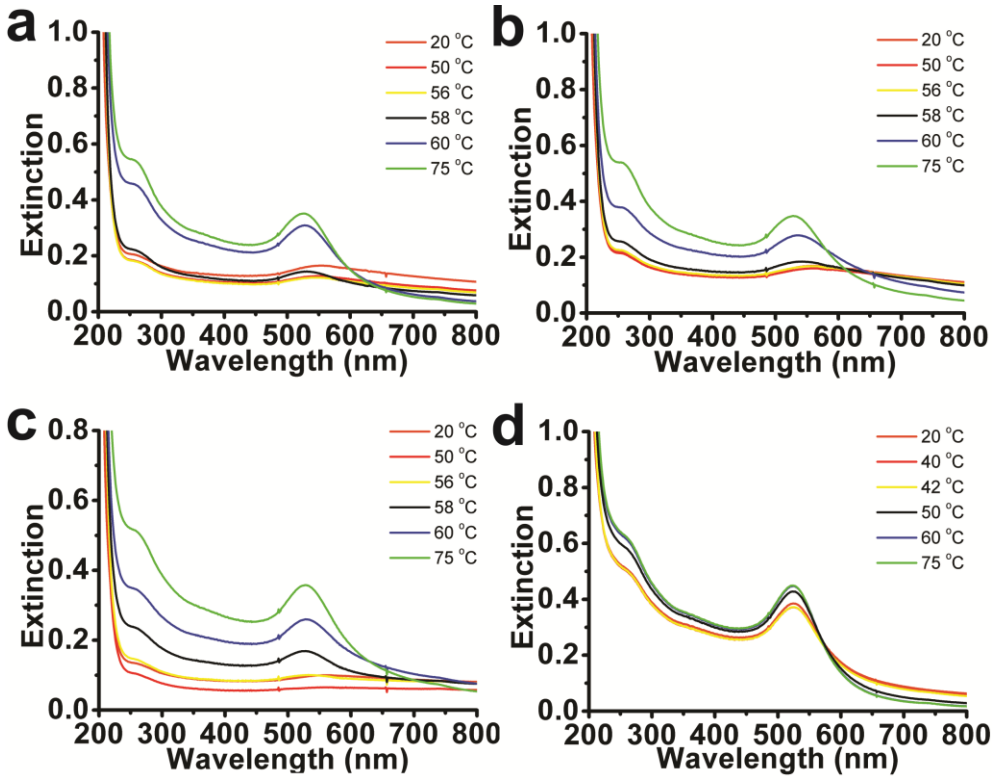

Figure 4.8. Temperature-dependent extinction spectra used to construct the melting curves shown in Figure 4.7 for mixed assemblies made of PBD-*b*-PEO and PBD-*b*-PEO-*b*-DNA with 100 mol% (a), 50 mol% (b) and 10 mol% (c) DNA block copolymer content, and assemblies made of PS-*b*-PEO and PS-*b*-PEO-*b*-DNA with 10 mol% DNA block copolymer content (d).

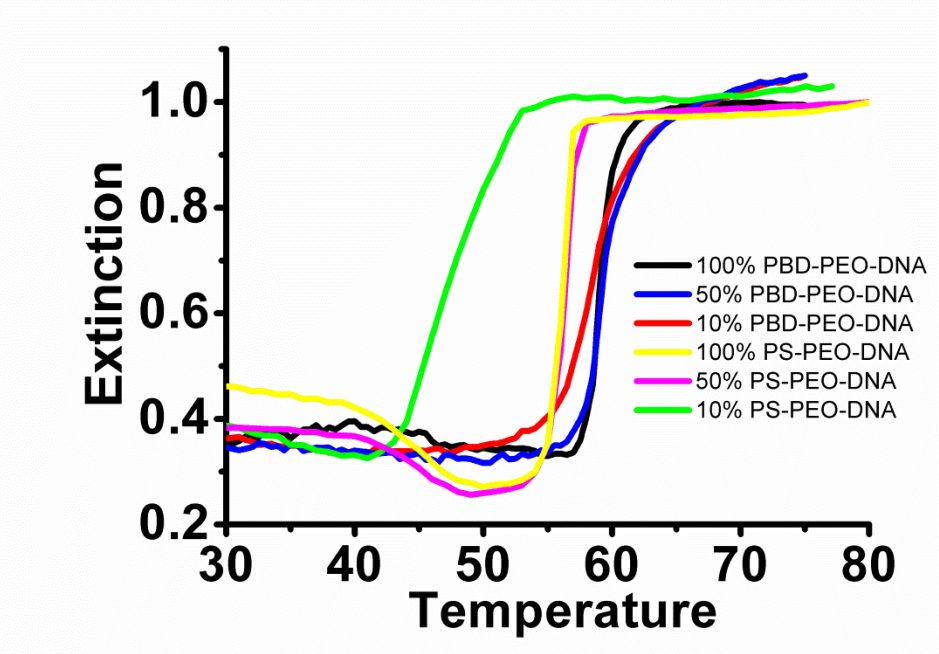

Figure 4.9. Melting profiles of two sets of mixed assemblies from PBD-*b*-PEO-*b*-DNA and PS-*b*-PEO-*b*-DNA with 100 mol%, 50 mol%, and 10 mol% DNA density on surfaces.

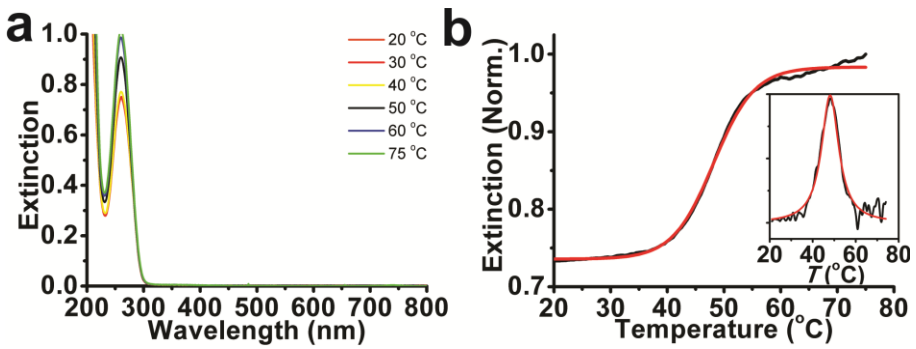

Figure 4.10. (a-b) Melting profile (b) of plain DNA, obtained by monitoring the absorbance at 260 nm with increasing temperature (a).

4.3.4 DNA melting properties of hybrid assemblies without pre-annealing. We also revealed the melting properties of hybrid DNA assemblies and DNA-funcaitonalized AuNPs aggregates without pre-annealing treatment. Similar to procedures mentioned above, AuNPs modified with DNA 2' (5'-A10-AATATTGATAAGGAT-3') were mixed with DNA triblock copolymer assemblies in 0.1 M PBS buffer. However, the mixtures were allowed to hybridize at room temperature overnight instead of incubating at 50 ℃ for 16 hr. The melting curves were also obtained by monitoring the extinction of gold nanoparticles at 520 nm. Sharp melting transitions were not found for the assemblies made of 50 mol% and 10 mol% for both DNA triblock copolymers. Comparing to assemblies composed of 100 mol% DNA triblock copolymer, hybrid assemblies containing 50 mol% or 10 mol% DNA block copolymers showed broadening in the transition with FWHM values (Table 4.2). More interestingly, for both 50 mol% and 10 mol% PBD-*b*-PEO-*b*-DNA assemblies, bumps were observed in pre-melting temperature region. We speculate that before double stranded DNA (dsDNA) sequences dehybridize, polymer strands undergo rearrangement and phase segregation. However, for assemblies made from high *Tg* polymer PS, since polymer strands lack of mobility, these observations were not found (Figure 4.12).

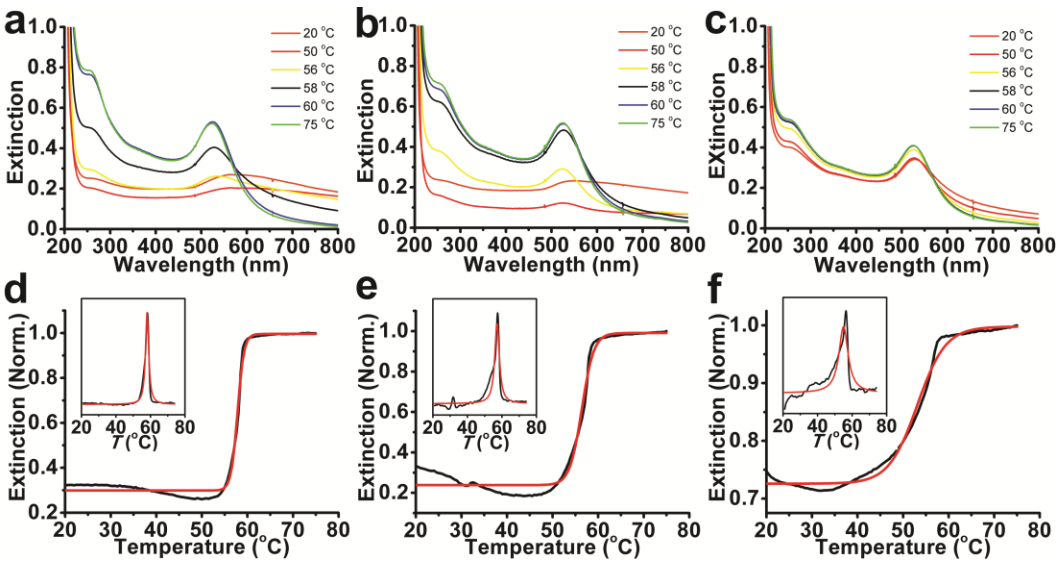

Figure 4.11. Melting profiles of gold nanoparticles and hybrid assemblies made of PBD-*b*-PEO and PBD-*b*-PEO-*b*-DNA with 100 mol% (a,d), 50 mol% (b,e) and 10 mol% (c,f) DNA block copolymer content without thermal annealing.

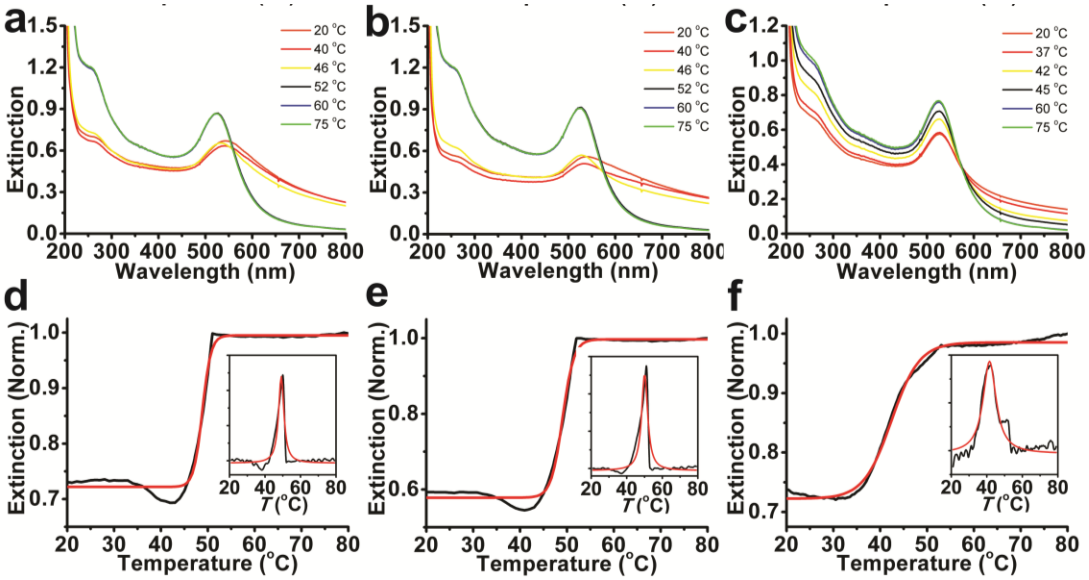

Figure 4.12. Melting profiles of gold nanoparticles and hybrid assemblies made of PS-*b*-PEO and PS-*b*-PEO-*b*-DNA with 100 mol% (a,d), 50 mol% (b,e) and 10 mol% (c,f) DNA block copolymer content without thermal annealing.

Table 4.2. List of *Tm* and FWHM of DNA triblock copolymer hybrid assemblies with or without annealing treatment in 0.1 M PBS.

	DNA mol%	Pre-annealing	*Tm* (℃)	FWHM (℃)
PBD-*b*-PEO-*b*-DNA	100	Yes	59.1	1.9
	50	Yes	59.1	2.4
	10	Yes	58.4	4.1
	100	No	58.1	2.2
	50	No	57.5	2.8
	10	No	56.6	6.7
PS-*b*-PEO-*b*-DNA	100	Yes	56.2	1.8
	50	Yes	56.3	2.0
	10	Yes	45.3	7.7
	100	No	49.9	3.6
	50	No	51.1	4.1
	10	No	41.8	8.9
	Contrl. plain DNA	Yes	48.2	9.8

4.4 Conclusions

In summary, we have fabricated mixed assemblies of DNA block copolymers (PBD-*b*-PEO-*b*-DNA, PS-*b*-PEO-*b*-DNA) and amphiphilic block copolymer of PBD-*b*-PEO and PS-*b*-PEO, respectively. Hybrid micelles formed from PBD-*b*-PEO-*b*-DNA and PBD-*b*-PEO at varying DNA triblock copolymer contents showed that the unique sharp melting transition of DNA block copolymer micelles is maintained in the micelles with 50% and 10% DNA block copolymer. However, mixed assemblies made by PS-*b*-PEO-*b*-DNA and PBD-*b*-PEO did not show sharp melting transition at low DNA concentration due to high *Tg* temperature of PS. Note that it is advantageous to use low DNA block copolymer content in forming DNA decorated polymer nanostructures, as DNA block copolymers are more costly to make than the matrix amphiphilic polymers. We believe that this work is the first to demonstrate the efficient DNA-induced phase segregation in mixed polymer assemblies and to show how it affects the DNA melting properties. The findings of this study demonstrate that the mixed assembly of DNA block copolymers and other commonly used amphiphilic polymers provides an opportunity to form various types of assembly structures that are difficult to make by DNA block copolymer by itself without losing its excellent DNA hybridization properties.

4.5 References

(1) Mirkin, C. A.; Letsinger, R. L.; Mucic, R. C.; Storhoff, J. J. *Nature* **1996**, *382*, 607-609.

(2) Estephan, Z. G.; Qian, Z.; Lee, D.; Crocker, J. C.; Park, S.-J. *Nano Lett.* **2013**, *13*, 4449-4455.

(3) Chan, W. C. W.; Nie, S. *Science* **1998**, *281*, 2016-2018.

(4) Rosi, N. L.; Mirkin, C. A. *Chemical Reviews* **2005**, *105*, 1547-1562.

(5) De, M.; Ghosh, P. S.; Rotello, V. M. *Adv. Mater.* **2008**, *20*, 4225-4241.

(6) Lee, K.; Drachev, V. P.; Irudayaraj, J. *ACS Nano* **2011**, *5*, 2109-2117.

(7) de Vries, J. W.; Zhang, F.; Herrmann, A. *J. Controlled Release* **2013**, *172*, 467-483.

(8) Jin, R.; Wu, G.; Li, Z.; Mirkin, C. A.; Schatz, G. C. *J. Am. Chem. Soc.* **2003**, *125*, 1643-1654.

(9) Hong, J. W.; Quake, S. R. *Nat Biotech* **2003**, *21*, 1179-1183.

(10) Torchilin, V. P. *Nat Rev Drug Discov* **2005**, *4*, 145-160.

(11) LaVan, D. A.; McGuire, T.; Langer, R. *Nat Biotech* **2003**, *21*, 1184-1191.

(12) Allen, T. M.; Cullis, P. R. *Science* **2004**, *303*, 1818-1822.

(13) Bonacucina, G.; Cespi, M.; Misici-Falzi, M.; Palmieri, G. F. *J. Pharm. Sci.* **2009**, *98*, 1-42.

(14) Hadorn, M.; Eggenberger Hotz, P. *PLoS ONE* **2010**, *5*, e9886.

(15) Beales, P. A.; Nam, J.; Vanderlick, T. K. *Soft Matter* **2011**, *7*, 1747-1755.

(16) Beales, P. A.; Vanderlick, T. K. *The Journal of Physical Chemistry A* **2007**, *111*, 12372-12380.

(17) Dave, N.; Liu, J. *ACS Nano* **2011**, *5*, 1304-1312.

(18) Banga, R. J.; Chernyak, N.; Narayan, S. P.; Nguyen, S. T.; Mirkin, C. A. *J. Am. Chem. Soc.* **2014**, *136*, 9866-9869.

(19) Schnitzler, T.; Herrmann, A. *Acc. Chem. Res.* **2012**, *45*, 1419-1430.

(20) Liu, H.; Zhu, Z.; Kang, H.; Wu, Y.; Sefan, K.; Tan, W. *Chemistry – A European Journal* **2010**, *16*, 3791-3797.

(21) Kwak, M.; Musser, A. J.; Lee, J.; Herrmann, A. *Chem. Commun.* **2010**, *46*, 4935-4937.

(22) Burke, S.; Shen, H.; Eisenberg, A. *Macromol. Symp.* **2001**, *175*, 273-284.

(23) Knowles, D. B.; LaCroix, A. S.; Deines, N. F.; Shkel, I.; Record, M. T. *Proceedings of the National Academy of Sciences* **2011**, *108*, 12699-12704.

(24) Rush, A. M.; Thompson, M. P.; Tatro, E. T.; Gianneschi, N. C. *ACS Nano* **2013**, *7*, 1379-1387.

(25) Crimmins, M. T.; Martin, T. J.; Martinot, T. A. *Org. Lett.* **2010**, *12*, 3890-3893.

(26) Storhoff, J. J.; Elghanian, R.; Mucic, R. C.; Mirkin, C. A.; Letsinger, R. L. *J. Am. Chem. Soc.* **1998**, *120*, 1959-1964.

(27) Li, Z.; Zhang, Y.; Fullhart, P.; Mirkin, C. A. *Nano Lett.* **2004**, *4*, 1055-1058.

4.6 Appendix

4.6.1 DNA liposome microarrays. DNA microarrays in a combination of PCR technology allow us to analyze the expression of hundreds of genes in improved speed and accuracy.[1-3] Interested DNA sequences extracted from cell samples are incubated with single stranded DNA sequences which are immobilized on a solid support of DNA microarray. Complementary DNA fragments hybridize with DNA sequences spotted on the array, which further allows for analysis or gene expression. In recent work, DNA-functionalized liposomes were immobilized on the chip and used as nanocontainer for protein detection.[4,5] Water soluble proteins are incorporated into liposome hydrophilic cavity to remain in their real states and avoid denaturation. Therefore, it opens up the possibility of a conversion of DNA chip to protein chip.

Amphiphilc biomolecules like membrane proteins are driven to insert into hydrophobic compartment of vesicles by the minimization of the number of hydrophobic carbon chains exposed to water. If this is the case, the hydrophobic wall of liposome is too thin to hold macromolecules, as its thickness is only about 3 nm.[6] It is revealed that hydrophobic walls of polymersomes have a thickness of 8 nm which is significantly greater than liposomes.[6] Moreover, amphiphilic block copolymers can self-assemble into other morphologies, such as micellar structures, and the loading capacity of hydrophobic cores is expected to be comparable. For example, our previous works have successfully encapsulated high mass percentage of nanoparticles (up to 44%) in a wide range of sizes (from 2 nm to 15 nm) into block co polymer micellar structures.[7-9] Therefore, by replacing lipid molecules with polymers, amphiphilic biomolecules which

usually possess high molecular weights can be encapsulated into more spacious hydrophobic compartment and macromolecule detection chip can be achieved.

4.6.2 Preparation of Streptavidin patterned glass slides *via* Polydimethylsiloxane (PDMS) stamps. Sylgard184 was mixed with curing agent in a 10:1 ratio. After degassing of the mixture, it was poured over the SU-8 photoresist master and baked at 80 ℃ for 60min. PDMS stamps of 1cm x 1cm were cut out directly from the master and then cleaned in 20% ethanol solution for 10 min applying sonication. The stamps were then extensively rinsed with Milli-Q water and dried with filtered air. Streptavidin was diluted in PBS buffer (pH 7.4, Sigma) to 0.2mg/ml and the stamp was inked with streptavidin solution for 60 min. After incubation, the stamp was rinsed with Milli-Q water and dried with filtered air. Glass cover slips were cleaned in air plasma for 10s prior to microcontact printing. Subsequently stamp and cover slip were brought into contact and streptavidin was printed.

4.6.3 Attachment of biotin-DNA to streptavidin patterned glass slides. Biotinylated DNA sequence (5’ TAA CAA TAA TCC-biotin-3’, 72.86 nmol) was dispersed 1 mL of 0.1 M PBS buffer solution (100 mM NaCl, 10 mM phosphate buffer, pH=7.17). Surface patterned streptavidin glass slide was immersed into biotinylated DNA buffer solution and allowed to conjugate overnight. Unbounded biotin-DNA sequences were removed by washing glass slide with excess amount of PBS buffer.

4.6.4 Attachment of 10 mol% DNA triblock copolymer hybrid assemblies to biotin pattern glass slides. Biotin patterned glass slide was incubated with linker DNA (5’ GGA TTA TTG TTA AAT ATT GAT AAG GAT 3’, 2.0 nmol) in 0.1 M PBS buffer for 3 hr at room temperature. Excess amount of linker DNA sequences were washed

away by multiple washes with PBS buffer. The glass slide was further incubated with 200 μL of 10 mol% DNA triblock copolymer hybrid assembly solution in 0.1 M PBS overnight. DNA triblock copolymer assembly surface patterned glass slide was thoroughly washed with 0.1 M PBS buffer before imaging (Scheme 4.3). Images of surface patterned glass slides were obtained using an Olympus Fluoview FV1000 confocal laser scanning microscope equipped with an inverted IX81 microscope. The objective lens (water immersion 40 x / 1.15 NA) imaged sample solutions by exciting 6-FAM with a 488 nm argon laser.

Scheme 4.3. Schematic description of surface patterning using DNA hybrid assemblies.

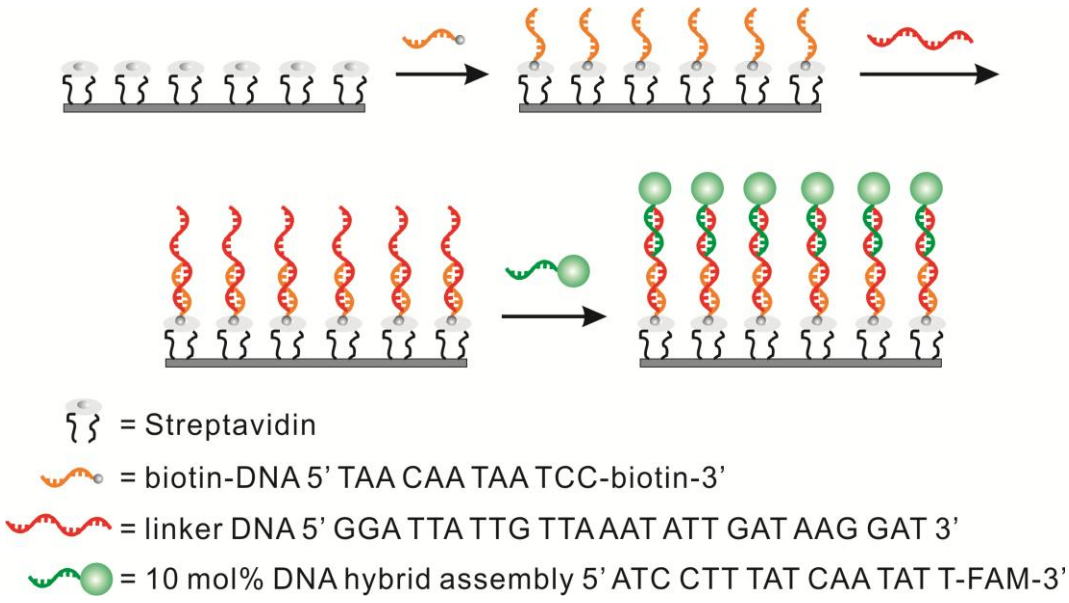

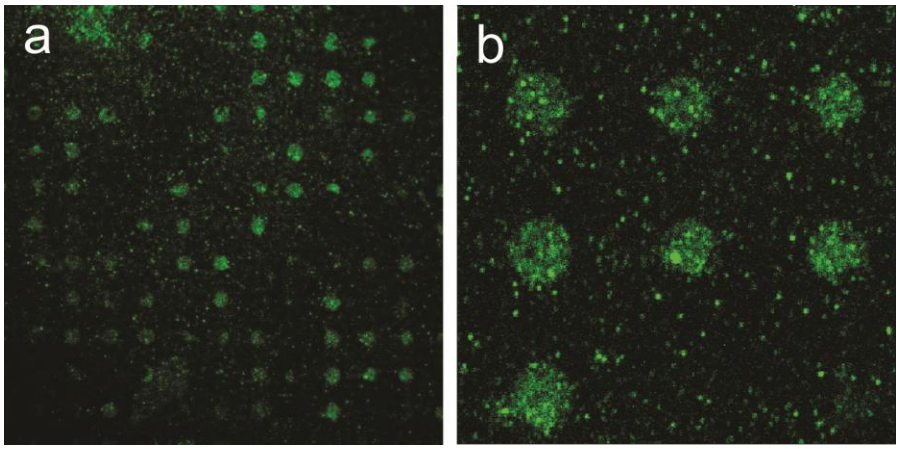

Figure 4.13. Patterning DNA hybrid assemblies. 10 mol% DNA triblock copolymer hybrid assemblies were patterned on an array of biotin with islands 10 μm in diameter and 10μm in spacing. (a,b) Fluorescence microscopy images of the streptavidin stamp overlayed with DNA hybrid assemblies.

4.6.6 References.

(1) Sanders, G. H. W.; Manz, A. *TrAC Trends in Analytical Chemistry* **2000**, *19*, 364-378.

(2) Heller, M. J. *Annu. Rev. Biomed. Eng.* **2002**, *4*, 129-153.

(3) Geschwind, D. H. *The Lancet Neurology*, *2*, 275-282.

(4) Städler, B.; Falconnet, D.; Pfeiffer, I.; Höök, F.; Vörös, J. *Langmuir* **2004**, *20*, 11348-11354.

(5) Chaize, B.; Nguyen, M.; Ruysschaert, T.; le Berre, V.; Trévisiol, E.; Caminade, A.-M.; Majoral, J. P.; Pratviel, G.; Meunier, B.; Winterhalter, M.; Fournier, D. *Bioconjugate Chem.* **2006**, *17*, 245-247.

(6) Discher, B. M.; Won, Y.-Y.; Ege, D. S.; Lee, J. C.-M.; Bates, F. S.; Discher, D. E.; Hammer, D. A. *Science* **1999**, *284*, 1143-1146.

(7) Chen, X.-J.; Sanchez-Gaytan, B. L.; Hayik, S. E. N.; Fryd, M.; Wayland, B. B.; Park, S.-J. *Small* **2010**, *6*, 2256-2260.

(8) Kamps, A. C.; Sanchez-Gaytan, B. L.; Hickey, R. J.; Clarke, N.; Fryd, M.; Park, S.-J. *Langmuir* **2010**, *26*, 14345-14350.

(9) Hickey, R. J.; Haynes, A. S.; Kikkawa, J. M.; Park, S.-J. *J. Am. Chem. Soc.* **2011**, *133*, 1517-1525.

Chapter 5. Lipid Bilayers Assisted Self-assembly of DNA-functionalized Gold Nanoparticles

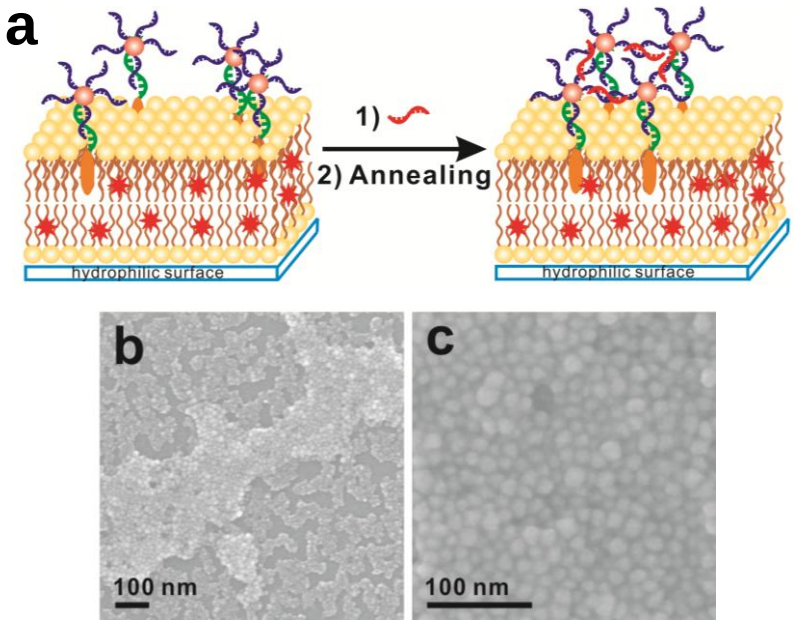

Self-assembly is a ubiquitous approach to fabricate novel supermolecular architectures. Here we demonstrate a strategy to self-assemble DNA-functionalized gold nanoparticles into macroscopic sheets assisted by DNA-tethered lipid bilayers. Cholesterol-DNA conjugates are tethered on lipid bilayers by hydrophobic interaction. We show that the DNA strands are mobile on modified lipid membrane surface by fluorescence recovery after photobleaching (FRAP) experiment. The DNA-tethered lipid bilayers can hybridize with complementary DNA-functionalized gold nanoparticles, and further self-assemble into micron-size nanoparticle sheets by adding linker DNA and annealing. By varying the amount of gold nanoparticles input, the surface coverage can be tuned. Our approach provides a new method for the preparation of versatile scaffolds for nanofabrication and paves the way for organizing functional nanoparticles in a micrometer space.

5.1 Introduction

There has been tremendous effort and interest in DNA-directed assembly which is a powerful means to create macroscopic nanoparticle ordered superlattices using DNA-functionalized nanoparticles as building blocks. Through specific interaction of DNA, nanoparticles functionalized with a dense layer of DNA sequences, can be programmable self-assembled into crystalline structures with controllable structural parameters, such as particle size, periodicity, and interparticle distance.[1] In addition to the three dimensional superlattice structures, previous studies have shown a variety of approaches to fabricate DNA gold nanoparticle conjugate layers on glass substrates, or even free-standing nanoparticle films. For example, early work was reported by Letsinger and co-workers where DNA was used as a particle interconnect for the formation of mono- and multilayers of gold nanoparticles showing application in the area of biodetection.[2,3] Our group has successfully fabricated responsive free-standing films of DNA-linked gold nanoparticles taking advantages of their unique sharp melting transition.[4] Recently, Mirkin and co-workers have shown the novel preparation method for transferrable free-standing DNA nanoparticle superlattice sheets which show a large degree of flexibility and can be post-process to increase their utility.[5] On the other hand, DNA-functionalized lipid bilayers have been widely used as planar platform to construct nanostructures. Because of their simple preparation, easy handling, planar geometry, and surface lateral mobility, lipid bilayers have been considered as ideal structural units for large-scale assemblies. For example, it has been demonstrated DNA origami units can be readily deposited

onto DNA-modified lipid bilayers and assembled into periodic lattices in micrometer-order dimensions.[6] Also the insertion of DNA nanostructures into lipid bilayers results in artificial ion channel mimics made from DNA, which is expected to have applications in basic biological research and nanotechnology.[7] Here, we combine the two useful building blocks and show gold nanoparticles assembly on lipid membranes driven by DNA hybridization event. In the future, appropriate design and careful selection of nanoparticles will allow for the generation of sensing, plasmonic devices.

5.2 Experimental Section

5.2.1 Materials. Cholesterol-modified DNA and thiol-modified DNA were purchased from TriLink BioTechnologies, Inc.: cholesteryl-5'-ATC CTT ATC AAT ATT-FAM-3', and 5'-(C6-S-S-C6)-A_{10}-AAT ATT GAT AAG GAT-3'. Linker DNA sequence was purchased from IDT: 5'-CGCG A ATC CTT ATC AAT ATT-3'. 1,2-dioleoyl-sn-glycero-3-phosphocholine (DOPC) was purchased from Avanti Polar Lipids, Inc. in a chloroform solution (25 mg/mL) and used without further purification.

5.2.2 Preparation of small unilamellar vesicles (SUVs). SUVs were prepared using a published procedure. Twenty five microliters of 25 mg/mL DOPC in chloroform stock solution plus 0.2 mol% fluorophore Texas Red was added to a glass vial and evaporated under air flow. The obtained lipid dry film was further dried under vacuum for at least 3 hr to remove trace of chloroform. The film was

then hydrated with 600 μL 0.1 M PBS buffer solution (100 mM NaCl, 10 mM phosphate pH=7.17) followed by 30 min sonication to form a liposomal suspension. The suspension was further vortexed, frozen, and thawed five times before applied membrane extrusion. To obtain narrow size distribution, the sample was extruded 19 times through a polycarbonate membrane (50 nm pore size, Avanti Polar Lipids, Inc.).

5.2.3 Spread of lipid membranes. Supported lipid bilayers were assembled by placing 30 μL of SUV solution and 70 μL 0.1 M PBS buffer over a glass coverslip (Fisherfinest Premium Cover Glass) on the bottom of a crystallization dish at room temperature. Before spreading liposomes, the coverslips were immersed into piranha solution (3:1 H_2SO_4: 30% H_2O_2 (aq)) for at least 45 min. After washing thoroughly with Milliphore H_2O and dried with air flow, the surfaces were further cleaned by plasma. Excess SUVs were removed from the newly formed supported lipid layer by multiple washings with 0.1 M PBS buffer.

5.2.4 Tether chol-DNAs to lipid bilayers. To prepare DNA-functionalized lipid bilayers, cholesterol modified DNA (0.4 nmol) was pipetted on top to a 2 cm in diameter vesicle membrane surface. At least 45 min was allowed for the chol-DNAs to diffuse into membrane. Excess chol-DNA sequences were washed away by multiple washing with 0.1 M PBS buffer.

5.2.5 Hybridization of AuNPs with DNA-functionalized lipid bilayers. Complementary DNA-modified AuNPs (26.8 pmol) were added to the freshly prepared DNA-functionalized lipid membrane and allowed to hybridize overnight. Again, excess AuNPs were removed by washing with 0.1 M PBS buffer. To prepare

gold nanoparticles assemblies, linker DNA (0.3 nmol) was added to lipid membranes hybridized with AuNPs and heated at 40 ℃ for 16 h and then cooled down to room temperature before imaging.

5.2.6 Thermal stability studies of DOPC lipid bilayers. DOPC lipid bilayers were incubated in 0.1 M PBS at 30 ℃ and 40 ℃ for different time periods. The lipid bilayers were cooled down to room temperature before imaging.

5.2.7 Control experiments. Two control experiments were performed to confirmation the retention of gold nanoparticles was indeed induced by DNA hybridization event. In the first control experiment, DNA-functionalized gold nanoparticles were incubated with complementary DNA-tethered lipid bilayers in pure water. In the second experiment, non-complementary DNA-functionalized gold nanoparticles were incubated with DNA-tethered lipid bilayers in 0.1 M PBS buffer. Another two control experiments were also carried out to proof both linker DNA and annealing are necessary for the formation of large scale nanoparticles assemblies. In the first experiment, DNA-functionalized gold nanoparticles were incubated with lipid bilayers at 40 ℃ overnight in the absence of linker DNA. In the second experiment, DNA-functionalized gold nanoparticles were mixed with lipid bilayers and linker DNA was later added to chamber. The chamber was allowed to sit at room temperature overnight.

5.2.8 Measurements and Instrumentation. Images of lipid bilayers, DNA-functionalized lipid bilayers and AuNP thin films were obtained using the Leica TCS SP8 confocal system. The objective lens was a Leica 20X. The fluorophore

Texas Red was excited by a laser at 552 nm and 6-FAM was excited at 488 nm. Scanning electron microscope (SEM) images were taken with a JEOL 7500F HRSEM at an accelerating voltage of 20 kV. Nanoparticles samples for SEM and GISAX measurements were first washed with excess amount of 0.3 M ammonium acetate solution. Coverslips with gold nanoparticles assemblies were further dried out under vacuum overnight before imaging. Samples for SEM imaging were first deposited with 4 nm Ir to increase conductivity. Samples for confocal microscope were directly imaged in chamber with 0.1 M PBS buffer.

5.3 Results and discussion

5.3.1 Formation of uniform lipid bilayers on hydrophilic glass substrate and their thermal stabilities.

Small unilamellar vesicles (SUVs) stock solution (1 mg/mL) was prepared from DOPC and 0.2 mol% of Texas Red. The solution was further diluted by 0.1 M PBS buffer solution (100 mM NaCl, 10 mM phosphate pH=7.17), and then brought into contact with a hydrophilic glass coverslip which was pretreated with piranha solution (3:1 H_2SO_4:H_2O_2). It is found that varying the concentration of SUV solution from 0.3 to 0.8 mg/mL does not have a big impact on the quality of membranes. Supported DOPC lipid membranes were formed rapidly within 20 min, and the formation of lipid bilayers is even and continuous over the entire slide (Figure 5.1a,b). The surface cleanness of glass slides is crucial to the quality of lipid bilayers. Glass coverslips need to be cleaned with piranha solution and subsequently treated with plasma. Otherwise, phase segregation or uneven surfaces was found. Also, the size of liposomes slightly affects the membrane

quality. Using small liposomes (50 nm), less defects on lipid bilayers were found; however, if larger liposomes were used to spread (> 100 nm), the area of phase segregation increased.

The thermal stability of lipid bilayers over time was also exploited. After lipid bilayers doped by Texas red were successfully formed on the hydrophilic glass substrate, different temperatures were used to incubate the lipid bilayers, and they were imaged at varied time intervals. The lipid bilayers maintain intact over long time period (>12 h) when incubated at 30 ℃, indicated by red fluorescence uniformly spread over the entire slide (Figure 5.2a,b). While a higher incubation temperature 40 ℃ was applied, the lipid bilayers were intact for the first few hours (~ 6 hr); however, overnight incubation led to the visualization of discrete lipid domains in red fluorescent images (Figure 5.2c,d). The continuity of DOPC lipid bilayers was perturbed by the long time incubation at high temperature. Further cooling down following the overnight incubation was attempted to regain the continuity, nevertheless, lipid domains were still presented and long range continuous lipid bilayers were not recovered. Therefore, the deformation of lipid bilayers caused by overnight incubation at high temperature is an irreversible process.

5.3.2 Fabrication of DNA-anchored lipid bilayers. One popular approach to anchor DNA nanostructures onto lipid membranes is employing the modification of nucleic acid with hydrophobic groups, such as porphyrin,[8,9] α-tocopherol[10] and cholesterol.[11,12] Cholesterol (chol) was chosen for surface functionalization in this work as the hydrophobic component. Due to its amphiphilicity, chol-DNA conjugate

buries its hydrophobic moiety into lipid bilayer hydrophobic core, anchoring DNA sequence onto the outer monolayer of lipid membranes. DNA surface functionalization process was carried out by incubating lipid membranes with chol-DNA conjugates in a home-built chamber for 60 min at room temperature. A green fluorescent dye (6-FAM) was attached at 3' end of DNA to monitor the presence of chol-DNA conjugate (Scheme 5.1). The unbound chol-DNA was then removed from the surface by exchanging 10 times the incubation buffer with 0.1 M PBS, never allowing the supported lipid bilayers to dry out. The preparation led to homogenous and continuous green fluorescence over the entire slide, indicating chol-DNA uniformly tethered on lipid surface (Figure 5.1c,d).

Scheme 5.1. Schematic Description of DNA-functionalized Lipid Bilayers Preparation.

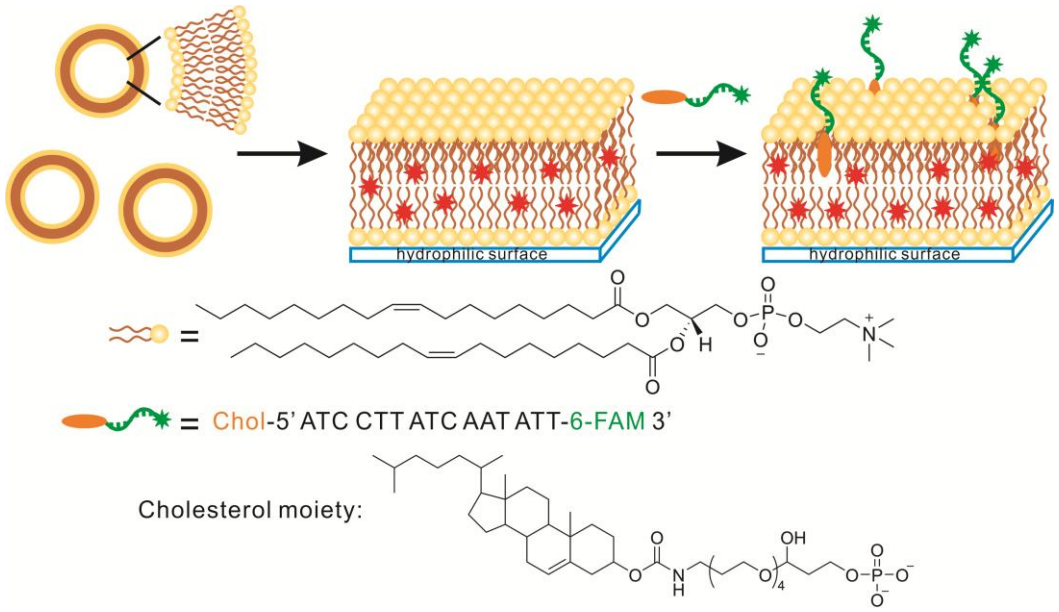

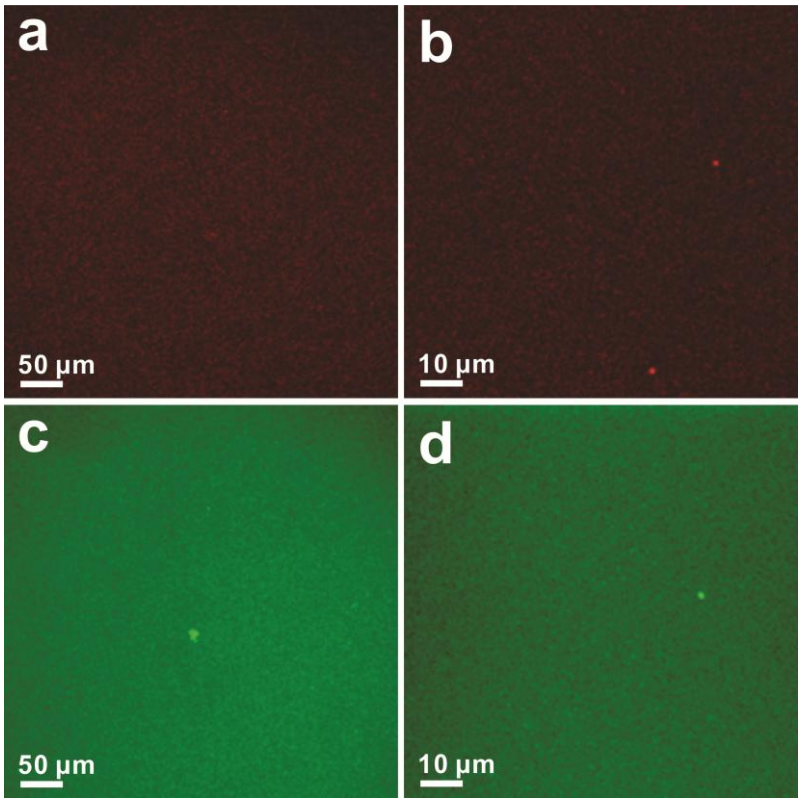

Figure 5.1. (a,b) Confocal laser scanning fluorescence image of Texas red doping DOPC lipid bilayers (ex @ 633 nm) on glass slides. (c,d) Confocal laser scanning fluorescence image of DNA-functionalized DOPC lipid bilayes (ex @ 488 nm).

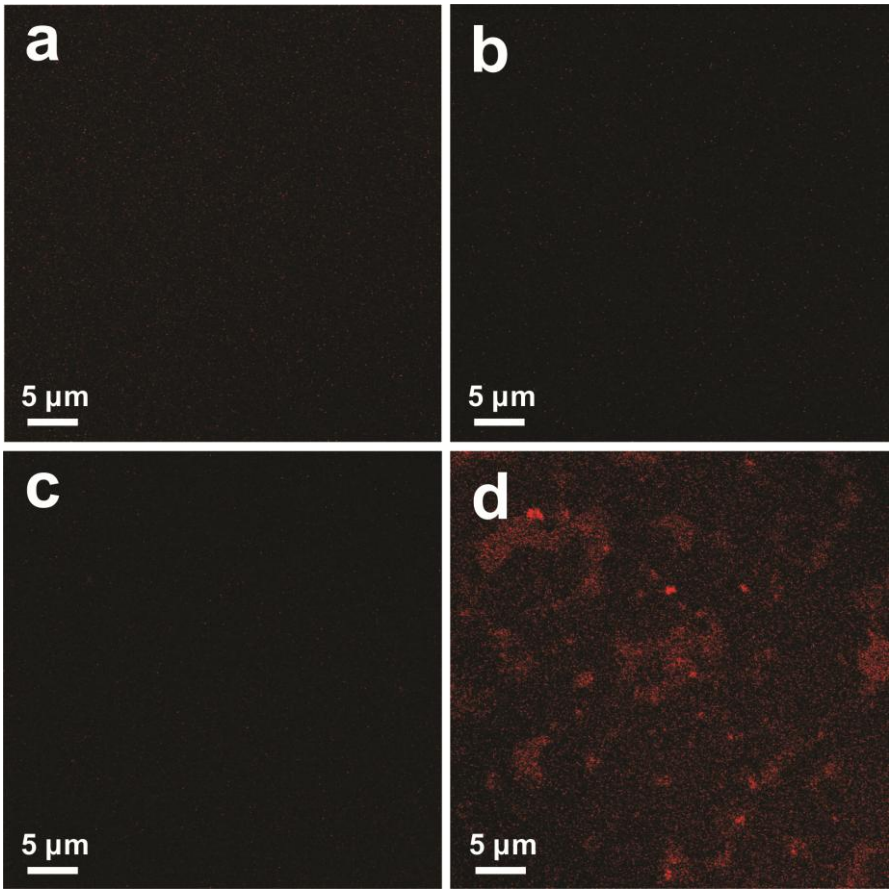

Figure 5.2. Confocal laser scanning fluorescence image of Texas red doped DOPC lipid bilayers incubate at 30 ℃ over (a) 6 hr and (b) overnight (ex @ 633 nm). Confocal laser scanning fluorescence image of Texas red doping DOPC lipid bilayes incubate at 40 ℃ over (c) 6 hr and (d) overnight (ex @ 633 nm).

5.3.3 Lateral mobility of DNA-anchored lipid bilayers via FRAP measurement. Next we studied the lateral mobility of the DNA-functionalized lipid bilayers. One of the most essential components of eukaryotic cell membranes is cholesterol molecule which orients in a phospholipid membrane with polar hydroxyl group encountering water and hydrophobic moiety buried in hydrocarbon chains of the phospholipids,[13] and its lateral mobility and distribution in membranes have been well documented.[14] On the other hand, fluorescence recovery after photobleaching (FRAP) is a widely used technology to measure molecular diffusion in membranes which is a determining factor in cell signaling and cell function.[15] To explore the lateral mobility of DAN-immobilized lipid bilayers constructed by chol-DNA conjugates in this study, fluorescein attached to DNA strand was used as a direct probe for the determination of chol-DNA conjugates diffusion in lipid membranes. The mobility can be presented as diffusion coefficient D, which is relevant to diffusion time $\tau_{1/2}$ and can be calculated from two-dimensional equation as following,[16,17]

$$\tau_{1/2} = 0.22R^2/D$$

where R is the radius of the bleach spot, and $\tau_{1/2}$ is the half-life for fluorescence intensity recovery. In the FRAP measurement (Figure 5.3a,b), bleach spot with a 27.25 μm radius was obtained by using high intensity laser beam. The half-life for recovery, that is, when fluorescence intensity returns to half of its pre-bleach number, was reached in 4 min (Figure 5.3c,d). Therefore, the diffusion constant of DNA-tethered lipid bilayer is 0.68 $\mu m^2/s$, which is comparable to typical lipid

membranes in previous report.[14] According to the percentage mobile fraction given by[18]

$$\%R = \frac{F(\infty) - F(0)}{F(t < 0) - F(0)}$$

where $F(t<0)$ is the pre-bleach fluorescence, the percent recovery %R is 72% in this study. Note that the beam also induced the photobleaching of fluorescein outside bleach spot during FRAP measurement,[19] thereby the actual %R is expected to be higher than 72%. The diffusion coefficient and percent recovery obtained from FRAP measurement show that DNA-anchored lipid bilayers have fluidity and undergo lateral diffusion, which plays an essential role in the following the DNA-induced gold nanoparticle self-assembly study.

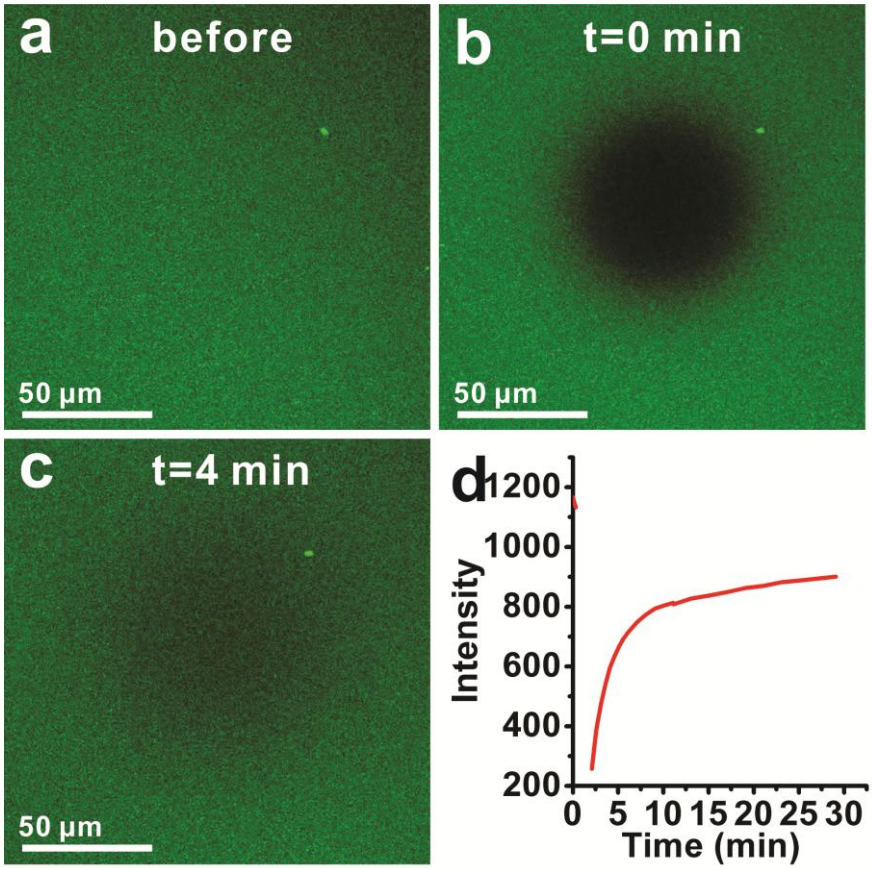

Figure 5.3. Fluorescence Recovery After Photobleaching (FRAP) on supported DNA-functionalized lipid bilayers. (a) Confocal laser scanning fluorescence image of DNA-functionalized lipid bilayers before photobleaching. 6-FAM was bleached by using a 488 nm laser at 100% intensity and image was acquired immediately after (t=0) (b) and a defined period after bleaching (t=4 min) (c), respectively. (d) Fractional fluorescence recovery curve obtained by FRAP.

5.3.4 Gold nanoparticle domains formed by hybridization of nanoparticles and lipid bilayers.

To fabricate gold nanoparticle self-assembly structure, complementary DNA-immobilized gold nanoparticles in 0.1 M PBS buffer were introduced to the DNA-tethered lipid membranes in home-built chamber, and allowed to hybridize with DNA sequences anchor on lipid surface at room temperature overnight (Scheme 5.2). After overnight incubation, a light pink color thin film by eye was obtained inside the chamber (Figure 5.4). The film was thoroughly washed by exchanging 10 times the incubation buffer with 0.1 M PBS to remove unbound nanoparticles, never allowing the supported lipid bilayers to dry out. To confirm that the formation of thin film is induced by DNA specific hybridization, two control experiments were performed, where gold nanoparticles were mixed with lipid bilayers in water, or gold nanoparticles functionalized with non-complementary DNA were added to the membranes (Figure 5.4). In both cases, since there was no DNA specific hybridization between nanoaprticles and lipid bilayers, gold nanoparticles were completely removed during the washing step, and no gold thin film formation was observed, as expected. These results confirm the retaining of nanoparticles is indeed due to the DNA specific interactions.

Scheme 5.2. Schematic Description of the Introduction of DNA-functionalized gold nanoparticles on DNA-functionalized Lipid Bilayers Preparation.

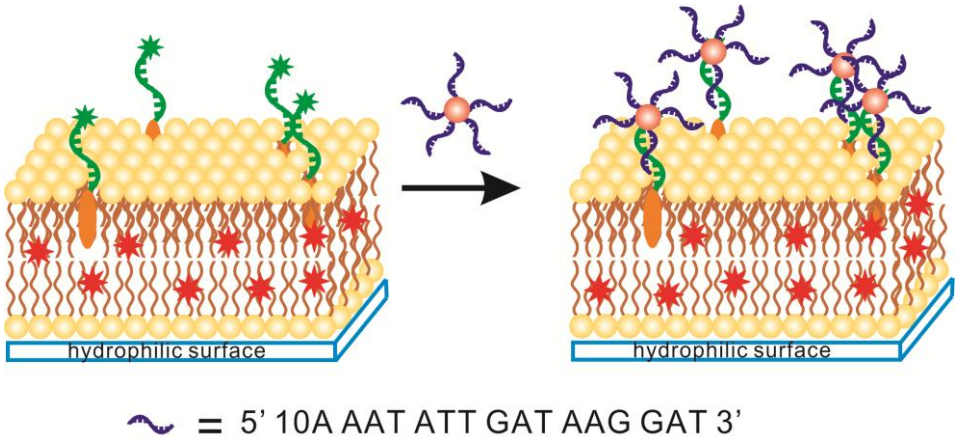

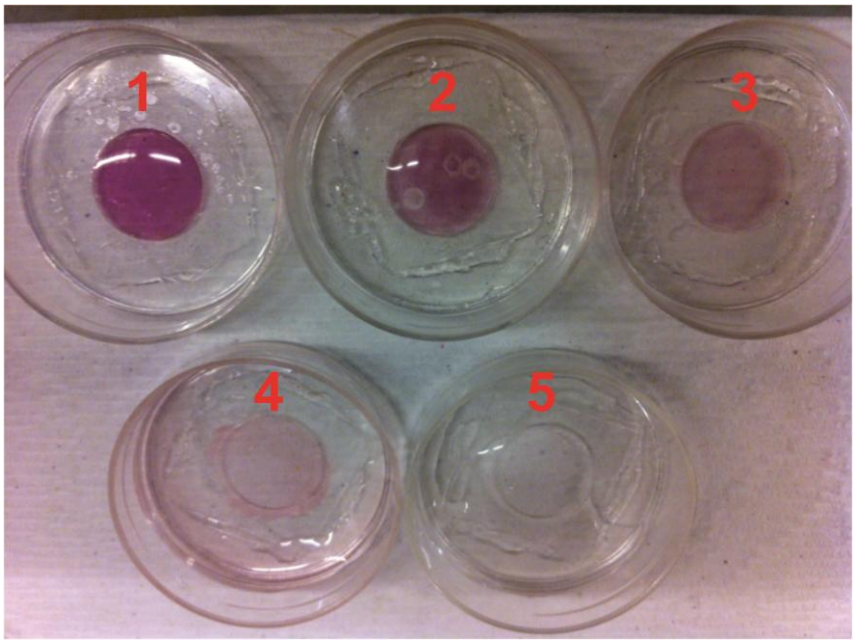

Figure 5.4. Thin films formed by the hybridization between DNA-functionalized gold nanoparticles and complementary DNA-tethered lipid bilayers using 600 μL (1), 300 μL (2), and 150 μL of gold nanoparticles stock solution, respectively. Two control experiments, gold nanoparticles were mixed with lipid bilayers in water (4), or gold nanoparticles functionalized with non-complementary DNA were added to the membranes (5).

We further investigated the structure of this as-deposit thin film by optical microscope. The optical microscope images reveal that the as-deposit film is actually incontinuous and composed of nanoparticle domains in the size range over micrometers. We attribute the formation of nanoparticle domains to the lateral mobility of chol-DNA conjugates as well as van de Waals attraction between gold nanoparticles.[20] Although gold nanoparticles bind to the lipid bilayer surface by DNA hybridization, they are free to diffuse parallel to the surface and further cluster up. More importantly, the emission intensities of Texas Red and fluorescein on confocal laser scanning fluorescence images are much dimmer compared to before nanoparticle deposition under the same laser power condition (Figure 5.5a,b), which further confirms that nanoparticles are brought into close contact with the two fluorescent dyes *via* DNA hybridization, and subsequently quenched the fluorescent of vicinity dye molecules due to energy transfer mechanism.[21] Interestingly, the emission of fluorescein follows the same patterns as nanoparticles domains implying chol-DNA conjugates move along with their counterpart gold nanoparticles and form green fluorescent domains right underneath nanoparticle clusters. We further reveal the nanostructure of as deposit film by SEM. Nanoparticle as-deposit films were washed with excess amount of 0.3 M ammonium acetate and deattached from the home-built chamber, and later dried out under vacuum to remove ammonium acetate before imaging. SEM images of as-deposit nanoparticle films clearly show that they are consisted of discrete nanoparticles. They also show that nanoparticles form domains whose sizes range from a hundred to several hundred nanometers when they

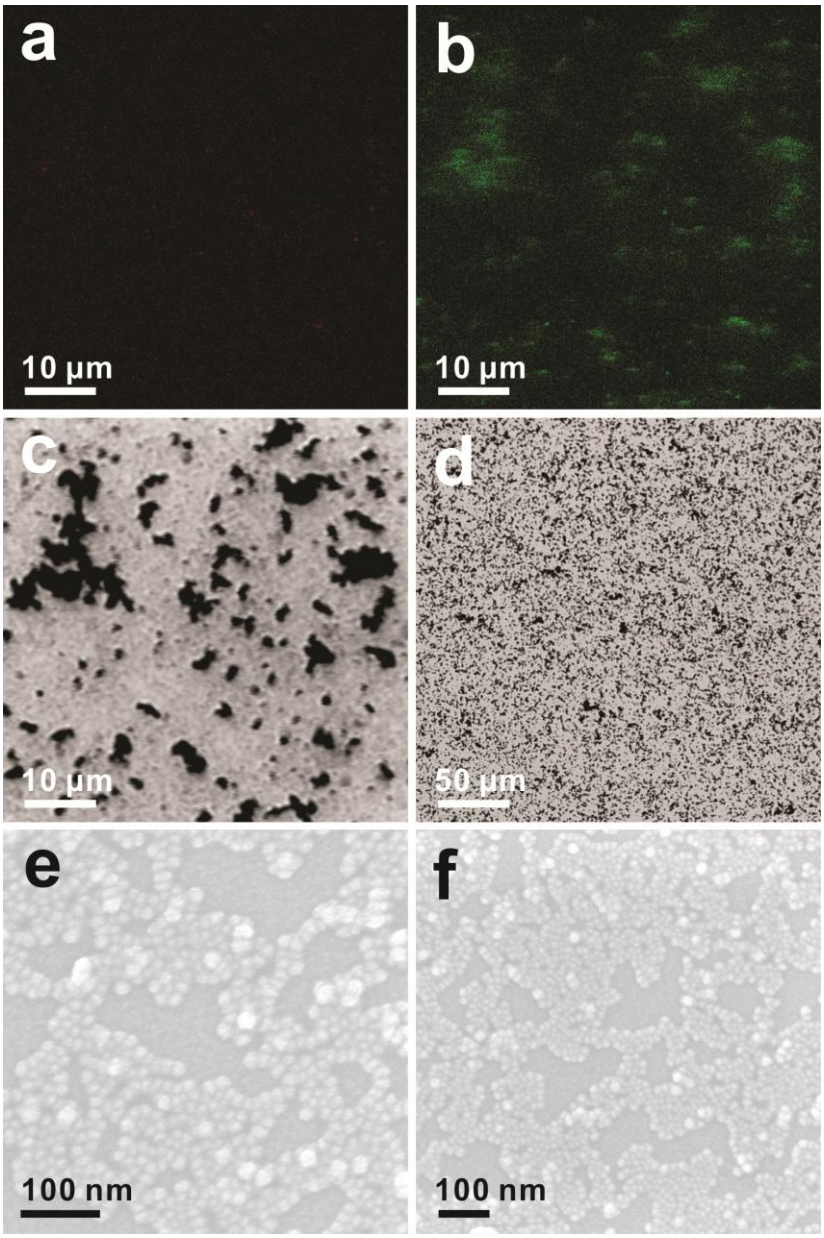

Figure 5.5. (a,b) Confocal laser scanning fluorescence image of Texas red (ex @ 633 nm) and 6-FAM (ex @ 488 nm) after hybridization with gold nanoparticles, respectively. (c,d) Transmission images of DNA-functionalized gold nanoparticle clusters on DOPC lipid bilayes. (e,f) SEM images of as-deposit gold nanoparticles.

are dried (Figure 5.5e,f).

5.3.5 Formation of gold nanoparticle self-assembly induced by DNA linker and thermal annealing. To induce the self-assembly within nanoparticle domains, a linker DNA which is complementary to the DNA sequences immobilized on nanoparticle surface and with a sticky end, was introduced to the system. The sample was then annealed at 40 ℃ overnight (Scheme 5.3). The color of nanoparticles films didn't change after the addition of linker DNA and annealing process. Note that the color of the nanoparticle sheets in this work is much lighter than those of gold nanoparticle films created by other methods reported on literatures due to fewer layers of nanoparticles.[4,5] Optical microscope images taken after 16 h annealing showed an optically uniform nanoparticle sheet with free nanoparticle sedimentation occasionally laid on top (Figure 5.6a). SEM was used to evaluate the arrangement of nanoparticle self-assembly. Glass slides were detached from culture dishes and washed with excess amount of 0.3 M ammonium acetate to replace with sodium chloride. The glass slides were dried under vacuum chamber for 16 hr to remove trace of ammonium acetate. In order to obtain good signal for samples on glass substrate which is not an ideal substrate for SEM imaging, 4 nm thick of Ir was deposited on top of the assembly to increase conductivity. The SEM images of gold nanoparticles after assembly process again show discrete nanoparticle features. Furthermore, nanoparticles domains grow bigger after the addition of linker DNA and annealing process compared to as-deposit nanoparticles films. The domain sizes span from a few hundred nanometers to micrometers indicated by SEM images

Scheme 5.3. Schematic Description of the formation of gold nanoparticle self-assemblies on DNA-functionalized lipid bilayers induced by linker DNA and annealing.

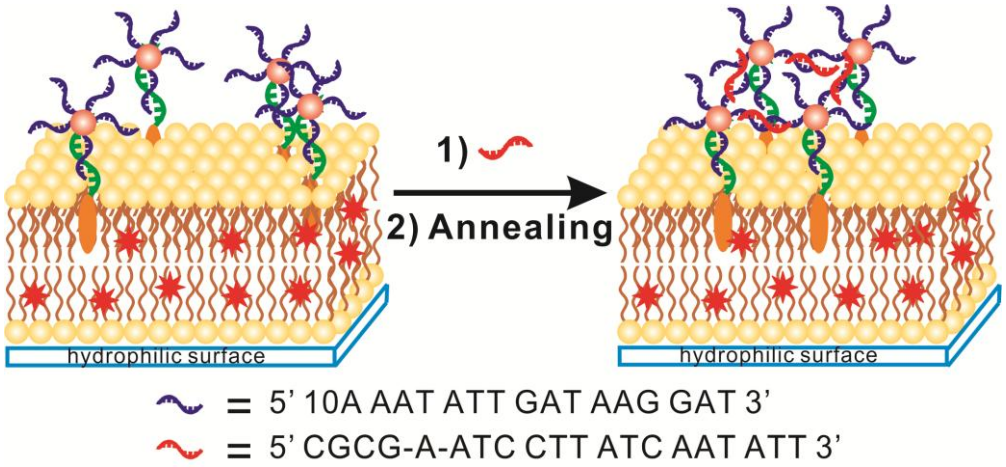

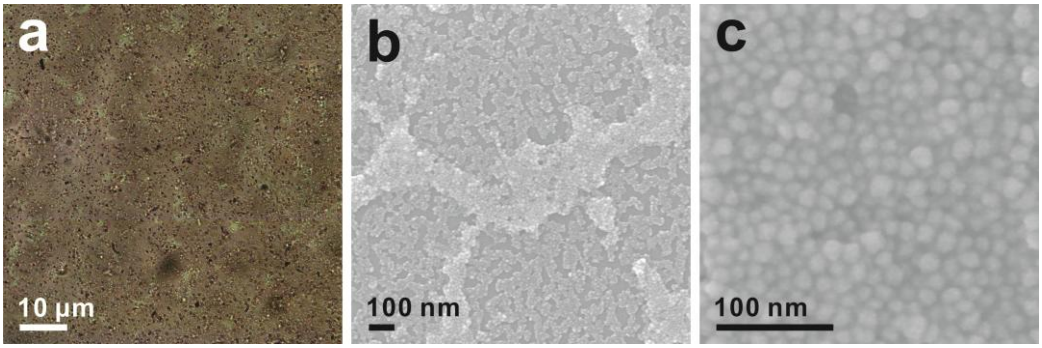

Figure 5.6. (a) Optical microscope image of gold nanoparticle assemblies induced by linker DNA and annealing. (b,c) SEM images of gold nanoparticle assemblies on lipid bilayers.

5.6b,c). We reason that the linker DNA connects adjacent gold nanoparticles and the annealing process provides sufficient energy to facilitate the lateral motions of nanoparticles on lipid bilayers. Two control experiments were carried out to examine the necessary conditions to create self-assembly structure. The first control experiment was performed annealing process in the absence of linker DNA. SEM image presents similar overall shape to as-deposit nanoparticle film whose domain sizes are small, indicating the self-assembly was not successfully achieved (Figure 5.7a). In the second control experiment, gold nanoparticles were allowed to hybridize with linker DNA at room temperature. Similar result was obtained and large domain size of assembly structures was not observed. The two control experiments emphasize the importance of linker DNA and annealing. The linker DNA offers the driven force for the lateral movements of nanoparticles *via* DNA hybridization, while the annealing process provides energy to promote the movements. And neither of them can be negligible.

The extent of order in nanoparticle self-assemblies was investigated using grazing incidence small-angle X-ray scattering (GISAXS). The sample preparation for GISAXS measurement was similar to the preparation for SEM. Nanoparticle film was first deattached from the home-built chamber and washed with large amount of 0.3 M ammonium acetate. The glass slide with nanoparticle film was further dried under vacuum overnight to remove ammonium acetate. The GISAXS data show broad rings, suggesting poorly ordered and essentially amorphous structure (Figure 5.8a). The rings indicate a preferred local packing distance, however, no

long-range coherent order. It is consistent with SEM images which are difficult to assign any type of crystal structures. In spite of lacking long-range order, we are still able to calculate the inter-particle distance d_{Au} according to the Bragg equation,

$$q = 2\pi/d$$

where q is the first order scattering vector. In our study, q_y is 0.04078 $Å^{-1}$ (Figure 5.8b), and d_{Au} is calculated to be 15.4 nm. The number of inter-particle distance in this study is two times smaller than the numbers reported on other literatures,[5] resulting from different sample preparation methods of GISAXS measurements. In previous papers, samples were coated with silica to maintain nanoparticles in the solid state. However, in our study, sample glass slides were completely dried out. We speculate that the drying process shrinks down the inter-particle distance. The UV-vis spectrum of gold nanoparticle assemblies on lipid bilayers in 0.1 M PBS buffer solution preserves nanoparticle plasmonic properties, yet the surface plasmon resonance (SPR) peak at 542 nm is red-shifted around 20 nm compared to isolated gold nanoparticles, indicating close nanoparticle distance (Figure 5.8c)

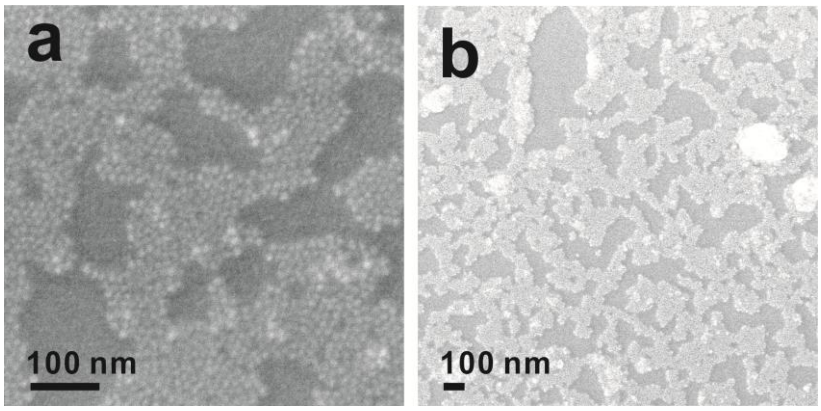

Figure 5.7. Two control experiments were performed to examine the importance of linker DNA and annealing. (a) SEM image of gold nanoparticles film incubated at 40 ℃ overnight in the absence of linker DNA. (b) SEM image of gold nanoparticles film incubated with linker DNA at room temperature overnight.

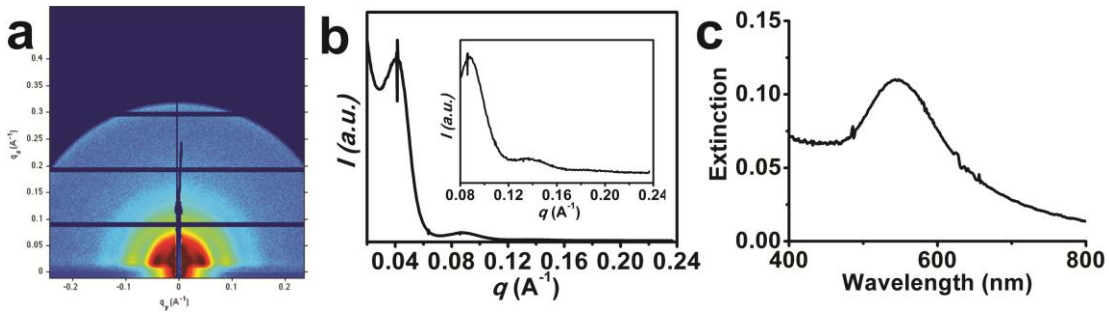

Figure 5.8. Characterization of gold nanoparticle assemblies on lipid bilayers. (a) GISAXS map of nanoparticle assemblies dry film, (b) linecuts from GISAXS scattering pattern, and (c) extinction spectrum of nanoparticle assembly film in 0.1 M PBS buffer solution.

5.3.6 Nanoparticle concentration dependency. We also investigated the influence of nanoparticle concentration to the formation of nanoparticle assemblies. Gold nanoparticle assemblies on lipid bilayers were prepared with varying gold nanoparticles concentrations. The initial gold nanoparticle amount added to the chamber (26.8 pmol) was not sufficient to cover the whole lipid membranes and left blank areas where few nanoparticles occupied. High nanoparticle density areas appear dark grey color, while low density areas are represented by light grey color (Figure 5.9a). As the amount of gold nanoparticles increases by two times, the blank areas reduce (Figure 5.9b). A further increase amount of nanoparticles to 107.2 pmol, the lipid membranes were covered by nanoparticles with occasional blank areas (Figure 5.9 c). Thus, the amount of nanoparticles influences the coverage of lipid membranes.

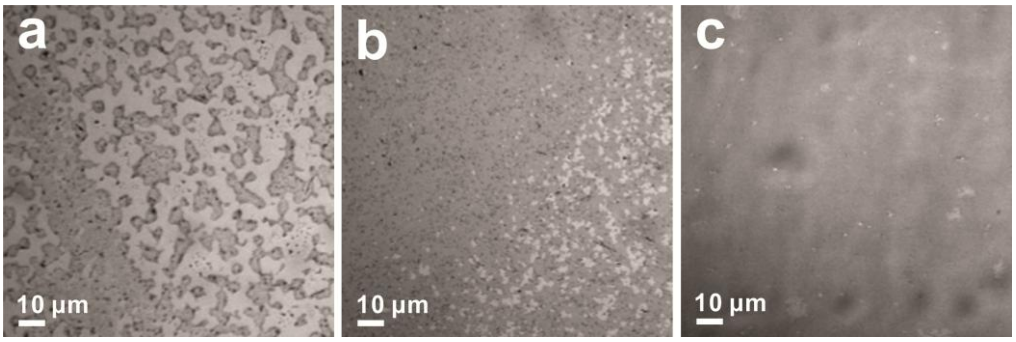

Figure 5.9. Transmission images of gold nanoparticle assembly thin films using different amount of gold nanoparticles, (a) 26.8 pm, (b) 53.6 pmol, and (c) 107.2 pmol.

5.4 Conclusions.

In summary, we demonstrate a strategy to assemble DNA-functionalized gold nanoparticles into macroscopic sheets assisted by DNA-tethered lipid bilayers. Cholesterol-DNA conjugates are tethered on lipid bilayers by hydrophobic interaction. We show that the DNA strands are mobile on modified lipid membrane surface by fluorescence recovery after photobleaching (FRAP) experiment. The DNA-tethered lipid bilayers can hybridize with complementary DNA-functionalized gold nanoparticles, and further self-assemble into micron-size nanoparticle sheets by adding linker DNA and annealing. By varying the amount of gold nanoparticles input, the surface coverage can be tuned. We believe our mobile DNA-functionalized lipid-bilayers will serve as a versatile platform for a diverse range of applications. And our assembly strategy provides a route to generate arrays of nanoparticles and organizing them into more sophisticated structures. For example, using this strategy, ordered arrangement of nanorods, such as end-to-end, may be achieved, which may show promising applications in surface-enhanced raman spectroscopy. We also anticipate that our approach will further expand the scope of nanoparticles that are used to organize to other nanomaterials, including carbon nanotube, nanowires, magnetic, electronic, and optical materials, and make them candidates for novel devices and sensors.

5.5 References.

(1) Macfarlane, R. J.; Lee, B.; Jones, M. R.; Harris, N.; Schatz, G. C.; Mirkin, C. A. *Science* **2011**, *334*, 204-208.

(2) Taton, T. A.; Mucic, R. C.; Mirkin, C. A.; Letsinger, R. L. *J. Am. Chem. Soc.* **2000**, *122*, 6305-6306.

(3) Taton, T. A.; Mirkin, C. A.; Letsinger, R. L. *Science* **2000**, *289*, 1757-1760.

(4) Estephan, Z. G.; Qian, Z.; Lee, D.; Crocker, J. C.; Park, S.-J. *Nano Lett.* **2013**, *13*, 4449-4455.

(5) Ku, J. C.; Ross, M. B.; Schatz, G. C.; Mirkin, C. A. *Adv. Mater.* **2015**, *27*, 3159-3163.

(6) Suzuki, Y.; Endo, M.; Sugiyama, H. *Nat Commun* **2015**, *6*.

(7) Langecker, M.; Arnaut, V.; List, J.; Simmel, F. C. *Acc. Chem. Res.* **2014**, *47*, 1807-1815.

(8) Börjesson, K.; Lundberg, E. P.; Woller, J. G.; Nordén, B.; Albinsson, B. *Angew. Chem., Int. Ed.* **2011**, *50*, 8312-8315.

(9) Burns, J. R.; Göpfrich, K.; Wood, J. W.; Thacker, V. V.; Stulz, E.; Keyser, U. F.; Howorka, S. *Angew. Chem., Int. Ed.* **2013**, *52*, 12069-12072.

(10) Banga, R. J.; Chernyak, N.; Narayan, S. P.; Nguyen, S. T.; Mirkin, C. A. *J. Am. Chem. Soc.* **2014**, *136*, 9866-9869.

(11) Gunnarsson, A.; Jönsson, P.; Marie, R.; Tegenfeldt, J. O.; Höök, F. *Nano Lett.* **2008**, *8*, 183-188.

(12) Stengel, G.; Zahn, R.; Höök, F. *J. Am. Chem. Soc.* **2007**, *129*, 9584-9585.

(13) Ohvo-Rekilä, H.; Ramstedt, B.; Leppimäki, P.; Peter Slotte, J. *Progress in Lipid Research* **2002**, *41*, 66-97.

(14) Alecio, M. R.; Golan, D. E.; Veatch, W. R.; Rando, R. R. *Proceedings of the National Academy of Sciences* **1982**, *79*, 5171-5174.

(15) Guo, L.; Har, J. Y.; Sankaran, J.; Hong, Y.; Kannan, B.; Wohland, T. *ChemPhysChem* **2008**, *9*, 721-728.

(16) Goertz, M. P.; Marks, L. E.; Montaño, G. A. *ACS Nano* **2012**, *6*, 1532-1540.

(17) Reits, E. A. J.; Neefjes, J. J. *Nat. Cell Biol.* **2001**, *3*, E145-E147.

(18) Ladha, S.; Mackie, A. R.; Harvey, L. J.; Clark, D. C.; Lea, E. J.; Brullemans, M.; Duclohier, H. *Biophys. J.* **1996**, *71*, 1364-1373.

(19) Song, L.; Hennink, E. J.; Young, I. T.; Tanke, H. J. *Biophys. J.* **1995**, *68*, 2588-2600.

(20) Prasad, B. L. V.; Stoeva, S. I.; Sorensen, C. M.; Klabunde, K. J. *Langmuir* **2002**, *18*, 7515-7520.

(21) Pustovit, V. N.; Shahbazyan, T. V. *The Journal of Chemical Physics* **2012**, *136*, 204701.

5.6 Appendix

5.6.1 Preparation of gold nanorods. Gold nanorods were synthesized by following the previously published silver-assisted growth procedures.[1] Hexadecyltrimethylammoniumbromide (CTAB) solution (1 mL, 0.2 M) was mixed with chloroauric acid ($HAuCl_4$) (1 mL, 0.0005 M), then ice cold sodium borohydride ($NaBH_4$) (120 μL, 0.01 M) was added to the mixture and vigorously mixed for 2 min. The seed solution was aging at 25 ℃ for 1 hr. To prepare growth solution, CTAB solution (5 mL, 0.2 M), silver nitrate ($AgNO_3$) (375 μL, 0.004 M), and $HAuCl_4$ (5 mL, 0.001 M) were mixed together. Reducing agent ascorbic acid (70 μL, 0.0788 M) was added to the mixture and a color change of growth solution from orange to colorless was observed immediately. In the final step, 12 μL of seed solution was added to the prepared growth solution and allowed to age at 25 ℃ overnight.

5.6.2 Preparation of DNA-functionalized gold nanorods. It was reported that as-synthesized nanorods made by silver-assisted growth procedures have difficulty in conjugation with thiolated-DNA due to the presence of a thin layer of silver on nanorod surface. To address this issue, an additional growth of gold on the nanorod was used to facilitate the DNA functionalization.[2] Gold nanorods (5 mL, LSPR=5) were spun down at 13400 rpm for 10 min and redispersed in 5 mL water. The nanorods were spun down again and resuspended in CTAB (5 mL, 0.01 M). Ascorbic acid (50 μL, 100 mM) and $HAuCl_4$ (50 μL, 0.5 mM) were added to the nanorod CTAB solution, and the mixture was allowed to wait an hour for the

overgrowth to complete. The solution was brought to 0.05 M CTAB by adding 1.335 mL of 0.2 M CTAB solution and later spun down twice at 13400 rpm for 10 min and redispersed in 5 mL of thiolated DNA water solution (DNA 1 5' 10A AAT ATT GAT AAG GAT 3', 15 $OD_{260\ nm}$) in a glass vial. The solution was aging on a shaker for 70 min. Sodium phosphate (555 μL, 100 mM) and sodium dodecyl sulfate (SDS, 17.3 μL, 100 mM) were added to the solution and waited for overnight. The solution was brought to 0.05 M, 0.1 M, 0.2 M, 0.3 M, 0.4 M and 0.5 M NaCl by adding 293 μL, 326 μL, 774 μL, 995 μL, 1326 μL, and 1857 μL of 0.1 M NaCl, sequentially. There was approximate an hr between each salt addition. After salt addition completed, nanorods were sit on the shaker overnight to achieve maximum functionalization. To remove unbounded DNA, nanorod solution was spun down twice at 8000 rpm for 10 min and resuspended in 0.01% SDS and the solution was later brought to 0.1 M sodium phosphate and 0.5 M NaCl for storage (Figure 5.10).

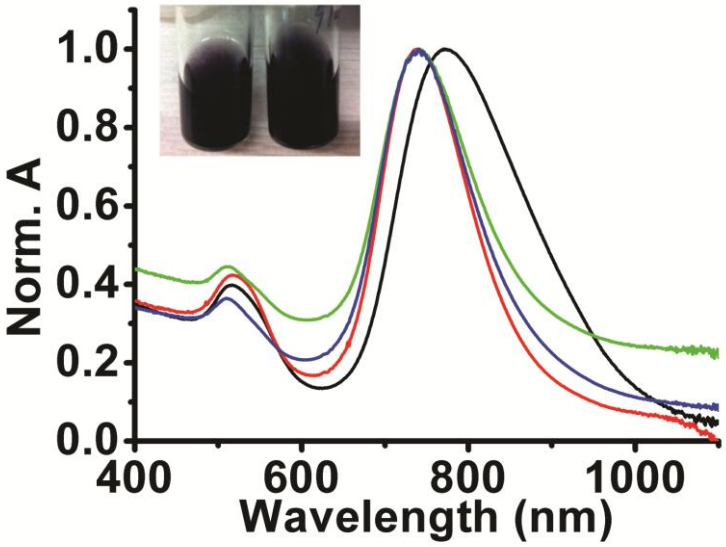

Figure 5.10. Extinction spectra of gold nanorods before (black) and after (red) deposition, DNA-modified gold nanorods (green) and over several days (> 3 days) (blue).

5.6.3 DNA-functionalized gold nanorods DNA recognition property.

DNA recognition properties of DNA-functionalized gold nanorods were evaluated by hybridizing gold nanorods to a complementary DNA sequence 2 (5'-ATC CTT ATC AAT ATT 6-FAM-3') labeled by a green fluorescent dye. Gold nanorods (100 μL) were mixed with DNA sequence 2 (0.022 nmol) at 55 ℃ for 5 min to facilitate the hybridization. A pronounced fluorescence quenching due to energy transfer between dye and nanorods was observed by fluorescence spectra, and the energy transfer process is reversible. As the temperature increases above the DNA melting temperature, dsDNA dehybridize and the distance between nanoparticles and fluorophores is increased resulting in the recovery of 6-FAM fluorescence intensity (Figure 5.11). Theses experimental observations confirm that after the modified DNA conjugation processes, gold nanorods were successfully coated with a dense layer of DNA sequences and possess DNA binding properties.

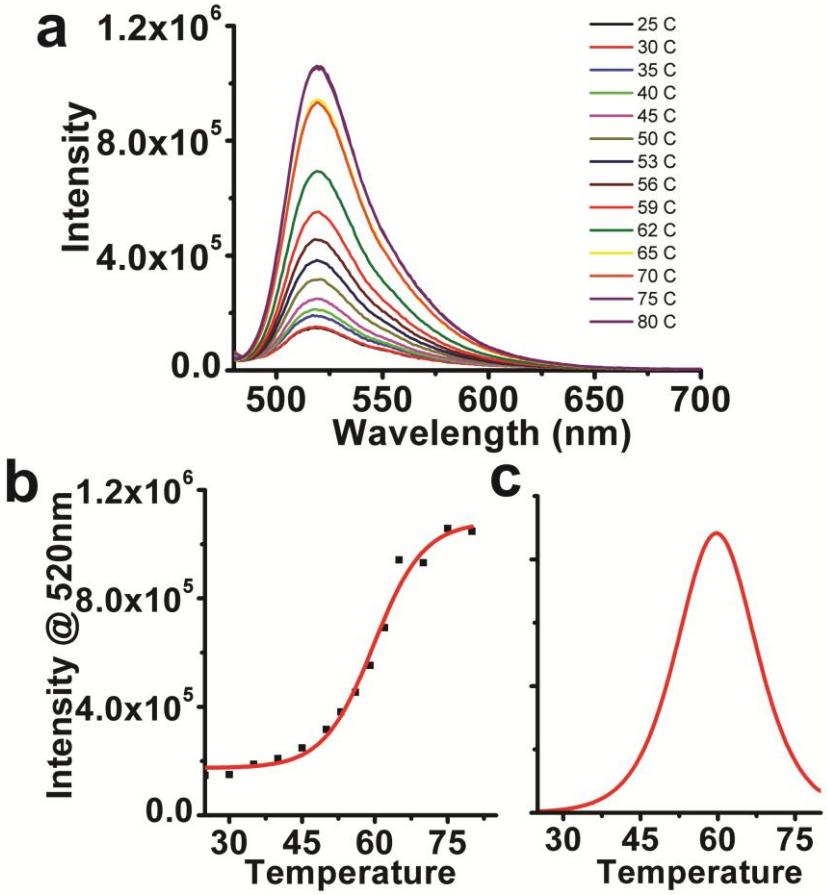

Figure 5.11. (a) Photoluminescence spectra of dehybridization of DNA-modified gold nanorods and complementary DNA strands in PBS buffer (0.5 M NaCl, 100 mM phosphate buffer, pH=7.17) with increasing temperatures. (b) Melting profile by monitoring fluorescence intensity at 520 nm with increasing temperature. (c) First derivative of the melting profile.

5.6.4 Hybridization of DNA-functionalized gold nanorods and DNA-modified lipid bilayers.

DNA-functionalized gold nanorods (200 μL) were hybridized with complementary DNA-modified DOPC lipid bilayers which were prepared by procedures described in Chapter 5. Following the protocols in Chapter 5, overnight incubation at room temperature only led to the sedimentation of gold nanorods. During washing step, most of DNA-functionalized gold nanorods were removed by buffer solution, leaving a very thin layer of nanoparticles on top of the lipid membranes (Figure 5.12 a). Confocal images (Figure 5.12 b,c) reveal that nanoparticles domains were also formed as expected; however, the density of nanorods hybridized with DNA-tagged lipid bilayers is much lower than that of spherical gold nanoparticles in Chapter 5. Linker DNA and annealing process were later applied to the gold nanorods thin films following the description in Chapter 5. After overnight incubation at 40 ℃, the formation of 2D nanorods self-assemblies was absent, instead gold nanorods clustered up and their aggregates floated inside the home-build chamber. Moreover, confocal images show that nanorods aggregates are surrounded by chol-DNA strands which are labeled by a green fluorescence dye while the fluorescence of lipid bilayers is much dimmer (Figure 5.13). We hypothesize that in DNA functionalization step, SDS as a water soluble surfactant was introduced to solution to stabilize the charged DNA-modified nanrods. When DNA-functionalized gold nanorods were mixed with lipid bilayers, free SDS

molecules in the solution solubilized and removed chol-DNA strands from lipid bilayers.

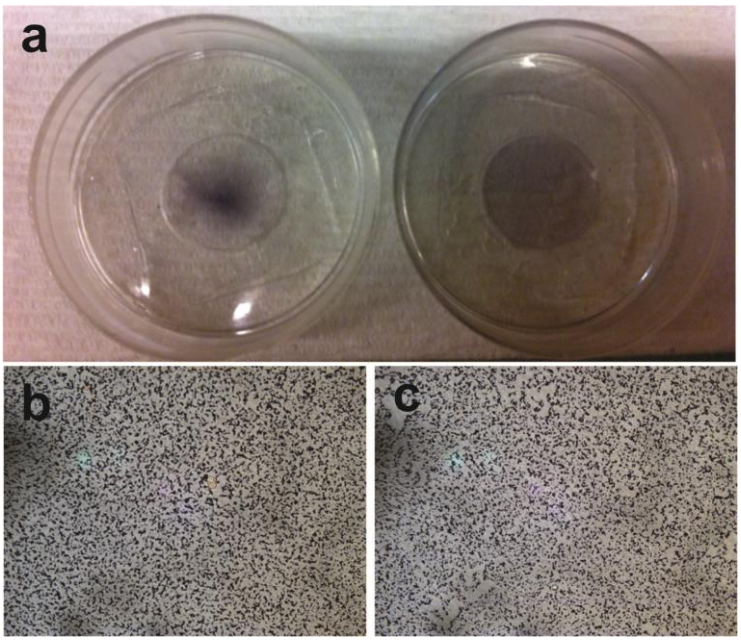

Figure 5.12. (a) Thin films formed by the hybridization between DNA-functionalized gold nanorods and complementary DNA-tethered lipid bilayers using as-modified gold nanorods (left) and extra cleaned gold nanorods (right). (b,c) Optical microscope images of gold nanorod thin films.

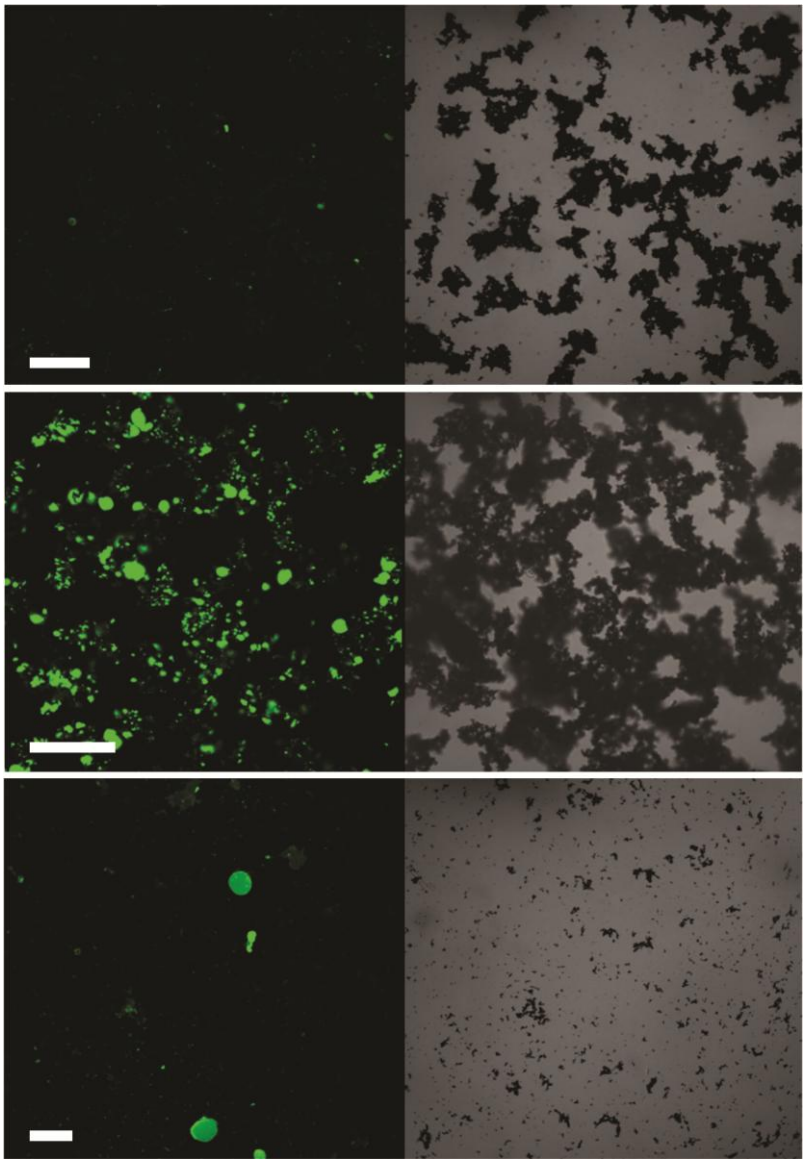

Figure 5.13. Representative confocal laser scanning and transmission images of gold nanorods thin films after overnight incubation (ex@488 nm). Scale bars: 10 μm.

5.6.5 Effect of SDS. Extra SDS was effectively removed by multiple centrifugation cycles. Before hybridized with DNA-tethered lipid bilayers, DNA-modified gold nanorods were spun down at 8000 rpm for 10 min and resuspended in water twice to remove excess SDS in the solution. As expected, purified gold nanorods readily bind with lipid bilayers and generate gold nanorod thin films which contain higher density of nanoparticles (Figure 5.14).

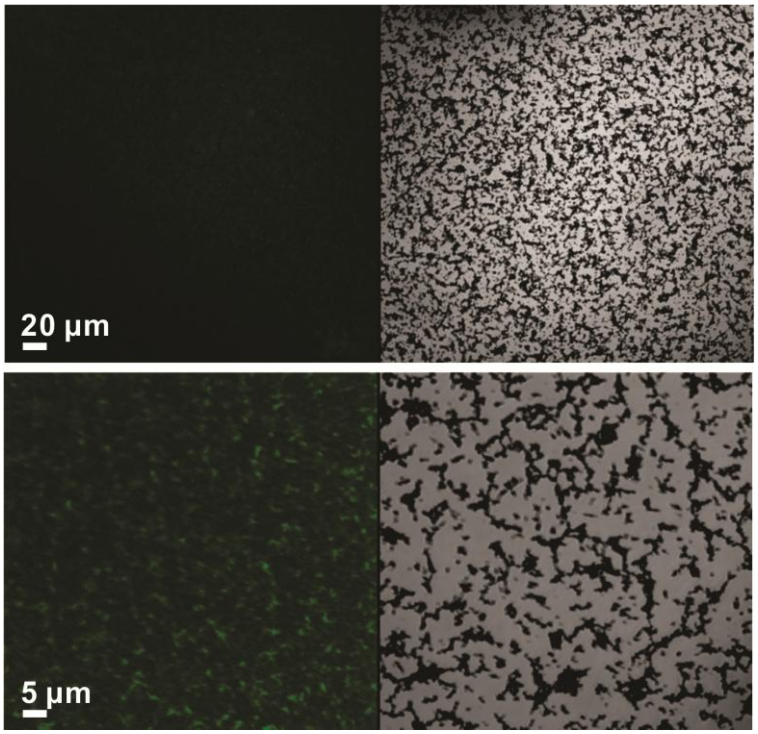

Figure 5.14. Representative confocal laser scanning and transmission images of gold nanorods thin films after overnight incubation using purified DNA-functionalized gold nanorods (ex@488 nm).

5.6.6 References

(1) Nikoobakht, B.; El-Sayed, M. A. Chem. Mater. 2003, 15, 1957-1962.

(2) Jones, M. R.; Macfarlane, R. J.; Lee, B.; Zhang, J.; Young, K. L.; Senesi, A. J.; Mirkin, C. A. Nat. Mater. 2010, 9, 913-917.

CHAPTER 6. Future Directions

6.1 Future directions

6.1.1 DNA rafts. In Chapter 3, we fabricated hybrid giant vesicles from DNA diblock copolymers of polymethylacrylate-*block*-DNA (PMA-*b*-DNA) using a prototypical block copolymer of poly(butadiene)-*block*-poly(ethylene oxide) (PBD-*b*-PEO) as a matrix polymer and demonstrated that the hybrid vesicles undergo efficient phase segregation upon the introduction of complementary DNA. The hybridization-induced phase segregation led to high density DNA rafts on the vesicle surface creating patchy assembly structures.

Booming interest in anisotropic particles, such as patchy, multicompartment and Janus particles, has predominately focused on their design and preparation, and higher order self-assembly in recent years, although their real world applications appear to be far away from realization. Given their unique structures, anisotropic particles have many applications as interface stabilizers,[1] controllable pores in lipid membranes,[2] biological sensors, and anisotropic building blocks for complex structures.[3] In nature, cell compartmentalization has been long identified as a critical role in enormous number of biological reactions and processes.[4] Other structural analogues are found useful in modern materials science. For example, hydrophobins which have hydrophilic and hydrophobic patches can form coatings and further attach to different surfaces.[5]

There are a variety of techniques for the preparation of patchy particles,

including templating, colloidal assembly, particle lithography, and electrospray usinga biphase nozzle.[6] As have shown in Chapter 3, the hybridization of complementary hybrid DNA polymersomes offers an extremely simple and efficient way to fabricate patchy particles. However, the patchy particles formed in this chapter are bound with their complementary analogues, and the stability of DNA rafts on isolated polymersomes has not been studied yet. It will be interesting to see whether or not the DNA rafts maintain even after hybrid DNA polymersomes dehybridize. Discher *et al* reported calcium cations crossbridge polyacrylic acid (PAA) which is a polyanionic polymer, and hence demix from matrix polymers and create spots or rafts in vesicle structures.[7] Likewise, DNA phosphate backbones which have similar electron structure to PAA can strongly chelate with multivalent cations to provide driving force for domain formation. It is expected that the addition of multivalent cations (e.g. Ca^{2+}) acting as glue in the solution during melting process will crosslink DNA amphiphiles and lead to the formation of DNA rich domains in an isolated patchy particle. The hybrid DNA polymersomes presents a good material candidate as anisotropic particles for targeted drug/gene delivery considering their unique DNA binding properties.

6.1.2 DNA hybrid assemblies on substrates. In Chapter 4, we prepared a new set of hybrid assemblies from a DNA triblock copolymer of poly(butadiene)-*block*-poly(ethylene oxide)-*block*-DNA (PBD-*b*-PEO-*b*-DNA) and used them for the fabrication of microarrays.

Colloidal science is beginning to face the challenge of organizing nanoparticles

into controllable architectures on micron- or even submicron-size substrates, which open the door to fabricate the new generation of microarrays and nanodevices. The most common strategy for nanoparticles immobilization is covalent reactions such as maleimides, amides and thiols. However, it will not necessarily be applicable as generic protocol to prepare complex nanoarrays where it needs different functional nanoparticles to be located on designated areas. In contrast to covalent bonds, DNA specific interaction has emerged as a promising substituent when using DNA nanoparticles. Unlike chemical bonds, DNA hybridization is a reversible process. In other words, the microarrays constructed *via* DNA hybridization response on and off to temperature or salt concentration change. The DNA hybrid assemblies shine light on the synthesis of much more complicated and multifunctional systems and patterned arrays. Owing to the spacious hydrophobic compartment of hybrid assemblies, various types of hydrophobic nanoparticles can be encapsulated into assembly cores and tagged on the same desired spot increasing the diversity of building blocks, which eventually leads to highly functionalized systems.

6.1.3 Alignments of anisotropic nanostructures on lipid bilayers. Anisotropic metallic nanoparticles (e.g. gold and silver nanorods or nanowires) have been extensively exploited for applications such as sensing, electronics, or optics because of their unique shape-dependent electronic and optical properties. Control of nanoparticles immobilization on substrates or their incorporation into soft material, like polymers,[8,9] is essential, for the reason that their performance is dictated by the orientation of anisotropic nanoparticles.

In Chapter 5, we developed a method to immobilize gold nanoparticles on lipid bilayers and furthermore form 2D self-assembly structures. However, in terms of gold nanorods, there is still difficulty in controlling their orientation on lipid bilayers, which eventually will weaken their real world applications. As shown in Chapter 5, due to strong attraction, gold nanorods easily aggregate into clusters before the addition of linker DNA and the alignment of gold nanorods was failed. Capping agents can be used not only as a stabilizer to prevent nanoparticles from aggregating, but also as a spacer to keep distance between nanoparticles. Therefore, in future study introducing longer length of ligands or even polymers can potentially help to minimize the aggregation effect. It is also imperative to study how the length of DNA sequences on gold nanorods surface would affect the orientation.

6.2 References

(1) Walther, A.; Matussek, K.; Müller, A. H. E. *ACS Nano* **2008**, *2*, 1167-1178.

(2) Yoshida, M.; Roh, K.-H.; Lahann, J. *Biomaterials* **2007**, *28*, 2446-2456.

(3) Glotzer, S. C.; Solomon, M. J. *Nat. Mater.* **2007**, *6*, 557-562.

(4) Bäumler, H.; Georgieva, R. *Biomacromolecules* **2010**, *11*, 1480-1487.

(5) Whiteford, J. R.; Spanu, P. D. *Molecular Plant Pathology* **2002**, *3*, 391-400.

(6) Pawar, A. B.; Kretzschmar, I. *Macromol. Rapid Commun.* **2010**, *31*, 150-168.

(7) Christian, D. A.; Tian, A.; Ellenbroek, W. G.; Levental, I.; Rajagopal, K.; Janmey, P. A.; Liu, A. J.; Baumgart, T.; Discher, D. E. *Nat. Mater.* **2009**, *8*, 843-849.

(8) Al-Rawashdeh, N. A. F.; Sandrock, M. L.; Seugling, C. J.; Foss, C. A. *The*

Journal of Physical Chemistry B **1998**, *102*, 361-371.

(9) van der Zande, B. M. I.; Pagès, L.; Hikmet, R. A. M.; van Blaaderen, A. *The Journal of Physical Chemistry B* **1999**, *103*, 5761-5767.